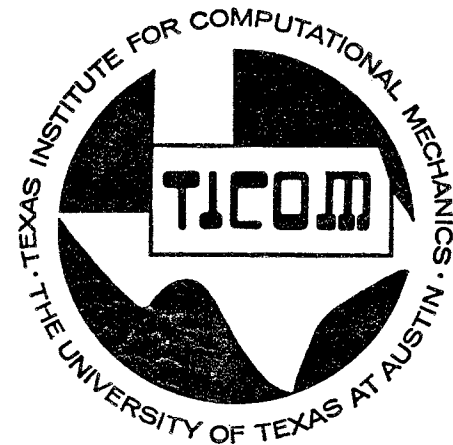FBR **8600**

Application of a Gradient Projection Technique to Minimum-Weight Design of Lifting Surfaces With Aeroelastic and Static Constraints

by I. O. Erbug

TICOM REPORT 74-3

Ph.D. Dissertation
Department of Civil Engineering
The University of Texas at Austin

THE TEXAS INSTITUTE *for* COMPUTATIONAL MECHANICS
COLLEGE OF ENGINEERING
THE UNIVERSITY OF TEXAS AT AUSTIN

June, 1974

20000111 060

APPLICATION OF A GRADIENT PROJECTION TECHNIQUE TO

MINIMUM-WEIGHT DESIGN OF LIFTING SURFACES WITH AEROELASTIC

AND STATIC CONSTRAINTS

by

Ibrahim Onur Erbuğ, B.S.C.E., M.S.C.E.

DISSERTATION

Presented to the Faculty of the Graduate School of

The University of Texas at Austin

in Partial Fulfillment

of the Requirements

for the Degree of

DOCTOR OF PHILOSOPHY

THE UNIVERSITY OF TEXAS AT AUSTIN

June 1974

ACKNOWLEDGEMENTS

APPLICATION OF A GRADIENT PROJECTION TECHNIQUE

TO MINIMUM-WEIGHT DESIGN OF LIFTING SURFACES WITH AEROELASTIC

AND STATIC CONSTRAINTS

Publication No._____

Ibrahim Onur Erbuğ, Ph.D.
The University of Texas at Austin, 1974

.

Supervising Professor: Roy R. Craig, Jr.

A parameter optimization algorithm is developed based on the gradient projection concept. The algorithm is applied to the aeroelastic optimization of a semi-infinite panel in supersonic flow and to the aeroelastic-stress optimization of a delta-wing in supersonic flow. The total weight is taken as the objective function. Constraints are placed on flutter speed and minimum thickness for the panel problem and on flutter speed, stress and minimum thickness for the delta wing problem.

Sandwich plate structural idealization is used for both the panel and the delta wing problem. During the optimization the core thickness is held constant while the cover skin thickness is varied. Finite element representation is used to model the structures. Constant thickness and tapered sandwich beam elements are used for the panel problem. A high precision triangular plate bending element, developed by Cowper, Kosko, Lindberg and Olson, is used for the delta-wing problem. The element stiffness and mass matrices are modified for linear

cover skin thickness variation. The element or the nodal point cover skin thicknesses are used as design variables (optimization parameters).

Two-dimensional, quasi-steady aerodynamic theory is used to obtain the aerodynamic forces. The aerodynamic damping is included. The same finite element functions are used in deriving the finite element mass, stiffness, aerodynamic and damping matrices, i.e. they are consistent.

In order to obtain the flutter constraint, system equations of motion are derived. These equations form a quadratic eigenvalue problem which can be reduced to a linear eigenvalue problem where the positive real parts of the eigenvalues indicate flutter. The optimization procedure required calculation of constraint gradients. Using analytical expressions, derivatives of the eigenvalues with respect to design variables are calculated efficiently.

For stress constraints only static loading is considered. Von Mises yield criterion is used to derive the equations for stress constraints. Stress constraints are placed at nodal points.

Due to nonlinearity of the constraints the optimization procedure incorporates constraint tolerances and provision for returning to the constraints when they are violated.

Different finite element combinations are studied for the panel problem. Using six tapered elements across the span, the effect of damping on the optimum shape is investigated.

For the delta wing problem a 3 x 3 grid of triangular bending elements is used. The natural boundary conditions are placed on curvatures for the free edges as well as geometric boundary conditions for the clamped edge. The effect of constraints on the optimum shape is studied by optimizing the structure first using only flutter and thickness constraints, then using only stress and thickness constraints, and finally using all three sets of constraints. Total weight reductions of 47% to 63% are obtained depending on the combinations of constraints.

TABLE OF CONTENTS

LIST OF TABLES

LIST OF FIGURES

CHAPTER 1

INTRODUCTION

1.1 Introduction to the Subject of Aeroelastic Optimization

The subject of this thesis is aeroelastic optimization, which falls under the general subject of structural optimization with eigenvalue (dynamic) constraints.

Although there are few earlier papers (mainly reference 25), the keen interest in this subject started in the late 1960's. Papers published on aeroelastic optimization since then present different approaches to the different aspects of the problem, namely the structural formulation, the aerodynamic formulation, the strength formulation, the formulation of the optimization problem and the solution of the optimization problem.

Generally the approach to the structural formulation falls into two groups;

1) Continuous formulation

2) Discrete formulation

Several theories are available for the aerodynamic formulation;

1) Strip theory

2) Piston theory

3) Quasi-steady aerodynamic theory

4) Three dimensional aerodynamic theory

Formulation of the optimization problem follows from

the structural formulation;

    1) Control theory formulation is applied when the continuous structural formulation is employed.

    2) Parameter optimization formulation follows the discrete structural formulation.

There exist several approaches to the solution of the control theory formulation. Among them are the following;

    1) Transition Matrix Method

    2) Gradient projection method

The solution methods for the parameter optimization problem have been independently developed by mathematicians and numerical analysts. Reference 13 is a good source for the numerical techniques available for structural optimization. There are two different approaches depending on the way that the eigenvalue constraint is handled;

    1) If the eigenvalue constraint is assumed to be an equality constraint, then the problem is reduced to a set of non-linear algebraic equations by introducing Lagrange multipliers. Several iterative numerical techniques exist for the solution of non-linear algebraic equations such as the Newton-Raphson method and its variations.

    2) If the eigenvalue constraint is assumed to be an inequality constraint, then the problem can be stated as a non-linear mathematical-programming problem. One of the iterative techniques based on gradient information can be used for the solution. The most commonly used algorithms in the aeroelastic

optimization field are;

    1)   Interior penalty function method

    2)   Usable-feasible directions method of Zoutendijk.

    3)   Gradient projection method

The predominant constraint in aeroelastic optimization is flutter. Few of the works published on aeroelastic optimization also consider other constraint such as deflections and stress. The process of handling such constraints has already been well established in the field of structural optimization.

In the following some of the important works on the aeroelastic optimization are briefly discussed:

In reference 4 Turner has extended his earlier work on structural optimization with constraints on natural frequencies (Ref. 26) to the optimization of structures with flutter constraints. He uses the discrete approach but handles the flutter constraint as an equality constraint. He obtains a set of non-linear algebraic equations by using complex Lagrange multipliers. The equations are solved using the Newton-Raphson method. Two examples are presented: 1) Panel Optimization 2) Cantilever Wing Optimization. His method can be used with any aerodynamic theory. He uses quasi-steady aerodynamic theory for the panel problem and strip theory for the cantilevered wing. The number of design variables is kept rather small (3 elements with constant mass and stiffness properties are used for both problems), presumably because of computational effort involved in solving non-linear equations. No other con-

straints are considered.

A paper by Ashley and McIntosh (Ref. 1) presents results using the continuous formulation. Several examples with eigenvalue constraints are discussed, among which are the optimization of a two-dimensional plate and of a cantilevered lifting surface with flutter constraints. Quasi-steady aerodynamic theory with zero aerodynamic damping is used. Equations are derived using control theory formulation but left unsolved for the two-dimensional plate problem. An analytical solution is given by inspection for the cantilevered wing. Placing constraints on minimum thickness is also considered.

Weisshaar, in reference 7, made significant contributions to both continuous and discrete approaches. Using control theory formulation, he obtains simultaneous non-linear differential equations and solves these equations using the "transition matrix" procedure (Ref. 27). Among examples with dynamic constraints he presents solutions for the first time to the optimum skin thickness distribution of a simply supported sandwich panel in supersonic flow with different thickness constraints and different mass ratios. Quasi-steady aerodynamic theory is employed. The aerodynamic damping is neglected. He also presents some results using finite elements and a first-order gradient technique (based on Rubin's work in reference 28) on the same problem. Flutter constraint gradients are calculated numerically.

A paper by Bhatia and Rudisill (Ref. 9) present their work on the optimization of complex structures with flutter

constraints using finite elements. The optimization procedure consists of three different search procedures, the first two are based on steepest-descent principle; one to increase the flutter speed, the other to decrease the structural weight. The third search procedure is based on gradient projection concept; it holds the structural weight constant while maximizing flutter speed. The main contribution is the analytical expressions for the calculation of flutter constraint gradients. A cantilevered box beam is optimized using three dimensional aerodynamic theory. With only flutter and thickness constraints approximately 40% total weight reduction is obtained after 22 design cycles.

A paper by Craig (Ref. 8) present results for flutter optimization of a simply supported sandwich panel using finite elements. Consistent element aerodynamic matrices are derived using quasi-steady theory with zero damping. Two different optimization modes are employed both based on the gradient projection concept. The weight minimization mode minimizes the weight while holding the flutter parameter constant. The Lambda-modification mode increases the flutter parameter while holding the weight constant. Optimum shapes are given for five and nine constant thickness beam elements across the span.

Rao in reference 19 presents a procedure for optimum design of aircraft wings to satisfy strength, stability, frequency and flutter constraints. Constant stress membrane elements and rectangular shear panels are used for structural idealization. Piston theory with zero damping is used to calcu-

late aerodynamic forces. An interior penalty function method is applied to the optimization problem. Eigenvalue gradients are calculated using exact expressions. Optimum shapes are obtained for several supersonic aircraft wings using 4 consecutive penalty parameters and 25 to 30 design cycles.

Miura, in reference 20, discusses a procedure to determine the optimum configuration of a lifting surface with aeroelastic constraints. Sandwich plate structural idealization is used. Ritz type displacement (modal) method is applied to derive system matrices. Aerodynamic forces are obtained using piston theory with negligible damping. The usable-feasible directions method of Zoutendijk is used to solve the optimization problem. Constraints are also placed on stresses and deflections. The paper by Fox, Miura and Rao (Ref. 10) summaries the above works by Rao and Miura.

A report put out by the Langley Research Center (Ref. 29) gives the optimum thickness distributions of a delta wing for stress and thickness constraints, for flutter and thickness constraints and for stress, flutter and thickness constraints. Sandwich plate idealization and piston theory are used. A finite-difference method is employed for discretization. An interior penalty function approach is chosen for the solution of the optimization problem.

Gwin, in reference 21, presents computer routines for the minimum-weight synthesis of a lifting surface with flutter constraint. Three-dimensional aerodynamic theory is used. Different finite elements can be used to represent the struc-

ture. A modified version of Zoutendijk's method is coded to solve the parameter optimization problem. System matrices are reduced using the first few natural vibration modes as generalized coordinates. Analytical expressions are used for flutter constraint gradients. Several subsonic examples are presented.

Recently, in reference 30, Pierson presented new contributions to the continuous approach. He applied what he calls a gradient projection optimal control method to control theory formulations. Results are presented for one and two dimensional solid and sandwich panels with different boundary conditions. Quasi-steady aerodynamic theory is used. A discussion is given to handle aerodynamic damping but the presented results are for zero damping.

1.2 Introduction to the Present Study:

In light of the above discussion the present work can be briefly described as follows:

The discrete approach is adopted for the structural formulation. Sandwich plate and finite element structural idealizations are used to represent the structure. Thickness parameters either associated with finite elements or with nodal points are used as design variables. The optimization problem is formulated as a non-linear mathematical-programming problem where the objective function is the total weight of the structure which is linear in the design variables. Flutter, stress and thickness constraints are considered. Quasi-steady aero-

dynamic theory with damping is used to calculate aerodynamic forces. However other aerodynamic theories can also be incorporated within the overall design procedure.

The consistent mass, stiffness, aerodynamic and damping matrices are derived for elements and for the system. The flutter constraint is represented as a quadratic eigenvalue problem in terms of these matrices. This is reduced to a linear eigenvalue problem where the eigenvalues are the complex frequencies and positive real parts of the eigenvalues indicate flutter. It is possible to detect flutter phenomena involving modes other than the two initial modes during the optimization. This way of handling the flutter constraint is unique to this study. In previous works on aeroelastic optimization the flutter constraint was placed on the flutter speed. That makes it very hard to predict flutter involving modes other than the initial two modes. Here the flutter speed is determined for the initial design and treated as a constant parameter during the optimization.

The stress constraints are only considered for uniform static loading, employed as a first approximation to the aeroelastic loading. This is consistent with the quasi-steady aerodynamic theory approximation. Von Mises yield criterion is used to obtain stress constraint equations. Constraints are placed at finite element nodal points. Thickness constraints are directly applied on design variables.

An algorithm based on the gradient projection concept is developed to solve the optimization problem. Due to non-

linearity of the constraints, the algorithm incorporates constraint tolerances. The design change vector is composed of two orthogonal vectors, one in the projected gradient direction to reduce the objective function; the other in the orthogonal direction for returning to the violated constraints.

The optimization procedure requires calculation of constraint gradients. Analytical expressions are derived to perform these calculations efficiently.

Two example problems are considered: A semi-infinite panel in supersonic flow and a cantilevered delta wing in supersonic flow. Different finite element representations are tried for the panel problem. Results are compared with Weisshaar's (Ref. 7) and Craig's (Ref. 9) results. Six tapered sandwich beam elements are used across the panel span to study the effect of damping on the optimum shape.

For the delta wing problem high precision triangular plate bending elements (Ref. 22) are used. Natural frequencies and flutter boundaries are checked against results given by Olson and others (Refs. 6 and 22). The minimum-weight designs are obtained for flutter and thickness constraints, for stress and thickness constraints and for flutter, stress and thickness constraints.

The main objectives of this study can be summarized as follows:

1) Development of a parameter optimization algorithm for the minimum-weight design of lifting surfaces; an algorithm capable of giving an approximate design using a small number

of iterations.

2) Development of equations for handling the flutter constraint such that is is possible to predict flutter involving higher modes during the optimization.

3) Development of analytical expressions for the constraint gradients so that these can be calculated with minimum time.

4) Study the effect of aerodynamic and structural damping on the minumum-weight design.

5) Study the effect of different combinations of flutter, stress and thickness constraints on the minimum-weight design.

1.3 Organization of the Thesis:

In Chapter 2 the optimization formulation is presented. Several popular algorithms for the solution of the nonlinear mathematical-programming problem are briefly discussed.

Chapter 3 is for structural formulation: Sandwich idealization is presented. Equations for stresses and bending moments in terms of transverse displacement second derivatives are given. Finite element representation is briefly explained.

Equations for aerodynamic forces are derived in Chapter 4. The derivation of element aerodynamic and damping matrices are discussed.

In Chapter 5 equations expressing flutter, stress and thickness constraints in terms of design variables are derived.

Chapter 6 gives the derivation of equations for the gradient projection algorithm. Figures explaining different design steps are also presented.

The analytical expressions for flutter, stress and thickness constraint gradients are developed in Chapter 7.

Chapter 8 and Chapter 9 present the results for the semi-infinite panel optimization and the cantilevered delta wing optimization respectively.

In Chapter 10 several conclusions and suggestions for further research are listed.

Appendices A, B and C are for the derivation of finite element matrices for the different finite elements used in the examples.

CHAPTER 2

FORMULATION OF THE OPTIMIZATION PROBLEM

Design of aircraft structures can be cast as a non-linear mathematical-programming problem of the form:

Find ρ

such that $F(\rho) \rightarrow$ minimum

subject to $C_j(\rho) \leq 0;$ $j = 1, 2, \ldots, m$

Here ρ, the vector of optimization parameters, should contain well chosen design variables such that when ρ is determined, the structure is essentially determined. $F(\rho)$, the merit (objective) function, should be so chosen that its minimization would drive us to a most desirable structural configuration, mainly a most economic one. $C_j(\rho)$, $j = 1, 2, \ldots, m$, the constraints, should include all the criteria the structure has to satisfy for its usability.

Most established algorithms for the solution of the non-linear programming problem require the calculations of the merit function gradient;

$$\nabla F(\rho)^T = \{\frac{\partial F}{\partial \rho_1}, \frac{\partial F}{\partial \rho_2}, \ldots, \frac{\partial F}{\partial \rho_n}\}(\rho) \qquad (2.1)$$

and the constraint gradients;

$$\nabla C_j(\rho)^T = \{\frac{\partial C_j}{\partial \rho_1}, \frac{\partial C_j}{\partial \rho_2}, \ldots, \frac{\partial C_j}{\partial \rho_n}\}(\rho), \quad j = 1, 2, \ldots, m$$

$$(2.2)$$

12

since along these directions the changes in $F(\rho)$ and $C_j(\rho)$, $j = 1,2,\ldots, m$, are maximum. For this reason the functional relationship between $F(\rho)$, $C_j(\rho)$, $j = 1,2,\ldots, m$, and ρ should be mathematically known to us.

The following definitions are in order for the clarity of the rest of this chapter:

1) Any design ρ_q is said to be feasible if it satisfies the relationships;

$$C_j(\rho_q) \leq 0; \quad j = 1,2,\ldots, m \tag{2.3}$$

2) Any design ρ_q is said to be usable with respect to a previous design ρ_{q-1}, if the relationship;

$$F(\rho_q) \leq F(\rho_{q-1}) \tag{2.4}$$

is valid.

3) A usable-feasible design change satisfies both of these conditions simultaneously.

4) A constraint is said to be "convex" if, any move made from the constraint along a direction orthogonal to the gradient vector, leads to a design in the infeasible region.

In figure 2.1 some of the concepts described above are illustrated on a 2-dimensional design space ($n = 2$).

2.1 Design Variables (Optimization Parameters)

Generally, sizing parameters of the structural members are used as design variables in structural optimization. The finite element representation makes the choice particularly
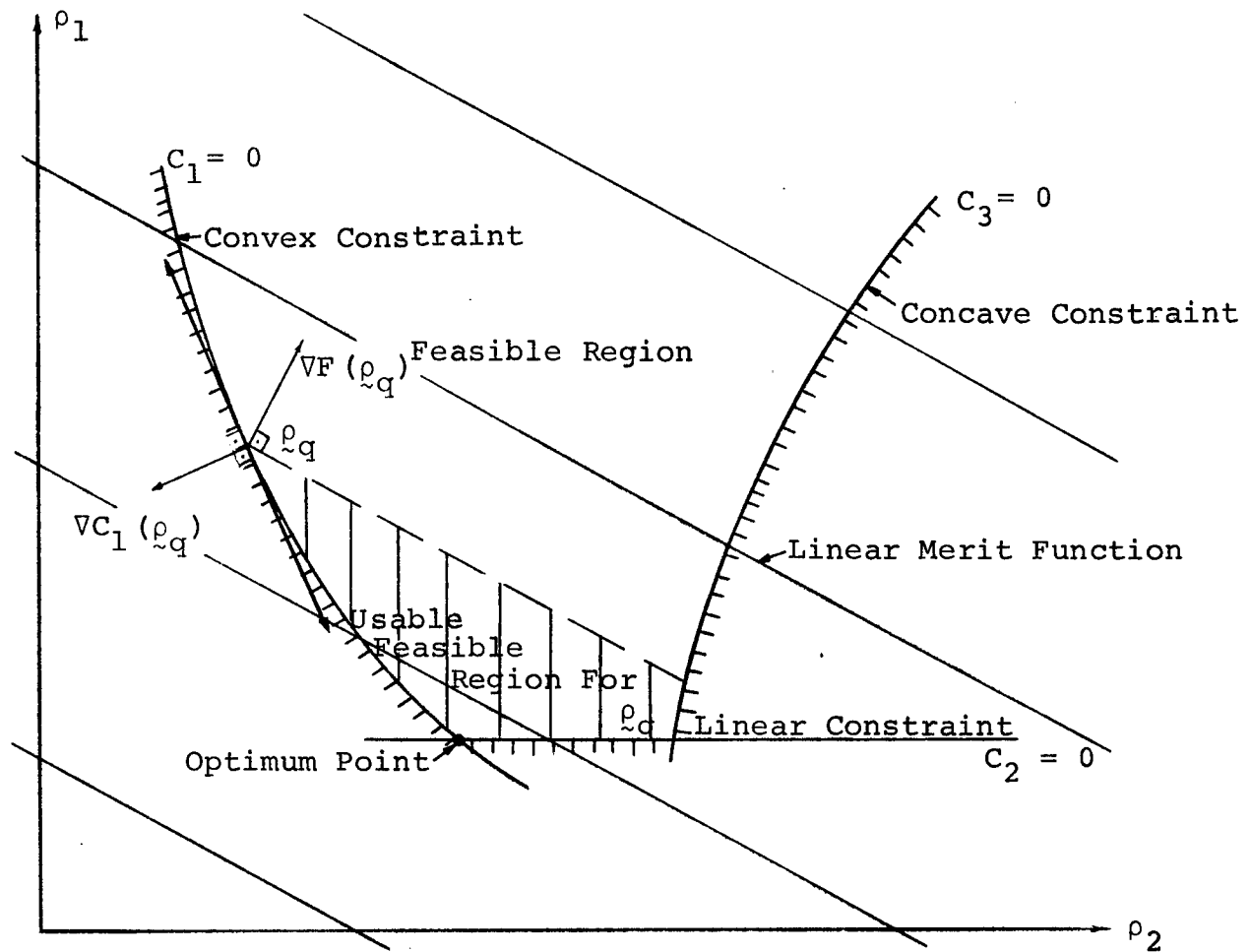
Fig. 2.1 Main Concepts for a Non-linear Mathematical Programming Problem

easy. In the problems considered here either the finite element thicknesses or the nodal point thicknesses are used as design variables.

2.2 Merit (Objective) Function

The structural weight is chosen to be the merit function in all the cases considered here. This choice is rather common for aeroelastic optimization since both the initial and operational costs of aircraft structures are closely related to the structural weight.

As shall be seen in the example problems it is very easy to express the structural weight in terms of either the finite element thicknesses or the nodal point thicknesses. In all cases the structural weight will be a linear function of the design variables. This fact makes the calculations of $F(\rho)$, the merit function, and of $\nabla F(\rho)$, the merit function gradients particularly simple and time-saving.

2.3 Constraints

Most aircraft structures are required to satisfy the following types of design criteria:

1. Combined stresses must be below yield for all structural members and for all specified loading conditions.

2. Deflections under all specified loading conditions must be within allowable limits.

3. Member sizes must be within practical limits.

4. Natural frequencies must fall within allowable

bands.

5. The structure must be aerodynamically stable, i.e., it must be free from flutter and divergence.

The following constraints, taken from the above list, are considered in the applications discussed here:

1. Flutter: The flutter speed of the final minimum-weight design must be greater than or equal to the flutter speed of the initial design.

2. Stress: The final minimum-weight design must satisfy the same yield criteria satisfied by the initial design.

3. Thickness: The member sizes of the final minimum-weight design must be greater than or equal to a certain percentage of the member sizes of the initial design.

In the examples discussed in Chapter 8 and Chapter 9, the effect of different combinations of constraints on the optimization is studied. Flutter + thickness, stress + thickness, and flutter + stress + thickness combinations are considered. Chapter 5 contains the explicit expressions for the constraints as functions of ρ. Stress and flutter constraints are non-linear; thickness constraints are linear constraints.

2.4 Optimization Algorithms

Three different algorithms, popular in structural optimization, are considered to drive the optimization process from ρ_o, the initial design variables, to ρ_f, the final (minimum-weight) design variables. These algorithms are briefly

discussed below:

1. Usable-Feasible Directions Method of Zoutendijk (Ref. 13, Sec. 7.2):

The idea is to generate a sequence of feasible designs ρ_o, ρ_1,...., ρ_q, ρ_{q+1} such that for all q the inequality

$$F(\rho_{q+1}) \leq F(\rho_q) \tag{2.5}$$

is satisfied. Here ρ_{q+1} is defined as:

$$\rho_{q+1} = \rho_q + \alpha_q^* S_q \tag{2.6}$$

so that the qth step of the process involves the calculation of the direction vector S_q and the step length α_q^* .

$C_j(\rho_q)$ is a critical constraint at ρ_q if $C_j(\rho_q) = 0$. For such critical constraints the feasibility of S_q is assured if S_q satisfies the inequality:

$$S_q^T \nabla C_j(\rho_q) < 0 \; ; \quad j \in J_c \tag{2.7}$$

where J_c is the set of all critical constraints.

The usability of S_q, on the other hand, is assured if S_q satisfies the inequality:

$$S_q^T \nabla F(\rho_q) < 0 \tag{2.8}$$

The determination of S_q satisfying the above inequalities can be cast as an auxiliary optimization problem as follows:

Maximize β

Subject to:

(1) $\quad \underset{\sim}{S}_q^T \nabla C_j (\underset{\sim}{\rho}_q) \; + \; \theta_j \beta \; \leq \; 0 \; ; \; j \; \epsilon \; J_c$ (2.9)

(2) $\quad \underset{\sim}{S}_q^T \nabla F (\underset{\sim}{\rho}_q) \; + \; \beta \; \leq \; 0$ (2.10)

(3) $\quad \underset{\sim}{S}_q$ is normalized

Here θ_j is a pre-selected non-negative parameter to account for the curvature of a non-linear convex constraint. $\theta_j = 0$ is used for a linear constraint.

This auxiliary optimization problem is linear, provided that a linear normalization is used for $\underset{\sim}{S}_q$, such as, $-1 \leq S_{qi} \leq 1$. Therefore the elements of $\underset{\sim}{S}_q$ and β can be easily calculated by using a linear programming algorithm (simplex method). If the auxiliary problem leads to $\beta > 0$, then $F(\underset{\sim}{\rho})$ can be improved within the feasible region. If, however, we obtain $\beta = 0$ then it can be shown that $\underset{\sim}{\rho}_q$ is the optimal solution.

Once the direction $\underset{\sim}{S}_q$ has been determined as above, determination of α_q^* for non-linear merit functions can be cast as a one-dimensional minimization problem (Ref. 13, sec. 6.2.2); Find α_q such that $F(\underset{\sim}{\rho}_q + \alpha_q \underset{\sim}{S}_q) \equiv F(\alpha_q)$ is minimum provided $\underset{\sim}{\rho}_{q+1} = \underset{\sim}{\rho}_q + \alpha_q \underset{\sim}{S}_q$ is in the feasible region. In practice $F(\alpha_q)$ is usually approximated by a quadratic function and determination of α_q^* requires calculation of $F(\alpha_q)$ for two different values of α_q other than $\alpha_q = 0$. If the gradients of the merit function are easily obtained, then a cubic approximation can be

used in which case calculation of $F(\alpha_q)$ and $\nabla F(\alpha_q)$ for one value of α_q other than $\alpha_q = 0$ is needed.

For linear merit functions the only consideration for the selection of α_q^* is the feasilibility of ρ_{q+1}. Therefore α_q^* can be supplied by the user (Ref. 21).

When α_q^* is so obtained, the constraints are checked. If there is a constraint violation, an interpolation procedure must be used to reduce the α_q^* so that we are on or near the violated constraint, within the feasible region (Ref. 21).

One way to increase the efficiency of the algorithm is to include the near-critical constraints, $-\varepsilon \le C_j(\rho_q) \le 0$ into the set of critical constraints. Here ε is a positive parameter which can be made successively smaller when small values of β indicate that ρ_q approaches the optimal solution.

It should be noted that the choice of scaling coefficients θ_j, $j = 1, 2, \ldots, m$, for non-linear constraints is intuitive, and it will affect the convergence speed of the algorithm considerably. Large values for θ_j's will push the iteration away from the constraints and most likely away from the optimum point too. Small values for θ_j's on the other hand will be ineffective in preventing the same constraints from being violated in the following steps.

The usable-feasible directions algorithm is terminated when either β or the change in $F(\rho)$ becomes small.

2. The Gradient Projection Method (Ref. 13, Sec. 7.3):

This method assumes that the optimum point lies on one or more constraints. Therefore the idea is to follow the constraints as closely as possible while reducing the merit function. For this purpose the method uses the projections of the steepest descent direction, $-\nabla F(\rho_q)$, into the manifold defined by currently active constraints, $C_j(\rho_q) = 0$, to calculate the vector S_q (same meaning as in equation 2.6). Thus S_q satisfies the relationships;

$$S_q^T \nabla F(\rho_q) \;\; < \;\; 0 \qquad\qquad (2.11)$$

and

$$S_q^T \nabla C_j(\rho_q) \;\; = \;\; 0 \; ; \quad j \; \varepsilon \; J_c \qquad\qquad (2.12)$$

where J_c is the set of all critical constraints.

It is possible to express S_q as:

$$S_q \;\; = \;\; - \; P_q \; \nabla F(\rho_q) \qquad\qquad (2.13)$$

where P_q is the projection matrix. P_q can be calculated by using the projection theorem of vector calculus. First it is convenient to introduce the rectangular matrix of constraint gradients:

$$G_q \;\; = \;\; \left[\nabla C_1(\rho_q), \; \nabla C_2(\rho_q), \ldots, \; \nabla C_m(\rho_q) \right] \qquad\qquad (2.14)$$

where m is the number of active constraints, so that we can write the feasibility condition (equations 2.12) concisely as

$$\underset{\sim}{G}_q^T \, \underset{\sim}{S}_q \;\; = \;\; \underset{\sim}{0} \qquad\qquad (2.15)$$

The projected vector $\underset{\sim}{P}_q \nabla F(\underset{\sim}{\rho}_q)$ can be obtained from $\nabla F(\underset{\sim}{\rho}_q)$ by substracting from it the vector $\underset{\sim}{G}_q \underset{\sim}{v}_q$, which is a linear combination of the constraint gradients. Now we can re-write the feasibility condition:

$$\underset{\sim}{G}_q^T \left[\underset{\sim}{P}_q \nabla F(\underset{\sim}{\rho}_q) \right] \;=\; \underset{\sim}{G}_q^T \left[\nabla F(\underset{\sim}{\rho}_q) \;-\; \underset{\sim}{G}_q \underset{\sim}{v}_q \right] \;=\; \underset{\sim}{0} \qquad (2.16)$$

This equation leads to:

$$\underset{\sim}{v}_q \;\;=\;\; \left[\underset{\sim}{G}_q^T \underset{\sim}{G}_q \right]^{-1} \underset{\sim}{G}_q^T \, \nabla F(\underset{\sim}{\rho}_q) \qquad\qquad (2.17)$$

and

$$\underset{\sim}{P}_q \;\;=\;\; \underset{\sim}{I} \;-\; \underset{\sim}{G}_q \left[\underset{\sim}{G}_q^T \underset{\sim}{G}_q \right]^{-1} \underset{\sim}{G}_q^T \qquad\qquad (2.18)$$

We should note that the matrix $[\underset{\sim}{G}_q^T \underset{\sim}{G}_q]$ is an m x m square matrix and can generally be inverted if the constraint gradients are linearly independent.

Once $\underset{\sim}{S}_q$ is so determined and normalized we have the usual equation for qth iteration step;

$$\underset{\sim}{\rho}_{q+1} \;\;=\;\; \underset{\sim}{\rho}_q \;+\; \alpha_q^* \, \underset{\sim}{S}_q \qquad\qquad (2.19)$$

The determination of α_q^* can again be cast as a one-dimensional minimization problem if the merit function is non-linear, if the merit function is linear it can be given a

priori. For either case α_q^* must be bounded not to violate any new constraints. Interpolation can be used to reduce α_q^* in case such a violation occurs.

As formulated above the gradient projection method is very powerful for linear constraints but will not work very well for non-linear constraints. When we are on a convex constraint any move performed along $\underset{\sim}{S}_q$ will take us out of the feasible region. An extra step has to be performed to come back to the feasible region (see Chapter 6 for a detailed discussion). For such cases, the choice of α_q^* becomes very important. A large value for α_q^* will increase the difficulty in coming back into the feasible region. On the other hand, a small value for α_q^* will mean that too many iterations will be required to converge to the optimum solution.

The idea of including the near critical constraints, $-\varepsilon \leq C_j(\underset{\sim}{\rho}_q) \leq 0$, into the set of critical constraints, to increase the efficiency of the algorithm also applies for the gradient projection method.

The convergence of the algorithm can be based either on the amount of variation of the objective function in one iteration step, $F(\underset{\sim}{\rho}_q) - F(\underset{\sim}{\rho}_{q+1})$, or on the product $\underset{\sim}{S}_q^T \nabla F(\underset{\sim}{\rho}_q)$ which tends to get smaller as the optimum point is approached.

3.   The Interior Penalty Function Method (Ref. 13, Sec. 6.3):

The idea is first to convert the constrained minimization problem into an unconstrained minimization problem and then solve the unconstrained minimization problem by one of the

well developed methods. The conversion is done by augmenting
the objective function with a penalty term which is small at
points away from the constraints in the feasible region, but
which gets very large as the constraints are approached. The
most commonly used form is the following:

$$\phi(\underset{\sim}{\rho},r) \;=\; F(\underset{\sim}{\rho}) \;-\; r \sum_{j=1}^{m} \frac{1}{C_j(\underset{\sim}{\rho})} \tag{2.20}$$

where $F(\underset{\sim}{\rho})$ is to be minimized over all $\underset{\sim}{\rho}$ satisfying
$C_j(\underset{\sim}{\rho}) \leq 0$, $j = 1,2,\ldots$, m. Here the penalty parameter r is a
positive number which must be made successively smaller in order
to come as close to the constraints as possible.

The most powerful mehtod so far developed to solve
the unconstrained minimization problem is the Davidon-Fletcher-
Powell variable metric method (Ref. 13, sec. 6.2.6) and it is
usually coupled in practice with the interior penalty function
approach to drive the optimization for decreasing r values.
It proceeds as follows:

$$(1) \quad \underset{\sim}{\rho}_{q+1} \;=\; \underset{\sim}{\rho}_q \;+\; \alpha_q^{*} \, \underset{\sim}{S}_q \tag{2.21}$$

where the directional vector $\underset{\sim}{S}_q$ is calculated as:

$$(2) \quad \underset{\sim}{S}_q \;=\; - \, \underset{\approx}{H}_q \nabla\phi(\underset{\sim}{\rho}_q,r) \tag{2.22}$$

Here $-\nabla\phi(\underset{\sim}{\rho}_q,r)$ is the well known steepest descent
direction. The matrix $\underset{\approx}{H}_q$ is a modifier which takes care of
the phenomenon called zig zagging which is the main cause of
inefficiency associated with steepest descent algorithms. We
can write

$$\underset{\sim}{H}_q \; = \; F(\underset{\sim}{H}_{q-1}, \; \underset{\sim}{S}_{q-1}, \; \underset{\sim}{g}_q, \; \underset{\sim}{g}_{q-1}, \; \alpha^*_{q-1}) \tag{2.23}$$

where $\quad \underset{\sim}{g}_q \; = \; \nabla\phi(\underset{\sim}{\rho}_q, r) \tag{2.24}$

and $\quad \underset{\sim}{g}_{q-1} \; = \; \nabla\phi(\underset{\sim}{\rho}_{q-1}, r) \tag{2.25}$

The calculation details of $\underset{\sim}{H}_q$ will be omitted here but may be found in reference 13. It can be shown that it is a positive definite approximation to the matrix of second partial derivatives (Ref. 13). $\underset{\sim}{H}_O$ usually is taken to be equal to the identity matrix $\underset{\sim}{I}$.

(3) Once $\underset{\sim}{S}_q$ is known, α^*_q is calculated by solving the one-dimensional minimization problem (Ref. 13, Sec. 6.2.2): Find α_q such that $\phi(\underset{\sim}{\rho}_q + \alpha_q\underset{\sim}{S}_q, r) \equiv \phi(\alpha_q)$ is minimum, provided $\underset{\sim}{\rho}_{q+1} = \underset{\sim}{\rho}_q + \alpha_q \underset{\sim}{S}_q$ is in the feasible region. Since $\phi(\underset{\sim}{\rho}, r)$ is non-linear, either a quadratic or a cubic approximation can be used for $\phi(\alpha_q)$ as was discussed for Zoutendijk's method. Once α^*_q is determined the qth step is completed.

The following points should be noted about the interior penalty function method:

1) The initial design must be in the feasible region, i.e., $C_j(\underset{\sim}{\rho}_O) \leq 0$, $j = 1,2,\ldots,$ m and care must be taken in calculating α^*_q to remain in the feasible region at all times. The augmented function loses its meaning outside the feasible region.

2) The selection of an initial value for the penalty

parameter r is intuitive. If the initial r is too large, the function $\phi(\rho,r)$ will be easy to minimize, but the minimum may lie far from the optimum point of the original constrained problem. If, on the other hand, the initial r is too small, the function $\phi(\rho,r)$ will be hard to minimize.

3) The minimum of the function $\phi(\rho,r_i)$ is determined for each r_i value and then r_i is reduced to its next value r_{i+1}. This process continues until the convergence criteria for function $F(\rho)$ is satisfied. This nature of the algorithm tends to increase the number of iteration steps since smaller step sizes have to be employed near minimum points (Ref. 19).

As described above, all three algorithms have certain common features which can be summarized as follows:

1) They all require the calculation of the merit function, the constraints, the merit function gradient and the constraint gradients at every iteration. In the interior penalty function approach this involves all the constraints; in the other two methods only the currently active constraints are involved.

2) All methods require a certain amount of algebra in the direction-finding process: The calculation of the matrix $\underset{\sim}{H}_q$ for the interior penalty function method, the linear programming solution for the Zoutendijk algorithm and the calculation of the matrix $\underset{\sim}{P}_q$ for the gradient projection approach.

3)   All the algorithms require the solution of a one-dimensional minimization problem, where care must be taken to remain in the feasible region. For the interior penalty function approach the one-dimensional minimization involves the calculations of the augmented function $\phi(\rho,t)$ which is always non-linear, whereas for the other two methods, only the merit function $F(\rho)$ is involved, which can be linear. On the other hand, remaining in the feasible region requires very little effort for the interior penalty function method since the constraints are inherent in the augmented function, for Zoutendijk's method it involves an interpolation only when new constraints are encountered, provided appropriate θ_j values are chosen, for the gradient projection method, assuming we are working with non-linear convex constraints, an extra step is always required to come back to the feasible region.

4)   All methods involve certain parameters which can only be properly selected after enough experience with the particular method and with the particular optimization problem. The penalty parameters r_i for the interior penalty function method, the scaling coefficients θ_j for the usable-feasible directions method and the step size α_q^* for the gradient projection method.

The above summary indicates that any choice of one of the algorithms over the other two is going to be problem dependent. We have the following preliminary data for the aeroelastic optimization problem:

1) Objective function is linear in design parameters.

2) Flutter and stress constraints are highly non-linear.

3) Thickness constraints are linear.

4) The calculation of the flutter constraint and its gradients are the major time consiming computational efforts.

With this much information it is possible to discard the penalty function method, since it will not take advantage of the linearity of the objective function and since it will include all the constraints at all times. Also because of its nature, (See page 25) it will tend to involve a larger number of iterations.

To make a choice between the other two is more difficult. Since the objective function is linear, a one-dimensional minimization procedure will not yield the step length α_q^* for either method. α_q^* must be determined some other way. This can be done empirically or can be based on some criteria such as the reduction in merit function (Ref. 21). In choosing α_q^*, the main concern for Zoutendijk's approach will be the violation of new constraints whereas the main concern for the gradient projection method will be staying close to the feasible region. Proper θ_j values must be selected for the Zoutendijk's approach whereas a proper way of coming back to the feasible region must be devised for the gradient projection method.

The final choice for the optimization algorithm in this study is the gradient projection concept which was sub-

sequently modified to handle the constraint violations. The main reason for this choice was to provide an alternative to the Zoutendijk's approach which has already been successfully used by several studies (Refs. 20, 21) on aeroelastic optimization in recent years.

CHAPTER 3

STRUCTURAL FORMULATION

3.1 Sandwich Idealization

For the examples considered here a sandwich type structural idealization is used. This type of structural idealization is well suited especially for the preliminary design of most types of lifting surfaces. This type of idealization, as will be seen later, is also computationally very efficient.

A sandwich plate (Figure 3.1) is the extension of the concept of I-beam into two-dimensions. It consists of shear-carrying core material with negligible bending stiffness, covered on both sides with skins having high inplane stiffness. The following assumptions further define the model:

1) $t \ll d$ i.e., cover skins can be considered to be membranes with negligible bending and transverse shear stiffness.

2) A line normal to the mid-surface in the undeformed state remains straight and normal to the mid-surface across the core and the skins after deformation.

3) Membrane stresses in the cover skins are constant across the thickness of the cover skins.

4) Both cover material and core material are isotropic.
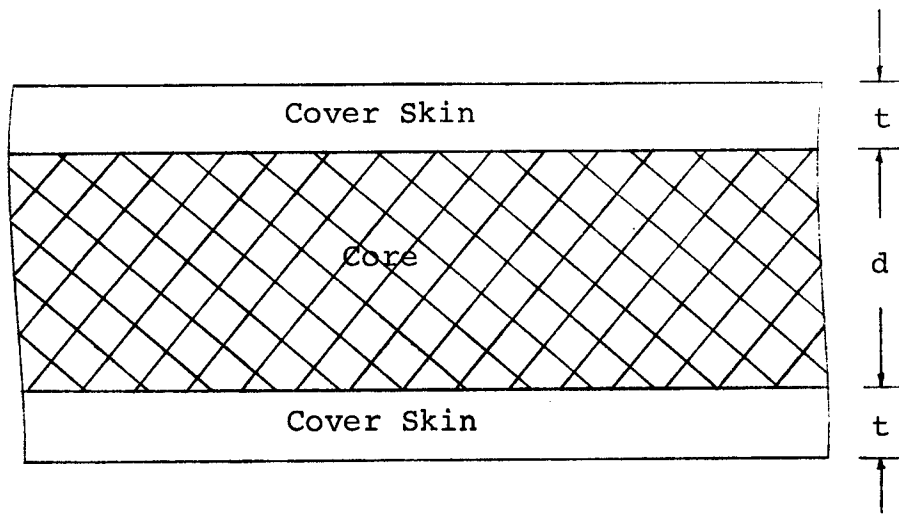
Fig. 3.1 Cross Section of a Sandwich Plate
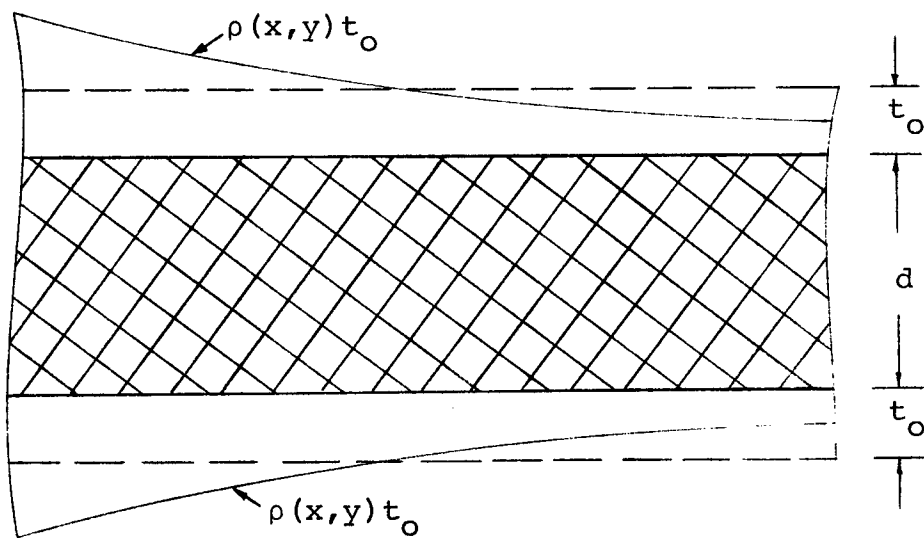
Fig. 3.2 Cover Skin Thickness Distribution

With these assumptions, the following equations expressing the membrane stresses in the cover skins in terms of second derivatives of the transverse displacement can be written:

$$\begin{Bmatrix} \sigma_x \\ \sigma_y \\ \tau_{xy} \end{Bmatrix} = \frac{-Ed}{2(1-\nu^2)} \begin{bmatrix} 1 & \nu & 0 \\ \nu & 1 & 0 \\ 0 & 0 & (1-\nu) \end{bmatrix} \begin{Bmatrix} W_{xx} \\ W_{yy} \\ W_{xy} \end{Bmatrix} \qquad (3.1)$$

The following equations give the plate bending moments in terms of second derivatives of the transverse displacement:

$$\begin{Bmatrix} M_x \\ M_y \\ M_{xy} \end{Bmatrix} = \frac{-E\, d^2 t}{2(1-\nu^2)} \begin{bmatrix} 1 & \nu & 0 \\ \nu & 1 & 0 \\ 0 & 0 & (1-\nu) \end{bmatrix} \begin{Bmatrix} W_{xx} \\ W_{yy} \\ W_{xy} \end{Bmatrix} \qquad (3.2)$$

In both of these equations ν, the Poisson's ratio and E, the Young's modulus, are of cover skin material. From equation (3.2) we can define the sandwich plate flexural rigidity term D as

$$D = \frac{E\, d^2 t}{2(1-\nu^2)} \qquad (3.3)$$

In all of the optimization problems discussed here, core thickness d is held constant and thickness t of both upper and lower skins is varied. By using a non-dimensional scaling function $\rho(x,y)$ it is possible to express a new skin

thickness distribution in terms of the initial uniform thickness distribution (Figure 3.2);

$$t(x,y) = \rho(x,y)t_o \qquad (3.4)$$

where t_o is the skin thickness of the initial design. From this definition we have

$$\rho_o(x,y) = 1 \qquad (3.5)$$

Since the plate flexural rigidity term D is a linear function of t, (Eq. 3.3) the varying flexural rigidity $D(x,y)$ can be expressed in terms of the initial uniform flexural rigidity as

$$D(x,y) = \rho(x,y)D_o \qquad (3.6)$$

The initial uniform mass per unit area of the sandwich plate can be divided into variable and constant mass such that

$$m_o = m_v + m_c = m_o\eta + m_o(1 - \eta) \qquad (3.7)$$

where

$$\eta = \frac{m_v}{m_o} \qquad (3.8)$$

Here variable mass is the mass of the cover skins; constant mass is the mass of the core material. For an actual wing, constant mass will include the mass of the spars, ribs and fuel. Since variable mass is a linear function of t, we can write

$$m(x,y) = m_o[\rho(x,y)\eta + 1 - \eta] \qquad (3.9)$$

where $m(x,y)$ is the total mass per unit area corresponding to a new cover skin thickness distribution.

As can be seen, at any step of the optimization, by specifying the non-dimensional scaling function $\rho(x,y)$ both

stiffness and mass parameters of the sandwich plate are easily
defined in terms of the initial stiffness and mass parameters.

3.2 Finite Element Idealization:

Finite element idealizations are used to discretize
the continuous structural examples. The following finite ele-
ments are employed:

1) Constant thickness sandwich beam element

2) Tapered sandwich beam element

3) High-precision triangular sandwich plate bending
element with linear thickness variation.

Details of the element characteristics are in Appen-
dices A, B, and C.

The scaling function $\rho(x,y)$ is discretized by either
associating a ρ_i with each element (for constant thickness ele-
ments) or with each nodal point (for elements with linear thick-
ness variation). In this way a continuous function $\rho(x,y)$ is
transformed into a design variable vector ρ. The initial design
vector used in the present studies will be

$$\rho_o^T = \{1, 1, 1, \ldots, 1, 1\} \qquad (3.10)$$

With this approach it is possible to write the mass
and stiffness matrices in the following form:

$$\underset{\approx}{K}(\underset{\sim}{\rho}) = \sum_i^n \rho_i \underset{\approx}{K}_i \qquad (3.11)$$

$$\underset{\approx}{M}(\underset{\sim}{\rho}) = \sum_i^n \rho_i \underset{\approx}{M}_i + \underset{\approx}{M}_c \qquad (3.12)$$

where M_C is the constant mass matrix, K_i and M_i are the individual contributions of the design variable ρ_i to stiffness and mass matrices respectively. We can further define initial mass and stiffness matrices as

$$K_O = K(\rho_O) \tag{3.13}$$

$$M_O = M(\rho_O) \tag{3.14}$$

Using M_O we can write

$$M_C = (1 - \eta)M_O \tag{3.15}$$

which can be used to generate M_C from the initial mass matrix.

The above representation of the mass and stiffness matrices enables us to generate mass and stiffness matrices for different design variable vectors ρ_q. Element matrices, which are independent of the design variables. Need only be computed and stored once at the beginning.

CHAPTER 4

AERODYNAMIC FORMULATION

This formulation basically follows Olson's in reference 6. Two-dimensional, quasi-steady aerodynamic theory is used to obtain the aerodynamic forces. It is assumed that the air flow is parallel to the x-axis (Figure 4.1) above the panel and the effect of any air below the panel may be neglected. In terms of the transverse displacement function, $W(x,y,t)$, the aerodynamic pressure acting on an infinitesimal element dxdy is

$$\Delta p(x,y,t) = \frac{2q}{(M_\infty^2-1)^{1/2}} \left[\frac{\partial W}{\partial x} + \frac{1}{u} \left(\frac{M_\infty^2 - 2}{M_\infty^2 - 1} \right) \frac{\partial W}{\partial t} \right] dxdy \qquad (4.1)$$

where q is the dynamic pressure, M_∞ is the free-stream Mach number, and u is the flow velocity.

It is possible to separate the transverse displacement function $W(x,y,t)$ into functions of space and time

$$W(x,y,t) = \bar{W}(x,y)e^{\mu t} \qquad (4.2)$$

where, in general, μ is a complex number

$$\mu = \beta + i\omega \qquad (4.3)$$

The borderline between stability and instability is defined by vanishing β. At the flutter condition the motion is given by $e^{i\omega t}$ which is harmonic.

$W(x,y,t) = \bar{W}(x,y)e^{\mu t}$

$\Delta p(x,y,t) = (\Delta p_a + \Delta p_d)e^{\mu t}$

$\Delta I = m_O(\rho\eta + 1-\eta)\mu^2\bar{W} \ dx \ dy$

$$\Delta p_a = \frac{2q}{(M_\infty^2 - 1)^{1/2}} \frac{\partial\bar{W}}{\partial x} \ dxdy$$

$$\Delta p_d = \left[\frac{2q}{u} \frac{M_\infty^2 - 2}{(M_\infty^2-1)^{3/2}}\right] \mu \ \bar{W} \ dxdy$$
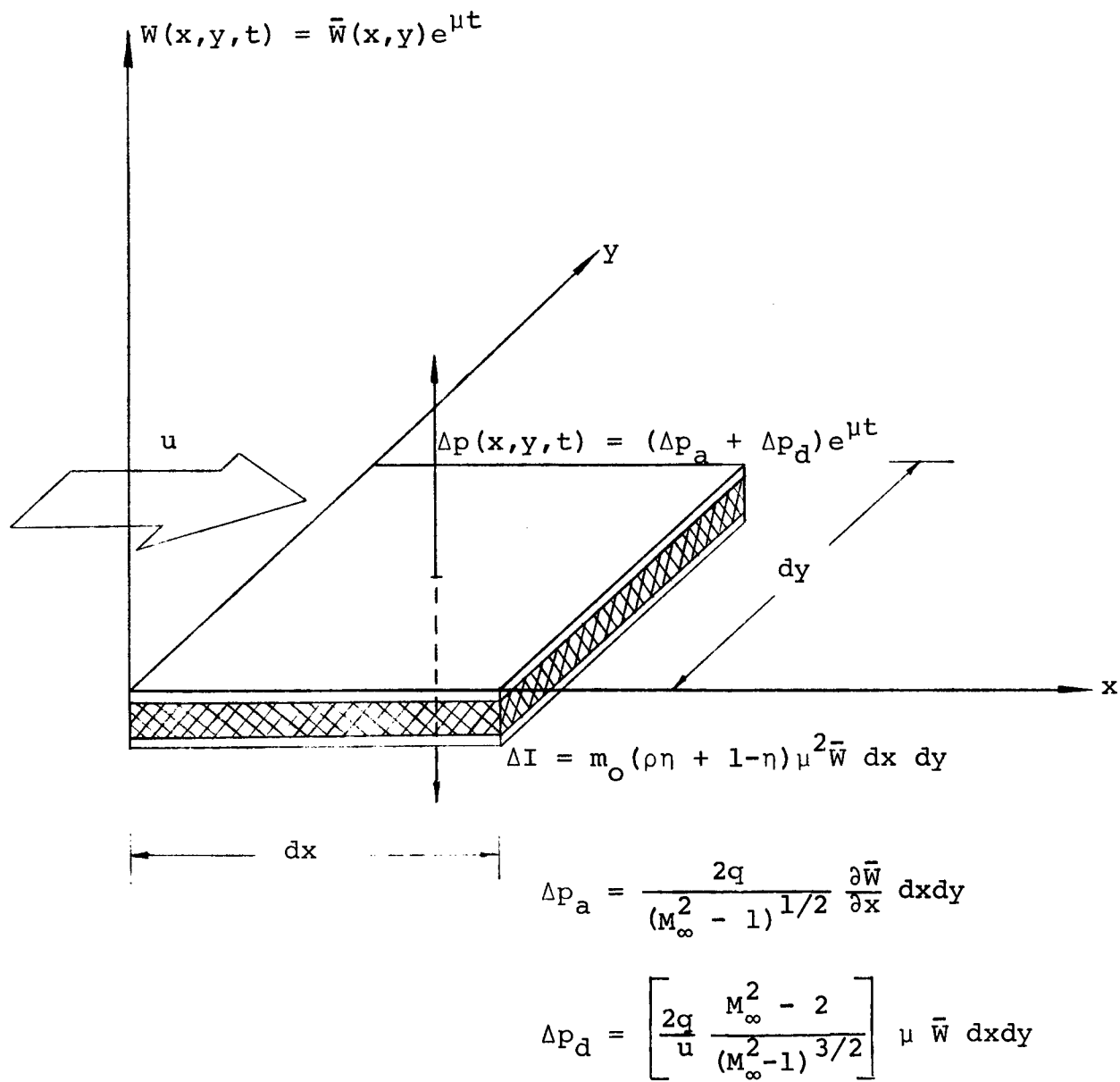
Fig. 4.1   Sandwich Panel in Supersonic Flow

Substitution of equation (4.2) into equation (4.1) allows the separation of the aerodynamic force into

$$\Delta p = [\Delta p_a + \Delta p_d] e^{\mu t} \qquad (4.4)$$

where

$$\Delta p_a = \frac{2q}{(M_\infty^2 - 1)^{1/2}} \frac{\partial \bar{W}}{\partial x} \, dxdy \qquad (4.5)$$

is the primary aerodynamic force, and

$$\Delta p_d = [\frac{2q}{u} \frac{M_\infty^2 - 2}{(M_\infty^2 - 1)^{3/2}}] \mu \, \bar{W} \, dxdy \qquad (4.6)$$

is the aerodynamic damping.

Δp_a is a function of $\frac{\partial \bar{W}}{\partial x}$; to include its effect into the matrix structural equation it is necessary to derive an aerodynamic matrix. This can be done by calculating the virtual work:

$$V_a = \iint \tilde{w} \, \Delta p_a = \frac{2q}{(M_\infty^2 - 1)^{1/2}} \iint \tilde{w} \frac{\partial \bar{W}}{\partial x} \, dxdy \qquad (4.7)$$

where $\tilde{w}(x,y)$ is the virtual displacement. In the finite element representation $\bar{W}(x,y)$ will usually have the following form:

$$\bar{W}(x,y) = \underset{\sim}{f}^T \underset{\approx}{T}_e \underset{\sim}{W}_e \qquad (4.8)$$

where $\underset{\sim}{f}$ is the vector of interpolation functions in x and y, $\underset{\approx}{T}_e$ is the transformation matrix that relates interpolation function coefficients to the element generalized displacements, and $\underset{\sim}{W}_e$ is the vector of element generalized displacements, which are element nodal point displacements.

Introducing equation (4.8) into equation (4.7) gives

$$V_a = \tilde{\underset{\sim}{W}}_e^T \; \underset{\approx}{A}_e \; \underset{\sim}{W}_e \qquad (4.9)$$

where

$$\underset{\approx}{A}_e = \underset{\sim}{T}^T \; \underset{\approx}{a}_e \; \underset{\sim}{T} \qquad (4.10)$$

and

$$\underset{\approx}{a}_e = \frac{2q}{(M_\infty^2 - 1)^{1/2}} \iint \underset{\sim}{f} \frac{\partial}{\partial x} (\underset{\sim}{f}^T) \; dxdy \qquad (4.11)$$

Here $\underset{\approx}{A}_e$ is the consistent aerodynamic matrix for an element.

Δp_d is a function of $\bar{W}(x,y)$. Its effect can be included by deriving an Aerodynamic Damping matrix, $\underset{\approx}{D}_e$. Following the same steps as above, we can obtain

$$\underset{\approx}{D}_e = \underset{\sim}{T}^T \; \underset{\approx}{d}_e \; \underset{\sim}{T} \qquad (4.12)$$

where

$$\underset{\approx}{d}_e = \frac{2q}{u} \frac{M_\infty^2 - 2}{(M_\infty^2 - 1)^{3/2}} \; \mu \iint \underset{\sim}{f}\underset{\sim}{f}^T dxdy \qquad (4.13)$$

It should be noted that the double integral in equation (4.13) is the same as the one required for the derivation of the element mass matrix for constant mass.

CHAPTER 5

CONSTRAINTS

In this chapter equations expressing the flutter, stress and thickness constraints in terms of the design variable vector ρ are derived.

5.1 Flutter Constraint

In order to express the flutter constraint in terms of ρ, it is necessary to write the equation of motion for the system. In the finite element approach this can be derived from the equation of motion for an element.

The element stiffness can be represented by the element stiffness matrix K_e which can be derived from strain energy. It will be a function of $\rho(x,y)$ which, in turn, can be expressed in terms of the elements of ρ.

The contribution, ΔI, of the inertia force (Figure 4.1),

$$\Delta I = m_o(\rho\eta + 1 - \eta)\mu^2 \bar{W} \, dxdy \qquad (5.1)$$

can be represented by the element mass matrix, M_e, which can be derived from either kinetic energy or from virtual work. It will also be a function of $\rho(x,y)$. References 15 and 16 can be mentioned as good sources for detailed derivations of mass and stiffness matrices.

The contributions of Δp_a, the primary aerodynamic

force (Equation 4.5), and Δp_d, the aerodynamic damping (Equation 4.6), can be represented by the element aerodynamic matrix, $\underset{\sim}{A}_e$, and element damping matrix, $\underset{\sim}{D}_e$, derivations of which have already been discussed in Chapter 4.

We can write the element equation of motion in terms of these matrices;

$$\underset{\sim}{F}_e = [\underset{\sim}{K}_e(\rho) + \mu^2 \underset{\sim}{M}_e(\rho) + \underset{\sim}{A}_e + \mu \underset{\sim}{D}_e]\underset{\sim}{W}_e \qquad (5.2)$$

where $\underset{\sim}{F}_e$ and $\underset{\sim}{W}_e$ are generalized forces and displacements respectively. They are related to the element nodal point degrees of freedom. We can rewrite equation (5.2) by using non-dimensional matrices $\underset{\sim}{\bar{K}}_e$, $\underset{\sim}{\bar{M}}_e$, $\underset{\sim}{\bar{A}}_e$ and $\underset{\sim}{\bar{D}}_e$;

$$\underset{\sim}{F}_e = [D_o \underset{\sim}{\bar{K}}_e(\rho) + m_o \ell^4 \mu^2 \underset{\sim}{\bar{M}}_e(\rho) + \frac{2q}{(M_\infty^2 -1)^{1/2}} \ell^3 \underset{\sim}{\bar{A}}_e$$

$$+ (\frac{2q}{u} \frac{M_\infty^2 - 2}{(M_\infty^2 - 1)^{1/2}}) \ell^4 \mu \underset{\sim}{\bar{D}}_e]\underset{\sim}{W}_e \qquad (5.3)$$

where ℓ is a convenient dimension used in scaling all finite element dimensions when deriving $\underset{\sim}{\bar{K}}_e$, $\underset{\sim}{\bar{M}}_e$, $\underset{\sim}{\bar{A}}_e$ and $\underset{\sim}{\bar{D}}_e$. It should be noted that $\underset{\sim}{\bar{D}}_e \equiv \underset{\sim}{\bar{M}}_e$ for $\rho = 1$. The matrix coefficients in equation (5.3) can be rearranged such that we have

$$\underset{\sim}{F}_e = D_o[\underset{\sim}{\bar{K}}_e(\rho) + (\frac{\mu}{\omega_o})^2 \underset{\sim}{\bar{M}}_e(\rho) + \alpha_o \underset{\sim}{\bar{A}}_e + g_{\alpha o}(\frac{\mu}{\omega o}) \underset{\sim}{\bar{D}}_e]\underset{\sim}{W}_e \qquad (5.4)$$

where

$$\omega_o = (\frac{D_o}{m_o \ell^4})^{1/2} \qquad (5.5)$$

is a convenient frequency scale factor

$$\alpha_O = \frac{2q}{(M_\infty^2 - 1)^{1/2}} \frac{\ell^3}{D_O} \tag{5.6}$$

is the non-dimensional dynamic pressure parameter, and

$$g_{\alpha O} = \frac{2q}{u} \frac{M_\infty^2 - 2}{(M_\infty^2 - 1)^{3/2}} \frac{1}{m_O \omega_O} \tag{5.7}$$

is the non-dimensional aerodynamic damping parameter.

The matrices $\bar{K}_e$, $\bar{M}_e$, $\bar{A}_e$ and $\bar{D}_e$, and vectors F_e and W_e can be assembled in the usual manner to form the system equations of motion. For no external forces, these equations can be written as

$$[K(\rho) + (\frac{\mu}{\omega_O})^2 M(\rho) + \alpha_O A + g_{\alpha O} (\frac{\mu}{\omega_O}) D]W = 0 \tag{5.8}$$

where W is the vector of system generalized displacements, which are related to the system nodal point degrees of freedom. Here $K(\rho)$ and $M(\rho)$ have the forms expressed in equations (3.11) and (3.12). It should be also noted that

$$D \equiv M_O \tag{5.9}$$

where M_O is the same as in equation (3.14).

For $g_{\alpha O} \neq 0$ Equation (5.8) can be recognized as a quadratic eigenvalue problem in $(\frac{\mu}{\omega_O})$. We can reduce this equation into a set of coupled first order equations by introducing

$$\lambda = \mu/\omega_O \tag{5.10}$$

$$V = \lambda W \tag{5.11}$$

and

$$U = \left\{ \begin{array}{c} V \\ W \end{array} \right\} \tag{5.12}$$

Using equations (5.10) and (5.11) in equation (5.8) we get

$$[K + \alpha_o A] \, W + g_{\alpha o} \, D \, V = -\lambda \, M \, V \tag{5.13}$$

and from equation (5.11) we have

$$V = \lambda \, W \tag{5.14}$$

or

$$-M^{-1} [K + \alpha_o A] \, W - g_{\alpha o} M^{-1} \, D \, V = \lambda \, V \tag{5.15}$$

and

$$V = \lambda \, W \tag{5.16}$$

Equations (5.15) and (5.16) can be rewritten by using U of equation (5.12);

$$C \, U = \lambda \, U \tag{5.17}$$

where

$$C = \left[\begin{array}{c|c} - g_{\alpha o} \, M^{-1} \, D & - M^{-1} [K + \alpha_o A] \\ \hline I & 0 \end{array} \right] \tag{5.18}$$

Equation (5.17) is a linear eigenvalue problem of size $2N \times 2N$ where N is the number of system degrees of freedom. For under damped systems (see ref. 24 for critical damping, under and over damped systems) equation (5.17) has N complex conjugate eigenvalues and corresponding N complex conjugate eigenvectors.

Recall that from (5.12), the last half of the eigenvectors (i.e., $\underset{\sim}{W}$) are modes shapes of motion, while the eigenvalues are the corresponding complex frequencies scaled by ω_o which is real and positive. In the complex frequency the real part is the damping part, the imaginary part is the frequency of oscillatory motion (equations 4.2 and 4.3). Complex mode shapes indicate that there are phase differences between different points of the structure in motion.

In Chapter 4 it has been pointed out that the border-line between stability and instability is defined by the real part of μ becoming zero. Since $\lambda = \mu/\omega_o$, the eigenvalues with positive real parts indicate aerodynamic instability, or flutter. This gives us the flutter constraint as;

$$C_f = \text{Real } (\lambda) \leq 0 \qquad (5.19)$$

where λ is any eigenvalue of the equation (5.17).

For a given damping parameter $g_{\alpha o}$ (it should be pointed out that any existing structural damping can be represented by adding a structural damping parameter to the aerodynamic damping parameter), and matrices $\underset{\sim}{K}$, $\underset{\sim}{M}$, $\underset{\sim}{D}$ and $\underset{\sim}{A}$, the flutter condition can be reached by increasing α_o from zero. The value of α_o that causes flutter is called α_{cr}. Since the final minimum-weight design is required to have the same flutter speed as the initial design we have the matrices $\underset{\sim}{K}_o$, $\underset{\sim}{M}_o$, $\underset{\sim}{D}$ and $\underset{\sim}{A}$ and the relationship

$$\underset{\sim}{M}_o \equiv \underset{\sim}{D}$$

which reduces the $\underset{\approx}{C}$ matrix to;

$$
\underset{\approx 0}{C} = \left[\begin{array}{c|c} -g_{\alpha 0} \, \underset{\approx}{I} & -\underset{\approx 0}{M}^{-1} \, [\underset{\approx 0}{K} + \alpha_0 \, \underset{\approx}{A}] \\ \hline \underset{\approx}{I} & \underset{\approx}{0} \end{array} \right] \tag{5.20}
$$

For $\alpha_0 = 0$, the eigenvalues of the $\underset{\approx 0}{C}$ matrix are simply the damped natural frequencies of the system. The real parts of all the eigenvalues will be $-g_{\alpha 0/2}$. As α_0 is increased; magnitudes of the imaginary parts of two complex conjugate pairs get closer (generally the lowest two frequency pairs are involved). The real parts remain the same until the imaginary parts become nearly equal (a required condition for energy transfer from one mode to the other). After that, the imaginary parts reamin equal but increase in magnitude, the damping of one pair increases as the damping of other pair decreases. At $\alpha_0 = \alpha_{cr}$ one pair will have $g_{\alpha 0}$, the other pair will have zero damping, which means the motion at flutter is pure harmonic. For $\alpha_0 > \alpha_{cr}$ the same trend continues; the real part of the flutter pair becomes positive (indicating instability), the other pair gets further damped, such that the equation

$$
\text{Real } (\lambda_1) + \text{Real } (\lambda_2) = -g_{\alpha 0} \tag{5.21}
$$

is always valid (see figure 5.1).

As α_0 is increased from zero to α_{cr} the real parts of all the other pairs remain at $-g_{\alpha 0/2}$; the imaginary parts change slightly.
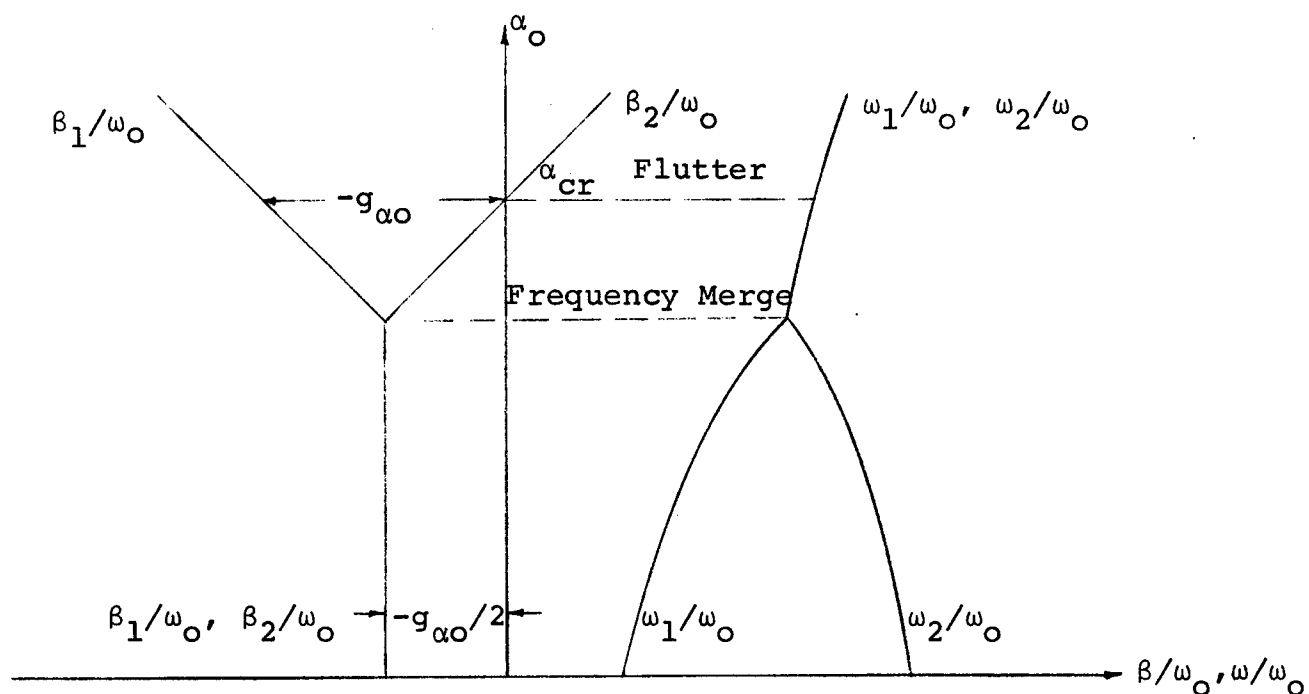
Fig. 5.1 The Real and Imaginary Parts of the Flutter Eigenvalues for Increasing α_o Values

The numerical determination of α_{cr} for the initial uniform design requires solving equation (5.17) for different α_o values with $\underset{\approx}{C}_o$ matrix of equation (5.20). Only the eigenvalues need to be calculated. By looking at the real parts of the eigenvalues it is possible to close in on α_{cr} using a bisection method.

During the optimization, in order to calculate the flutter constraint, matrix $\underset{\approx}{C}$ of equation (5.18) has to be formed. The aerodynamic matrix $\underset{\approx}{A}$ is already generated for the preliminary flutter analysis, the damping matrix $\underset{\approx}{D}$ is obtained by storing $\underset{\approx}{M}_o$. Matrices $\underset{\approx}{M}$ and $\underset{\approx}{K}$ need to be generated at every design step according to the equations (3.11), (3.12) and (3.15). In the problems considered here, the flutter constraint is kept active

at all design steps. The eigenvalues of the $\underset{\approx}{C}$ matrix are calculated by first reducing the matrix into a Hessenberg form (Ref. 18) and then applying QR iterations (Ref. 18) on the Hessenberg form. Among the eigenvalues the pair with the largest positive real part is chosen to be the flutter eigenvalue. For cases where all the eigenvalues have negative real parts, the pair with the smallest imaginary part in magnitude is chosen to be the flutter eigenvalue.

Other points of interest: a) During the optimization process, this way of expressing the flutter constraint enables us to detect flutter involving modes other than the original two modes. b) The flutter constraint is highly non-linear in ρ; the functional relationship of the matrix $\underset{\approx}{C}$ to ρ is through matrices $\underset{\approx}{K}$ and $\underset{\approx}{M}$ which are functions of ρ as expressed in equations (3.11) and (3.12).

5.2 Stress Constraint

Stress constraints are considered only for the specified uniform static loading conditions used as a first approximation to the aeroelastic loading.

Von Mises yield criterion is used to obtain stress constraint equations. For cover skin stresses where $\sigma_{zz} = \sigma_{zy} = \sigma_{zx} = 0$, the Von Mises yield criterion reduces to

$$\frac{1}{6} \left[(\sigma_x - \sigma_y)^2 + \sigma_y^2 + \sigma_x^2 + 6 \tau_{xy}^2 \right] = K^2 \tag{5.22}$$

or

$$\sigma_x^2 - \sigma_x \sigma_y + \sigma_y^2 + 3 \tau_{xy}^2 = 3K^2 \tag{5.23}$$

Here K is yield strength in pure shear or

$$K = \frac{1}{\sqrt{3}} \, (\sigma_{\text{yield pure tension}}) \qquad (5.24)$$

Using equation (3.1) for stresses we can write equation (5.23) in terms of curvatures W_{xx}, W_{yy} and W_{xy};

$$\frac{Ed}{2(1-\nu)^2}[(W_{xx} + \nu W_{yy})^2 - (W_{xx} + \nu W_{yy})(\nu W_{xx} + W_{yy})$$

$$+ (\nu W_{xx} + W_{yy})^2 + 3(1-\nu)^2 \, W_{xy}^2] = 3K^2 \qquad (5.25)$$

We can reduce equation (5.25) to a standard constraint form:

$$C_s = (\nu^2 - \nu + 1)(W_{xx}^2 + W_{yy}^2) - (\nu^2 - 4\nu + 1)W_{xx}W_{yy}$$

$$+ 3(1-\nu)^2 W_{xy}^2 - A \leq 0 \qquad (5.26)$$

where

$$A = \frac{6K^2(1-\nu)^2}{Ed} \qquad (5.27)$$

In the finite element analysis, for any point on the structure where a stress constraint is applied, curvatures W_{xx}, W_{yy} and W_{xy} can be calculated from the element nodal point displacement vector $\underset{\sim}{W}_e$. Using equation (4.8) we can write

$$\left\{ \begin{array}{c} W_{xx} \\ W_{yy} \\ W_{xy} \end{array} \right\}_{(x,y)} = \left[\begin{array}{c} \underset{\sim}{f}_{xx}^T \\ \underset{\sim}{f}_{yy}^T \\ \underset{\sim}{f}_{xy}^T \end{array} \right]_{(x,y)} \underset{\approx}{T}_e \underset{\sim}{W}_e \qquad (5.28)$$

W_e can be obtained from the system nodal point dis-
placement vector W, which in turn can be calculated from the
equation of equilibrium for static loading;

$$K(\rho)W = L \qquad (5.29)$$

where K is the system stiffness matrix and L is the load vector.

From equations (5.28) and (5.29) we get

$$\begin{Bmatrix} W_{xx} \\ W_{yy} \\ W_{xy} \end{Bmatrix}_{(x,y)} = \begin{bmatrix} f_{xx}^T \\ f_{yy}^T \\ f_{xy}^T \end{bmatrix}_{(x,y)} T_e X_e \; W \qquad (5.30)$$

where the rectangular matrix X_e picks up the vector W_e from W
i.e:

$$W_e = X_e \; W \qquad (5.31)$$

It should be noted that, in equation (5.30) only W
is a function of ρ (according to equation (5.29)). This fact
will be used in deriving the equations for stress gradients in
Chapter 7.

Stress constraints are only considered for the delta
wing problem. The load vector is calculated for a uniform load
distribution by condensing loads at the nodal points. The in-
tensity of the uniform load distribution is determined to pro-
duce yield for the uniform initial design. The constraints are
applied at the nodal points where transverse displacement

second derivatives are obtained directly from nodal point degrees of freedom (see Chapter 9 for details).

5.3 Thickness Constraint

Thickness constraints are applied on the elements of the design variable vector ρ. Since negative thickness is not physically possible, the condition $\rho_i \geq 0$ must be satisfied by all ρ_i at all stages of the optimization. The following is the standard constraint equation for the ith design variable

$$c_{ti} = \rho_{min} - \rho_i \leq 0; \quad 0 \leq \rho_{min} \leq 1 \qquad (5.32)$$

For cases where nodal point cover skin thickness parameters used as design variables, the above equation is sufficient to constrain thickness within elements since linear thickness distribution is assumed.

$\rho_{min} = 0.1$ is used in the optimization examples.

CHAPTER 6

GRADIENT PROJECTION ALGORITHM WITH MULTIPLE CONSTRAINTS

The basic ideas of the gradient projection method have been discussed in Section 2.4 in forming a comparison with the other popular algorithms. It was pointed out that the main problem with the algorithm was to stay on or within the convex constraints. The equations for the algorithm used in this study, where the minimization of the objective function and returning to violated constraints are performed in the same step, will now be derived.

We assume that at the design point ρ_q there are m_c critical constraints, which for convenience are considered to be numbered 1, 2, ..., m_c, i.e. constraints for which

$$C_j(\rho_q) \geq 0 \, , \, j = 1, \, ..., \, m_c \qquad (6.1)$$

we want to calculate a new design point ρ_{q+1} where;

$$F(\rho_{q+1}) < F(\rho_q) \qquad (6.2)$$

and

$$C_j(\rho_{q+1}) \leq 0 \, , \, j = 1, \, ..., \, m_c \qquad (6.3)$$

We define $\Delta\rho_q$ as the vector required to take us from ρ_q to ρ_{q+1}, i.e.

50

$$\varrho_{q+1} \;\; = \;\; \varrho_q \;\; + \;\; \Delta\varrho_q \qquad\qquad (6.4)$$

Using linear approximations for $F(\varrho)$ and $C_j(\varrho)$,
$j = 1, \ldots, m_c$ at ϱ_q, we can write ΔF, the change in the objective function, and ΔC_j, $j = 1, \ldots, m_c$, changes in the critical constraints along $\Delta\varrho_q$ as;

$$\Delta F \;\; = \;\; \Delta\varrho_q{}^T \; \nabla F(\varrho_q) \qquad\qquad (6.5)$$

$$\Delta C_j \;\; = \;\; \Delta\varrho_q{}^T \; \nabla C_j(\varrho_q), \;\; j = 1, \ldots, m_c \qquad (6.6)$$

We define a norm for $\Delta\varrho_q$;

$$R_q{}^2 \;\; = \;\; \Delta\varrho_q{}^T \; \Delta\varrho_q \qquad\qquad (6.7)$$

where R_q, the step size, is a pre-selected positive number for this particular design step (see Sections 8.3, 9.4, 9.5 and Chapter 10 for the selection of the step size).

Now the calculation of $\Delta\varrho_q$ can be cast as an optimization problem with equality constraints:

Maximize $\;\;(-\Delta F)$

Subject to $\;\; \Delta C_j \;\; = \;\; - C_j(\varrho_q), \;\; j = 1, \ldots, m_c$

and $\;\;\; R_q{}^2 \; - \; \Delta\varrho_q{}^T \; \Delta\varrho_q \;\; = \;\; 0$

so that the requirements in equations (6.2) and (6.3) are met to within a linear approximation.

Using Lagrange multipliers μ_j, $j = 1, \ldots, m_c$ and ν_R we define the following functional:

$$\Gamma = -\Delta\rho_q^T \, \nabla F(\rho_q) \quad + \quad \sum_j^{m_c} \mu_j \, [\Delta\rho_q^T \, \nabla C_j(\rho_q) \quad + \quad C_j(\rho_q)]$$

$$+ \quad \nu_R(R_q^2 - \Delta\rho_q^T \, \Delta\rho_q) \tag{6.8}$$

$\delta\Gamma \; = \; 0$ gives

$$-\nabla F(\rho_q) \quad + \quad \sum_j^{m_c} \mu_j \nabla C_j(\rho_q) - 2\nu_R\Delta\rho_q \; = \; 0 \tag{6.9}$$

$$\Delta\rho_q^T \, \nabla C_j(\rho_q) \quad + \quad C_j(\rho_q) \; = \; 0, \; j = 1, \, \ldots, \, m_c \tag{6.10}$$

$$R_q^2 \; - \; \Delta\rho_q^T \, \Delta\rho_q \; = \; 0 \tag{6.11}$$

We can rewrite equations (6.9) and (6.10) using matrix notations as follows:

$$-\nabla F(\rho_q) \quad + \quad G_q \, \mu - 2\nu_R\Delta\rho_q \; = \; 0 \tag{6.12}$$

$$G_q^T \, \Delta\rho_q \quad + \quad C_q \; = \; 0 \tag{6.13}$$

where

$$G_q \; = \; [\nabla C_1(\rho_q), \; \nabla C_2(\rho_q), \; \ldots, \; \nabla C_{mc}(\rho_q)] \tag{6.14}$$

$$\mu^T \; = \; [\mu_1, \; \mu_2, \; \ldots, \; \mu_{mc}] \tag{6.15}$$

$$C_q^T \; = \; [C_1(\rho_q), \; C_2(\rho_q), \; \ldots, \; C_{mc}(\rho_q)] \tag{6.16}$$

From equation (6.12) we obtain

$$\Delta\rho_q \; = \; \frac{1}{2\nu_R} \, [-\nabla F(\rho_q) \quad + \quad G_q \, \mu] \tag{6.17}$$

which can be substituted in equation (6.13) to give

$$\frac{1}{2\nu_R} \underset{\approx}{G}_q^T [-\nabla F(\underset{\sim}{\rho}_q) + \underset{\approx}{G}_q \underset{\sim}{\mu}] + \underset{\sim}{C}_q = \underset{\sim}{0} \qquad (6.18)$$

or

$$\underset{\approx}{G}_q^T \underset{\approx}{G}_q \underset{\sim}{\mu} = -2\nu_R \underset{\sim}{C}_q + \underset{\approx}{G}_q^T \nabla F(\underset{\sim}{\rho}_q) \qquad (6.19)$$

Assuming columns of $\underset{\approx}{G}_q$ are linearly independent, the matrix $[\underset{\approx}{G}_q^T \underset{\approx}{G}_q]$ is nonsingular and can be inverted. Thus equation (6.19) yields:

$$\underset{\sim}{\mu} = -2\nu_R [\underset{\approx}{G}_q^T \underset{\approx}{G}_q]^{-1} \underset{\sim}{C}_q + [\underset{\approx}{G}_q^T \underset{\approx}{G}_q]^{-1} \underset{\approx}{G}_q^T \nabla F(\underset{\sim}{\rho}_q) \qquad (6.20)$$

Using this expression for μ in equation (6.17) we get

$$\Delta\underset{\sim}{\rho}_q = \frac{1}{2\nu_R} [\underset{\approx}{G}_q [\underset{\approx}{G}_q^T \underset{\approx}{G}_q]^{-1} \underset{\approx}{G}_q^T - \underset{\approx}{I}] \nabla F(\underset{\sim}{\rho}_q)$$

$$-\underset{\approx}{G}_q [\underset{\approx}{G}_q^T \underset{\approx}{G}_q]^{-1} \underset{\sim}{C}_q \qquad (6.21)$$

ν_R can be calculated by using equation (6.11). For simplicity we can write

$$\Delta\underset{\sim}{\rho}_q = \frac{1}{\nu_R} \underset{\sim}{e} + \underset{\sim}{f} \qquad (6.22)$$

where $\underset{\sim}{e} = \frac{1}{2} [\underset{\approx}{G}_q [\underset{\approx}{G}_q^T \underset{\approx}{G}_q]^{-1} \underset{\approx}{G}_q^T - \underset{\approx}{I}] \nabla F(\underset{\sim}{\rho}_q) \qquad (6.23)$

$$\underset{\sim}{f} = -\underset{\approx}{G}_q [\underset{\approx}{G}_q^T \underset{\approx}{G}_q]^{-1} \underset{\sim}{C}_q \qquad (6.24)$$

Now equation (6.11) can be written as

$$R_q^2 - (\frac{1}{\nu_R} \underset{\sim}{e}^T + \underset{\sim}{f}^T)(\frac{1}{\nu_R} \underset{\sim}{e} + \underset{\sim}{f}) = 0 \qquad (6.25)$$

54

which reduces to

$$[R_q^2 - c]\nu_R^2 - b\nu_R - a = 0 \tag{6.26}$$

where $\quad a = \underset{\sim}{e}^T\underset{\sim}{e}$ (6.27)

$$b = 2\underset{\sim}{e}^T\underset{\sim}{f} \tag{6.28}$$

$$c = \underset{\sim}{f}^T\underset{\sim}{f} \tag{6.29}$$

Using expressions for $\underset{\sim}{e}$ and $\underset{\sim}{f}$ we get

$$b = \nabla F(\underset{\sim}{\rho}_q)^T [\underset{\sim}{G}_q[\underset{\sim}{G}_q^T\underset{\sim}{G}_q]^{-1} \underset{\sim}{G}_q^T - \underset{\sim}{I}] [-\underset{\sim}{G}_q[\underset{\sim}{G}_q^T\underset{\sim}{G}_q]^{-1}]\underset{\sim}{C}_q \tag{6.30}$$

or

$$b = \nabla F(\underset{\sim}{\rho}_q)^T [\underset{\sim}{0}]\underset{\sim}{C}_q = 0 \tag{6.31}$$

which means that $\underset{\sim}{e}$ is orthogonal to $\underset{\sim}{f}$. Using this information in equation (6.26) we get

$$\nu_R = \left(\frac{a}{R_q^2 - c}\right)^{1/2} \tag{6.32}$$

and finally $\Delta\underset{\sim}{\rho}_q$ becomes

$$\Delta\underset{\sim}{\rho}_q = \left(\frac{R_q^2 - c}{a}\right)^{1/2} \underset{\sim}{e} + \underset{\sim}{f} \tag{6.33}$$

where all the terms have already been defined.

It should be noted that

$$2\underset{\sim}{e} \equiv \underset{\sim}{S}_q \tag{6.34}$$

where $\underset{\sim}{S}_q$ has been defined in equation (2.13). So we have the design change vector $\Delta\underset{\sim}{\rho}_q$ as being composed of two orthogonal

vectors, $\underset{\sim}{e}' = (\frac{R_q^2-c}{a})^{1/2} \underset{\sim}{e}$, and $\underset{\sim}{f}$, where $\underset{\sim}{e}'$ is in the projected gradient direction along which the changes in constraints are zero and $\underset{\sim}{f}$ is in an orthogonal direction along which the changes in constraints are equal to the constraint violations at $\underset{\sim}{\rho}_q$ in magnitude with opposite signs, that is

$$\underset{\approx}{G}_q^T \underset{\approx}{e}' = \underset{\sim}{0} \tag{6.35}$$

and

$$\underset{\approx}{G}_q^T \underset{\sim}{f} = -\underset{\sim}{C}_q \tag{6.36}$$

For cases where the norm of the vector $\underset{\sim}{f}$ (i.e. c) is bigger than R_q^2, the equation (6.33) cannot be used for the calculation of $\Delta\underset{\sim}{\rho}_q$, since the term inside the square root becomes negative. For such cases the following relationship is used to calculate $\Delta\underset{\sim}{\rho}_q$:

$$\Delta\underset{\sim}{\rho}_q = \frac{R_q}{\sqrt{c}} \underset{\sim}{f} \tag{6.37}$$

where only the component required to come back to the violated constraints is employed and the relationship

$$R_q^2 = \Delta\underset{\sim}{\rho}_q^T \Delta\underset{\sim}{\rho}_q$$

is still valid.

Figures 6.1 and 6.2 illustrate the design steps given by equations 6.33 and 6.37 on a two-dimensional design space.

For the example problems presented in Chapters 8 and
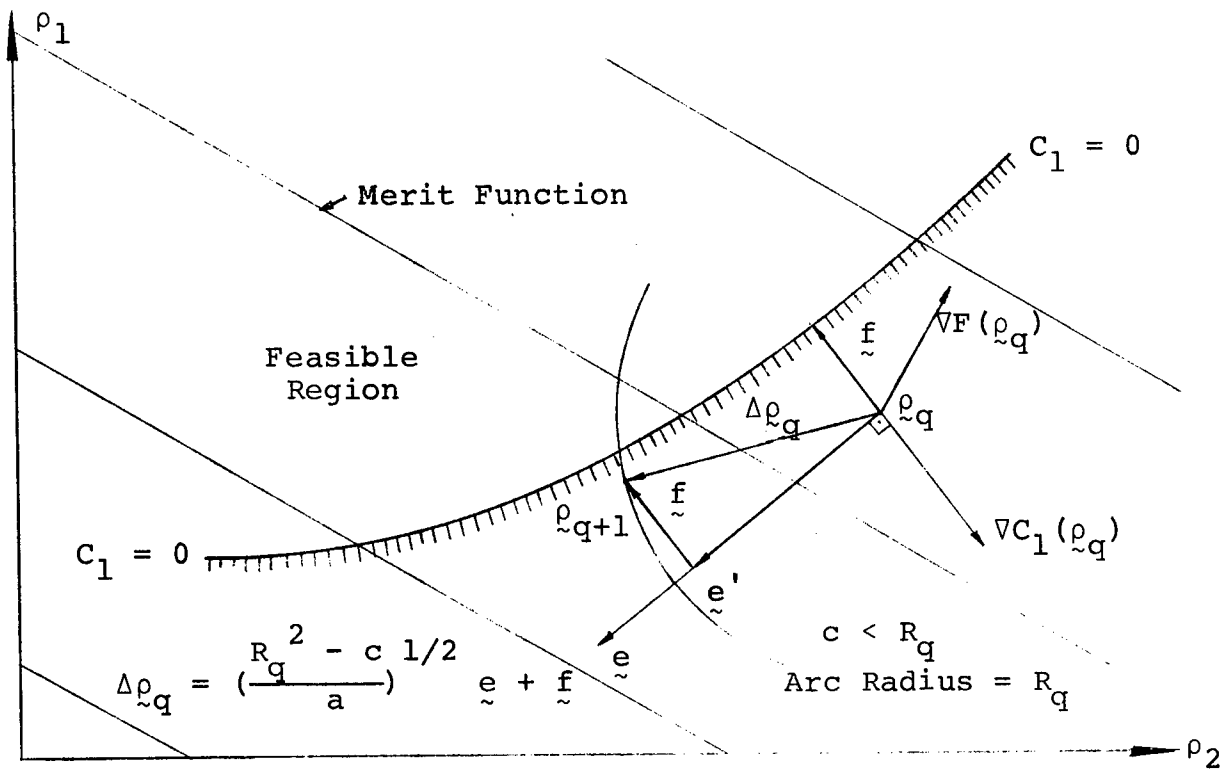
Fig. 6.1 Primary Design Change Vector

$$\Delta \rho_q = \left(\frac{R_q^2 - c}{a} \right)^{1/2} e + f$$

$$c < R_q$$
Arc Radius $= R_q$
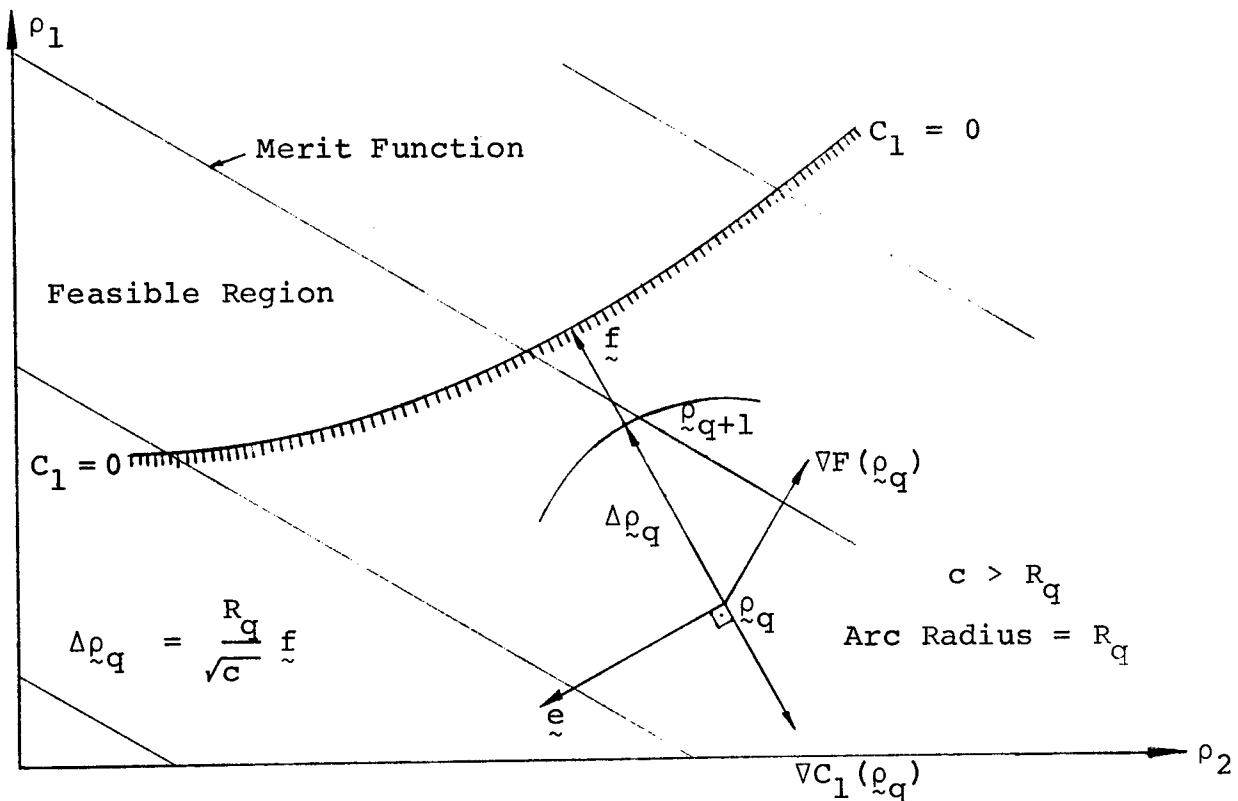
Fig. 6.2 Secondary Design Change Vector

$$\Delta \rho_q = \frac{R_q}{\sqrt{c}} f$$

$$c > R_q$$
Arc Radius $= R_q$

9, the flutter constraint is kept active at all design steps. Since α_o is determined to produce flutter for the initial uniform design, ρ_o is on the flutter constraint. For design steps where $C_f < 0$, C_f is set equal to zero when constructing the vector C_q.

For the delta-wing problem the stress constraints are considered to become active when the condition $C_s \geq -\epsilon$ is satisfied for any nodal point. Here ϵ is a positive parameter which is made successively smaller as the optimum design is approached (see section 9.4). For cases where $-\epsilon \leq C_s \leq 0$, C_s is set equal to zero when constructing the vector C_q.

Thickness constraints become active when there is a violation (i.e. $\rho_i \leq \rho_{min}$).

It should be noted that the derivation of $\Delta\rho_q$ as outlined above does not include any provision for stress or thickness constraints which are not active for ρ_q but becomes active for ρ_{q+1}. This fact created some problems in the earlier runs for the delta wing optimization; mainly a stress or thickness constraint which was not active at a particular ρ_q became severely violated at ρ_{q+1} and it took several iterations to bring the design back into the feasible region during which the flutter constraint had to be calculated several times. Since the calculation of the flutter constraint is the main time-consuming computational effort, the following procedure is used to reduce the computation time: After calculating ρ_{q+1} the stress and thickness constraints were checked, if there was a new stress

or thickness constraint violation, a parameter $\alpha_R (0 \le \alpha_R \le 1)$ is calculated using linear interpolation to scale $\Delta\rho_q$ so that

$$\bar{\rho}_{q+1} = \rho_q + \alpha_R \Delta\rho_q \qquad (6.38)$$

is in the feasible region (see Figure 6.3 for a 2-dimensional illustration). The procedure proved to be very successful.

Other points of interest about the algorithm and its application to the aeroelastic-stress optimization are:

1) The method maximizes $(-\Delta F)$ subject to returning back to the feasible region, but there is no guarantee that the condition $F(\rho_{q+1}) < F(\rho_q)$ will be satisfied, especially for cases where $\Delta\rho_q$ is required primarily for coming back to constraints. However the application of the algorithm showed that this fact does not create problems in practice.

2) Considering the fact that the structural weight is a linear function of the design variables, equation (6.5) is an exact expression, however the equations (6.6) are exact only for linear constraints (e.g. thickness constraints) and are approximate for non-linear constraints (e.g. flutter and stress constraints). Their accuracy for non-linear constraints is a function of R_q, the step size, and the curvature of the constraints.

3) Although the algorithm is capable of handling constraint violations, getting far away from the feasible region would be undesirable since the gradient information obtained at such points would be misleading.
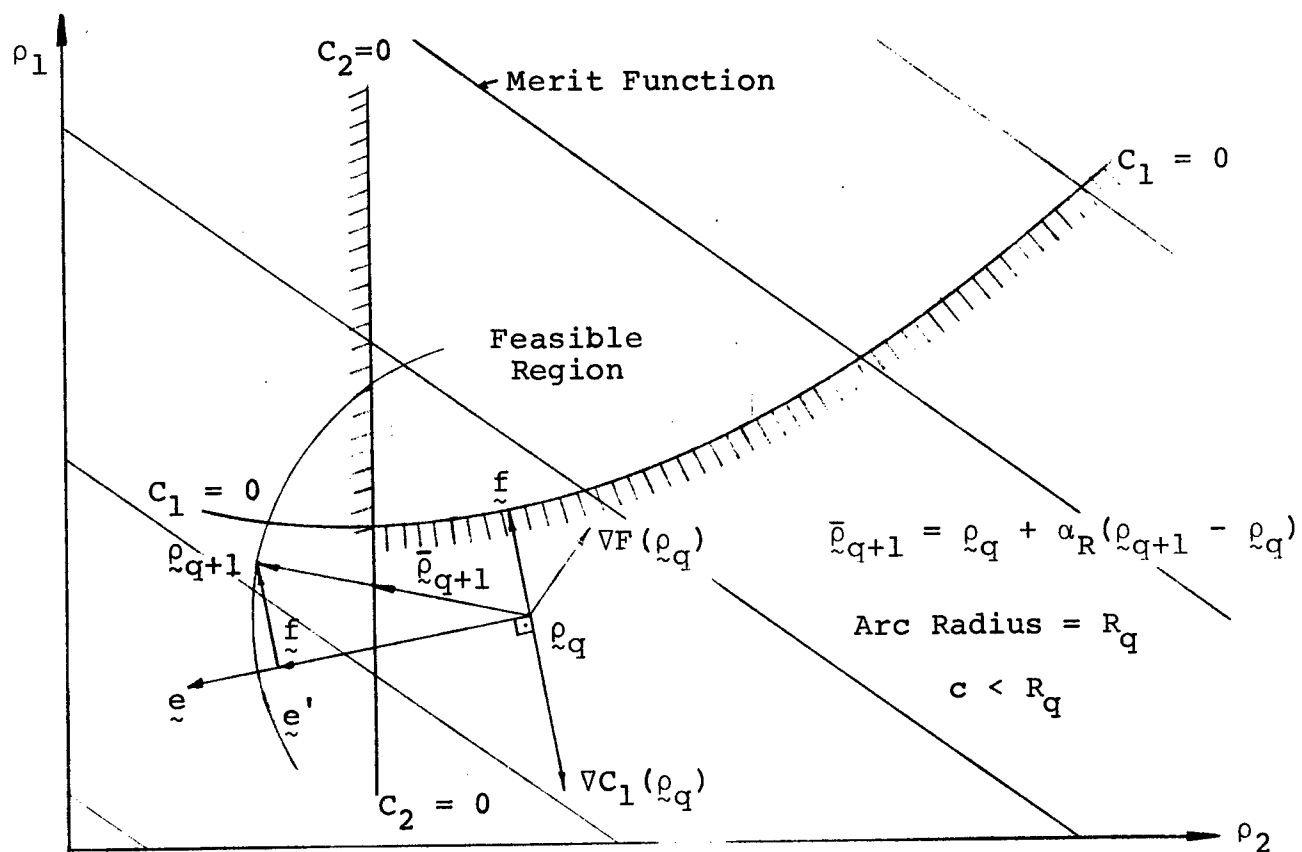
Fig. 6.3   Reduction in the Design Change Vector Due to a
New Constraint Violation

4) From 2) and 3) it becomes apparent that the choice of R_q is extremely important. A very large value for R_q could make the algorithm unstable. On the other hand a very small value for R_q would mean an increased number of iterations for convergence.

5) The change in the merit function from one design to the next, is used as the convergence criteria for the applications (see results in Chapters 8 and 9).

6) For a single constraint the above equations can be simplified by replacing G_q with $\nabla C(\rho_q)$. Equation (6.21) becomes

$$\Delta \rho_q = \frac{1}{2 \nu_R} [\frac{A}{B} \nabla C(\rho_q) - \nabla F(\rho_q)] - \frac{C_q}{B} \nabla C(\rho_q) \tag{6.39}$$

where

$$A = \nabla C(\rho_q)^T \nabla F(\rho_q)$$

$$B = \nabla C(\rho_q)^T \nabla C(\rho_q)$$

ν_R can be calculated using equation (6.32). Employing equation (6.39) we now have

$$a = \frac{1}{4} [D - \frac{A^2}{B}] \tag{6.40}$$

$$c = \frac{C_q^2}{B} \tag{6.41}$$

where

$$D = \nabla F(\rho_q)^T \nabla F(\rho_q)$$

For a given ρ_q find the critical constraints, calculate G_q and C_q

Form $A = G_q^T G_q$

Invert A

Form $C = B G_q^T - I$

Form $B = G_q A^{-1}$

Calculate

$e = \frac{1}{2} C \nabla F(\rho_q)^*$

$f = - B C_q$

$a = e^T e$ and $c = f^T f$

R_q is given

Is $R_q^2 > c$

Yes

No

Replace

$\rho_q = \rho_{q+1}$ (or $\bar{\rho}_{q+1}$)

Calculate

$\Delta \rho_q = \left(\frac{R_q^2 - c}{a}\right)^{1/2} e + f$

Calculate

$\Delta \rho_q = \frac{R_q}{\sqrt{c}} f$

No

Check Convergence

No

Check for new Constraint Violations

Calculate

$\rho_{q+1} = \rho_q + \Delta \rho_q$

Yes

Out

Yes

Calculate α_R

*$\nabla F(\rho_q)$ is constant and need to be calculated only once

Calculate

$\bar{\rho}_{q+1} = \rho_q + \alpha_R \Delta \rho_q$

Fig. 6.4 Flow Chart for the Gradient Projection Algorithm

These equations yield

$$\frac{1}{2\nu_R} = (\frac{BR_q^2 - C_q^2}{BD - A^2})^{1/2} \tag{6.42}$$

and equation (6.39) becomes

$$\Delta\rho_q = (\frac{BR_q^2 - C_q^2}{BD - A^2})^{1/2} [\frac{A}{B} \nabla C(\rho_q) - \nabla F(\rho_q)] - \frac{C_q}{B} \nabla C(\rho_q) \tag{6.43}$$

Figure 6.4 shows a simplified flow chart of the algorithm based on the above developments.

CHAPTER 7

GRADIENT CALCULATIONS

The gradient projection algorithm developed in Chapter 6 requires the calculation of the gradients of the objective function and the gradients of the critical constraints. In this chapter the analytical expressions used for these calculations are derived.

7.1 Gradients of the Objective Function

It has already been indicated that the objective function used in this study is linear in the design variables. This means that the gradient vector $\nabla F(\underset{\sim}{\rho}_q)$ is a constant vector everywhere in the design space. It needs to be calculated only once and stored. The expressions for objective functions and the gradients are given in the text whenever the need arises (Chapters 8 and 9).

7.2 Gradients of the Flutter Constraint

The flutter constraint was given in equation (5.19) as

$$C_f = \text{Real } (\lambda) \leq 0$$

where λ was determined by the complex eigenvalue problem (5.17). In equation (5.17) the coefficient matrix $\underset{\approx}{C}$ contains the mass and stiffness matrices $\underset{\approx}{M}$ and $\underset{\approx}{K}$, which are functions of $\underset{\sim}{\rho}$. For the gradient calculations we need the terms $\frac{\partial}{\partial \rho_i}[\text{Real } (\lambda)]$

expressed analytically.

Equations derived by Rogers (Ref. 11, similar equations were given by Van de Vooren in Ref. 12) are employed to achieve this. For the general eigenvalue problems with real or complex eigenvalues and eigenvectors

$$\alpha_i \underset{\approx}{A}(x) \underset{\sim}{\phi}_i + \underset{\approx}{B}(x) \underset{\sim}{\phi}_i = \underset{\sim}{0} \tag{7.1}$$

and

$$\alpha_i \underset{\approx}{A}^T(x) \underset{\sim}{\theta}_i + \underset{\approx}{B}^T(x) \underset{\sim}{\theta}_i = \underset{\sim}{0} \tag{7.2}$$

where the right and left hand eigenvectors are normalized such that:

$$\underset{\sim}{\theta}_i^T \underset{\approx}{A} \underset{\sim}{\phi}_i = 1 \tag{7.3}$$

Rogers (11) gives the following expression

$$\alpha_{i,x} = - \underset{\sim}{\theta}_i^T [\alpha_i \underset{\approx}{A}_{,x} + \underset{\approx}{B}_{,x}] \underset{\sim}{\phi}_i \tag{7.4}$$

where ,x means differentiation with respect to x.

The flutter equation (5.17) can be put into the forms of equations (7.1) and (7.2). We start from equations (5.13) and (5.14) and rewrite them as:

$$g_{\alpha 0} \underset{\approx}{D} \underset{\sim}{V} + [\underset{\approx}{K} + \alpha_0 \underset{\approx}{A}] \underset{\sim}{W} = - \lambda \underset{\approx}{M} \underset{\sim}{V} \tag{7.5}$$

$$- \underset{\approx}{M} \underset{\sim}{V} = - \lambda \underset{\approx}{M} \underset{\sim}{W} \tag{7.6}$$

which can be reduced to

$$\lambda \begin{bmatrix} \underset{\approx}{M} & \vdots & \underset{\approx}{O} \\ \cdots & \vdots & \cdots \\ \underset{\approx}{O} & \vdots & \underset{\approx}{M} \end{bmatrix} \underset{\sim}{U} + \begin{bmatrix} g_{\alpha 0} \underset{\approx}{D} & \vdots & \underset{\approx}{K} + \alpha_0 \underset{\approx}{A} \\ \cdots & \vdots & \cdots \\ -\underset{\approx}{M} & \vdots & \underset{\approx}{O} \end{bmatrix} \underset{\sim}{U} = \underset{\sim}{0} \tag{7.7}$$

where $\underset{\sim}{U} = \left\{ \begin{array}{c} \underset{\sim}{V} \\ \underset{\sim}{W} \end{array} \right\}$ as defined in equation (5.12).

Equation (7.7) is of the same form as equation (7.1). By transposing equation (7.7) we get

$$\lambda \left[\begin{array}{c|c} \underset{\approx}{M} & \underset{\approx}{O} \\ \hline \underset{\approx}{O} & \underset{\approx}{M} \end{array} \right] \underset{\sim}{\bar{U}} + \left[\begin{array}{c|c} g_{\alpha O} \underset{\approx}{D} & -\underset{\approx}{M} \\ \hline \underset{\approx}{K} + \alpha_O \underset{\approx}{A}^T & \underset{\approx}{O} \end{array} \right] \underset{\sim}{\bar{U}} = \underset{\sim}{O} \qquad (7.8)$$

which is analogous to equation (7.2). Here the symmetry property of matrices $\underset{\approx}{M}$, $\underset{\approx}{D}$ and $\underset{\approx}{K}$ are used. $\underset{\approx}{A}$ is not symmetrical. Equation (7.8) can be reduced to the form

$$\underset{\approx}{\bar{C}} \, \underset{\sim}{\bar{U}} = \lambda \, \underset{\sim}{\bar{U}} \qquad (7.9)$$

where

$$\underset{\approx}{\bar{C}} = \left[\begin{array}{c|c} -g_{\alpha O} \underset{\approx}{M}^{-1} \underset{\approx}{D} & \underset{\approx}{I} \\ \hline -\underset{\approx}{M}^{-1} [\underset{\approx}{K} + \alpha_O \underset{\sim}{A}^T] & \underset{\approx}{O} \end{array} \right] \qquad (7.10)$$

from which the left hand eigenvectors, $\underset{\sim}{\bar{U}}$, can be calculated using the eigenvalues of $\underset{\approx}{C}$ matrix.

Similar to equation (7.3) we can write

$$\underset{\sim}{\bar{U}}^T \left[\begin{array}{c|c} \underset{\approx}{M} & \underset{\approx}{O} \\ \hline \underset{\approx}{O} & \underset{\approx}{M} \end{array} \right] \underset{\sim}{U} = 1 \qquad (7.11)$$

by which the left and right hand eigenvectors can be normalized.

Using the analogy of equation (7.4) and remembering that only $\underset{\approx}{M}$ and $\underset{\approx}{K}$ are functions of $\underset{\sim}{\rho}$, we get

$$\lambda_{i,\rho_j} = - \underset{\sim i}{\bar{U}}^T \left\{ \lambda_i \left[\begin{array}{c|c} \underset{\approx}{M}_{,\rho_j} & \underset{\approx}{O} \\ \hline \underset{\approx}{O} & \underset{\approx}{M}_{,\rho_j} \end{array} \right] \left[\begin{array}{c|c} \underset{\approx}{O} & \underset{\approx}{K}_{,\rho_j} \\ \hline -\underset{\approx}{M}_{,\rho_j} & \underset{\approx}{O} \end{array} \right] \right\} \underset{\sim i}{U}$$

$$(7.12)$$

substituting

$$\lambda_i = (\beta_i + i\,\omega_i)/\omega_o = \bar{\beta}_i + i\,\omega_i \qquad (7.13)$$

reduces equation (7.12) to

$$\bar{\beta}_{i,\rho_j} + i\omega_{i,\rho_j} = - \underset{\sim i}{\bar{U}}^T \left\{ \left[\begin{array}{c|c} \bar{\beta}_i \underset{\approx}{M}_{,\rho_j} & \underset{\approx}{K}_{,\rho_j} \\ \hline -\underset{\approx}{M}_{,\rho_j} & \bar{\beta}_i \underset{\approx}{M}_{,\rho_j} \end{array} \right] + i \left[\begin{array}{c|c} \bar{\omega}_i \underset{\approx}{M}_{,\rho_j} & \underset{\approx}{O} \\ \hline \underset{\approx}{O} & \bar{\omega}_i \underset{\approx}{M}_{,\rho_j} \end{array} \right] \right\} \underset{\sim i}{U}$$

$$(7.14)$$

When right hand and left hand eigenvectors $\underset{\sim}{U}$ and $\underset{\sim}{\bar{U}}$ are

calculated from equations (5.17) and (7.9) and normalized

according to equation (7.11), the real part of the equation

(7.14) will give us the required gradients.

Using equations (3.11) and (3.12) for $\underset{\approx}{K}$ and $\underset{\approx}{M}$, we can

write:

$$\underset{\approx}{K}_{,\rho_j} = \underset{\approx j}{K} \qquad (7.15)$$

and

$$\underset{\approx}{M}_{,\rho_j} = \underset{\approx j}{M} \qquad (7.16)$$

where $\underset{\approx j}{K}$ and $\underset{\approx j}{M}$ are the individual contributions of the design

variable ρ_j to the stiffness and mass matrices respectively. These matrices can be assembled from element mass and stiffness matrices in a process similar to assembling system mass and stiffness matrices. This time, however, only the elements associated with a particular ρ_j will contribute.

It should be noted that $\bar{\underset{\approx}{C}}$ is not $\underset{\approx}{C}^T$, since

$$\underset{\approx}{C}^T = \left[\begin{array}{c|c} -g_{\alpha O} \underset{\approx}{M}^{-1} \underset{\approx}{D} & \underset{\approx}{I} \\ \hline -[\underset{\approx}{K} + \alpha_O \underset{\approx}{A}^T]\underset{\approx}{M}^{-1} & \underset{\approx}{O} \end{array} \right] \tag{7.17}$$

which is different. Even though $\underset{\approx}{C}^T$ will have the same eigenvalues as $\bar{\underset{\approx}{C}}$, its eigenvectors are different from those of $\bar{\underset{\approx}{C}}$.

In practice the right and left hand eigenvectors are calculated by employing inverse power iteration (Ref. 18) using flutter eigenvalue as the spectrum shift.

7.3 Gradients of the Stress Constraints

Differentiation of equation (5.26) with respect to ρ_j yields

$$\begin{aligned} C_{s,\rho_j} = {} & 2(\nu^2 - \nu + 1)(W_{xx}W_{xx,\rho_j} + W_{yy}W_{yy,\rho_j}) \\ & - (\nu^2 - 4\nu + 1)(W_{xx}W_{yy,\rho_j} + W_{yy}W_{xx,\rho_j}) \\ & + 6(1 - \nu)^2 W_{xy}W_{xy,\rho_j} \end{aligned} \tag{7.18}$$

The gradients of the curvatures can be obtained from the gradients of the element nodal point displacement vector;

similar to equation 5.28 we can write

$$
\left\{
\begin{array}{c}
W_{xx,\rho_j} \\
W_{yy,\rho_j} \\
W_{xy,\rho_j}
\end{array}
\right\}_{(x,y)}
=
\left[
\begin{array}{c}
\underset{\sim}{f}{}^T_{xx} \\
\underset{\sim}{f}{}^T_{yy} \\
\underset{\sim}{f}{}^T_{xy}
\end{array}
\right]_{(x,y)}
\underset{\approx}{T}_e \underset{\sim}{W}_{e,\rho_j}
\qquad (7.19)
$$

Here $\underset{\sim}{W}_{e,\rho_j}$ can be obtained from the gradients of the system nodal point displacements vector $\underset{\sim}{W}$. These in turn can be calculated from the equation of equilibrium (Eq. 5.29):

$$
\underset{\approx}{K}(\underset{\sim}{\rho})\underset{\sim}{W} = \underset{\sim}{L}
\qquad (7.20)
$$

$$
\underset{\approx}{K}_{,\rho_j}\underset{\sim}{W} + \underset{\approx}{K}(\underset{\sim}{\rho})\underset{\sim}{W}_{,\rho_j} = \underset{\sim}{L}_{,\rho_j} = \underset{\sim}{0}
\qquad (7.21)
$$

or

$$
\underset{\approx}{K}(\underset{\sim}{\rho})\underset{\sim}{W}_{,\rho_j} = - \underset{\approx}{K}_{,\rho_j}\underset{\sim}{W}
\qquad (7.22)
$$

$\underset{\sim}{W}$ can be solved from equation (7.20) and $\underset{\sim}{W}_{,\rho_j}$ can be solved from equation (7.22). Using the rectangular matrix $\underset{\approx}{X}_e$ defined in section 5.2, we get;

$$
\left\{
\begin{array}{c}
W_{xx,\rho_j} \\
W_{yy,\rho_j} \\
W_{xy,\rho_j}
\end{array}
\right\}_{(x,y)}
= -
\left[
\begin{array}{c}
\underset{\sim}{f}{}^T_{xx} \\
\underset{\sim}{f}{}^T_{yy} \\
\underset{\sim}{f}{}^T_{xy}
\end{array}
\right]_{(x,y)}
\underset{\approx}{T}_e \underset{\approx}{X}_e \underset{\sim}{W}_{,\rho_j}
\qquad (7.23)
$$

The calculation of $\underset{\approx}{K}_{,\rho_j}$ was discussed in connection with the flutter constraint gradients.

7.4 Gradients of the Thickness Constraints

From equation (5.32) we get

$$C_{ti,\rho_j} = -\delta_{ij} \qquad (7.24)$$

where δ_{ij} is the Kronecker's delta.

CHAPTER 8

SEMI-INFINITE PANEL OPTIMIZATION

The problem of semi-infinite panel optimization with flutter constraint is considered first since there are control theory and finite element solutions to this problem available for comparison in literature (references 7 and 8). First, the computer routines to determine α_{cr} are developed, then the routines to calculate the flutter gradients based on equations of section 7.2 are coded. The results are checked against gradients calculated numerically. Once these routines are established, a gradient projection routine is applied to optimize the panel with only a flutter constraint. This routine had already been developed and applied to problems involving simple algebraic merit functions of a few variables with non-linear constraints whose gradients were easy to evaluate. Different finite element combinations are tried in order to find the best representation from the point of view of optimization. Later, the multiple-constraint gradient projection routine, that was developed primarily for the delta wing problem is applied to the best finite element representation to study the effect of damping on optimization.

8.1 Structural Model

The following assumptions define the structural model:
1) The panel has length ℓ, is simply supported at

both ends in the direction of the air flow and is free of in-plane forces.

2) The panel is of infinite dimension in the direction perpendicular to the air flow, i.e. the problem is one dimensional.

3) The panel is of sandwich construction.

4) The effect of any air below the panel can be neglected.

Figure 8.1 shows the cross section of the structural model.
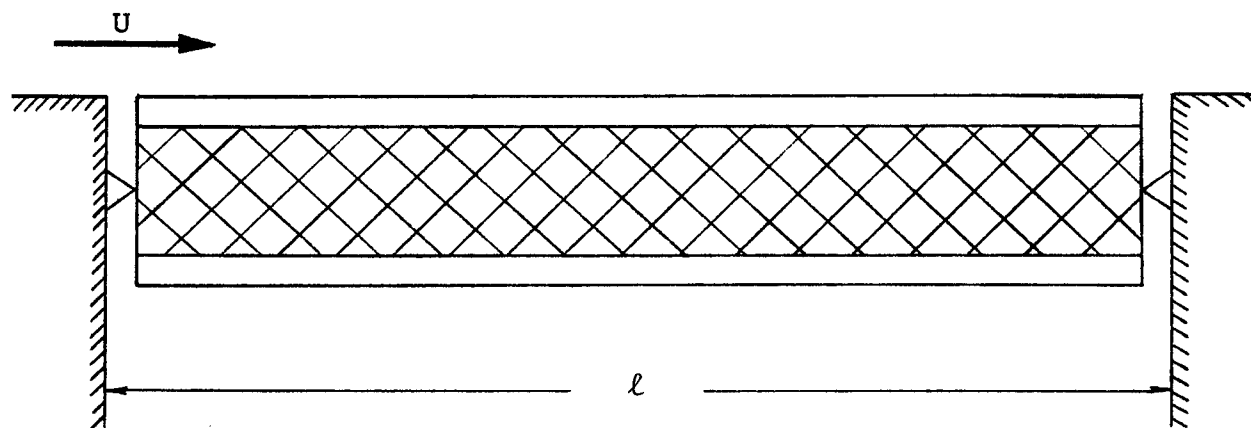
Fig. 8.1 Semi-Infinite Simply Supported Sandwich Panel in Supersonic Flow

8.2 Analysis to Determine α_{cr}

Five constant thickness beam elements are used across the span ℓ to represent the panel. Mass, stiffness, aerodynamic and damping matrices for a constant thickness sandwich beam element are given in appendix A. Span length ℓ is used to scale the finite element dimensions. α_{cr} is determined for different damping values, $g_{\alpha o}$.

In Table 8.1 first two eigenvalue pairs of the $\underset{\approx}{C}_o$ matrix are presented for increasing α_o values and for different damping parameters, $g_{\alpha o}$. The starting α_o values are estimated from a graph developed by Houbolt (Ref. 23) which is reproduced in reference 3. There is a π^2 factor difference between the damping parameter g_α used by Houbolt and the damping parameter $g_{\alpha o}$ used in this study such that:

$$g_\alpha = g_{\alpha o}/\pi^2 \qquad\qquad (8.1)$$

Numbers in Table 8.1 exhibit the flutter phenomenon clearly. It can be seen that for small damping values the α_o for which the imaginary parts become equal is very close to α_{cr}, whereas for high damping values α_{cr} is much higher than the α_o for which the frequencies merge (as illustrated in figure 5.1). In Table 8.2 α_{cr} values and flutter frequencies are given for all of the damping cases considered. In Figure 8.2, the α_{cr} values versus $g_{\alpha o}/\pi^2$ are plotted against the curve given by Houbolt, (His solutions are obtained by solving the differential equation of flutter). This shows that the α_{cr} values

TABLE 8.1 CRITICAL EIGENVALUES FOR INCREASING α_o VALUES

α_o	$\lambda_1 = (\beta_1 \mp i\, \omega_1)/\omega o$	$\lambda_2 = (\beta_i \mp i\, \omega_2)/\omega o$
$g_{\alpha o} = 0.0$		
341.25	$0.000 \mp i\ 31.20$	$0.000 \mp i\ 33.45$
342.50	$0.000 \mp i\ 31.81$	$0.000 \mp i\ 32.92$
* 342.901	$0.000 \mp i\ 32.38$	$0.000 \mp i\ 32.38$
343.75	$+\ 0.804 \mp i\ 32.40$	$-\ 0.804 \mp i\ 32.40$
$g_{\alpha o} = 2.0$		
341.25	$-\ 1.000 \mp i\ 31.19$	$-\ 1.000 \mp i\ 33.43$
343.75	$-\ 0.196 \mp i\ 32.39$	$-\ 1.804 \mp i\ 32.39$
* 344.214	$0.000 \mp i\ 32.40$	$-\ 2.000 \mp i\ 32.40$
345.00	$+\ 0.264 \mp i\ 32.43$	$-\ 2.264 \mp i\ 32.43$
$g_{\alpha o} = 1.0\pi^2 \qquad g_{\alpha o/2} = 4.935$		
361.25	$-\ 1.168 \mp i\ 32.59$	$-\ 8.702 \mp i\ 32.59$
367.50	$-\ 0.579 \mp i\ 32.80$	$-\ 9.290 \mp i\ 32.80$
* 374.570	$-\ 0.001 \mp i\ 33.03$	$-\ 9.869 \mp i\ 33.03$
400.00	$+\ 1.651 \mp i\ 33.87$	$-11.52 \mp i\ 33.87$
$g_{\alpha o} = 2.0\pi^2 \qquad g_{\alpha o/2} = 9.87$		
457.50	$-\ 0.414 \mp i\ 34.83$	$-19.33 \mp i\ 34.83$
463.75	$-\ 0.178 \mp i\ 35.06$	$-19.56 \mp i\ 35.06$
* 468.594	$0.000 \mp i\ 35.23$	$-19.74 \mp i\ 35.23$
477.50	$+\ 0.315 \mp i\ 35.54$	$-20.05 \mp i\ 35.54$

*Indicates α_{cr}

TABLE 8.2 PANEL FLUTTER BOUNDARIES AND FLUTTER
FREQUENCIES FOR DIFFERENT DAMPING VALUES

$g_{\alpha o}$	α_{cr}	$\lambda_f = \mp i(\omega_{f/\omega o})$
0.0	342.901	$\mp i$ 32.38
1.0	343.230	$\mp i$ 32.38
2.0	344.214	$\mp i$ 32.40
$1.0\pi^2$	374.570	$\mp i$ 33.03
$1.5\pi^2$	414.375	$\mp i$ 33.95
$2.0\pi^2$	468.594	$\mp i$ 35.54
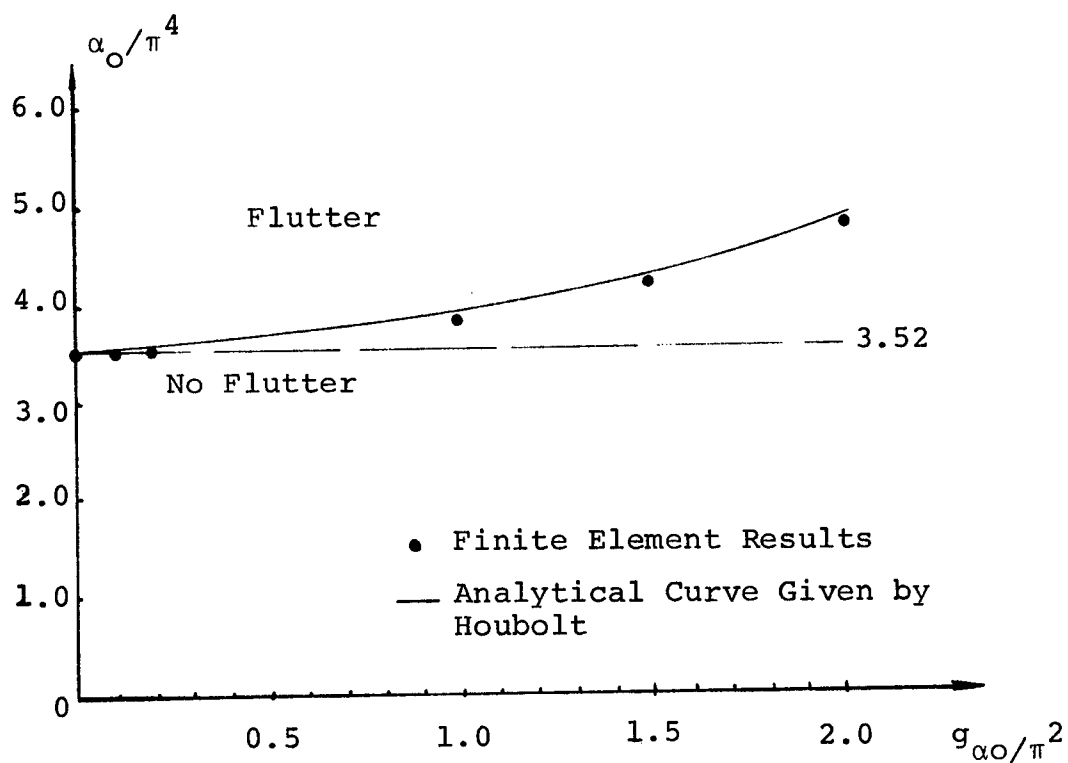
Fig. 8.2 Flutter Boundaries for Different Damping Values

obtained by using five constant thickness beam elements are slightly lower but in good agreement with the analytical solutions.

8.3 Optimization Results

The first set of optimization results were obtained by using a gradient projection subroutine which can only handle one constraint. It is based on equations (6.39 - 43). For this set of results only the flutter constraint was considered and it was kept active all the times. Various methods of R_q selection and various convergence criteria were used with different success in terms of number of iterations and the accuracy of the final results. However the main purpose of this initial study was to determine a proper finite element model to get the optimum shapes comparable to other methods (mainly control theory method used by Weisshaar, in ref. 7).

The first optimization attempt was made using the same model used for calculating the α_{cr} values, i.e., five constant thickness beam elements across the span with a mass ratio ρ_i associated with each element. Using equation (A.2) the merit function for this model can be written as

$$F(\underset{\sim}{\rho}) = \sum_{i=1}^{5} \rho_i \qquad (8.2)$$

with the gradient

$$\nabla F(\underset{\sim}{\rho})^T = \{1, 1, 1, 1, 1\} \qquad (8.3)$$

A damping parameter of $g_{\alpha o} = 1.0\pi^2$ was used to-

gether with $\alpha_o = 375.00$ which is slightly (0.11%) higher than the $\alpha_{cr} = 374.57$ (Table 8.1) for this damping. $\eta = 0.80$ was used for the ratio of initial cover skin mass to total mass.

The initial flutter gradients, $\nabla C_f(\rho_o)$, were checked against numerical gradients which were obtained by calculating the flutter eigenvalue with a small increment ($\varepsilon = 10^{-5}$) to each design variable ρ_i successively. The agreement was found to be extremely good. During the optimization, the gradients were calculated for all ρ_i and the symmetry property was used to check the accuracy of the gradients (i.e. $\frac{\partial C_f}{\partial \rho_1} = \frac{\partial C_f}{\partial \rho_5}$, $\frac{\partial C_f}{\partial \rho_2} = \frac{\partial C_f}{\partial \rho_4}$. See ref. 4 for the proof that the optimum shape is symmetrical about mid span).

The initial and final values for the merit function, the design parameters (ρ_4 and ρ_5 are omitted because of symmetry), and the flutter eigenvalue pair are given in table 8.3. The results are also plotted in figure 8.3. It can be seen that thickness constraints never come into the picture. The other point of interest is that the flutter frequency of the optimum shape is 1.62% higher than the initial value. This model produced 4.96% structural weight reduction which means 3.97% reduction in total weight. These results are very close to the results presented by Craig (Ref. 8) using 5-constant thickness elements and zero damping.

The crudeness of the optimum shape for constant thickness element suggested that linearly tapered elements be used. Therefore the same problem was solved using 5 tapered elements across the span. The element mass, stiffness, aero-

TABLE 8.3   PANEL OPTIMIZATION - 5 CONSTANT THICKNESS ELEMENTS
(NO THICKNESS CONSTRAINT)

$g_{\alpha o} = 1.0\pi^2$		$\eta = 0.80$			$\alpha_o = 375.00$
	$F(\rho)$	ρ_1	ρ_2	ρ_3	λ_f
INITIAL	5.000	1.000	1.000	1.000	0.0319 $\mp$i 33.041
FINAL	4.752	0.7998	1.2377	0.6772	0.0319 $\mp$i 33.576

TABLE 8.4   PANEL OPTIMIZATION - 5 TAPERED ELEMENTS
(NO THICKNESS CONSTRAINT)

$g_{\alpha o} = 1.0\pi^2$		$\eta = 0.80$			$\alpha_o = 375.00$
	$F(\rho)$	ρ_1	ρ_2	ρ_3	λ_f
INITIAL	5.000	1.000	1.000	1.000	0.0319 $\mp$i 33.041
FINAL	4.546	0.0795	1.2457	0.9479	0.0319 $\mp$i 33.268

TABLE 8.5   PANEL OPTIMIZATION - 6 TAPERED ELEMENTS
(NO THICKNESS CONSTRAINT)

$g_{\alpha o} = 1.0\pi^2$		$\eta = 0.80$				$\alpha = 375.00$
	$F(\rho)$	ρ_1	ρ_2	ρ_3	ρ_4	λ_f
INITIAL	6.000	1.000	1.000	1.000	1.000	0.0021 $\mp$i 33.068
FINAL	5.057	0.0846	1.0918	1.4552	-0.1211	0.0021 $\mp$i 35.727
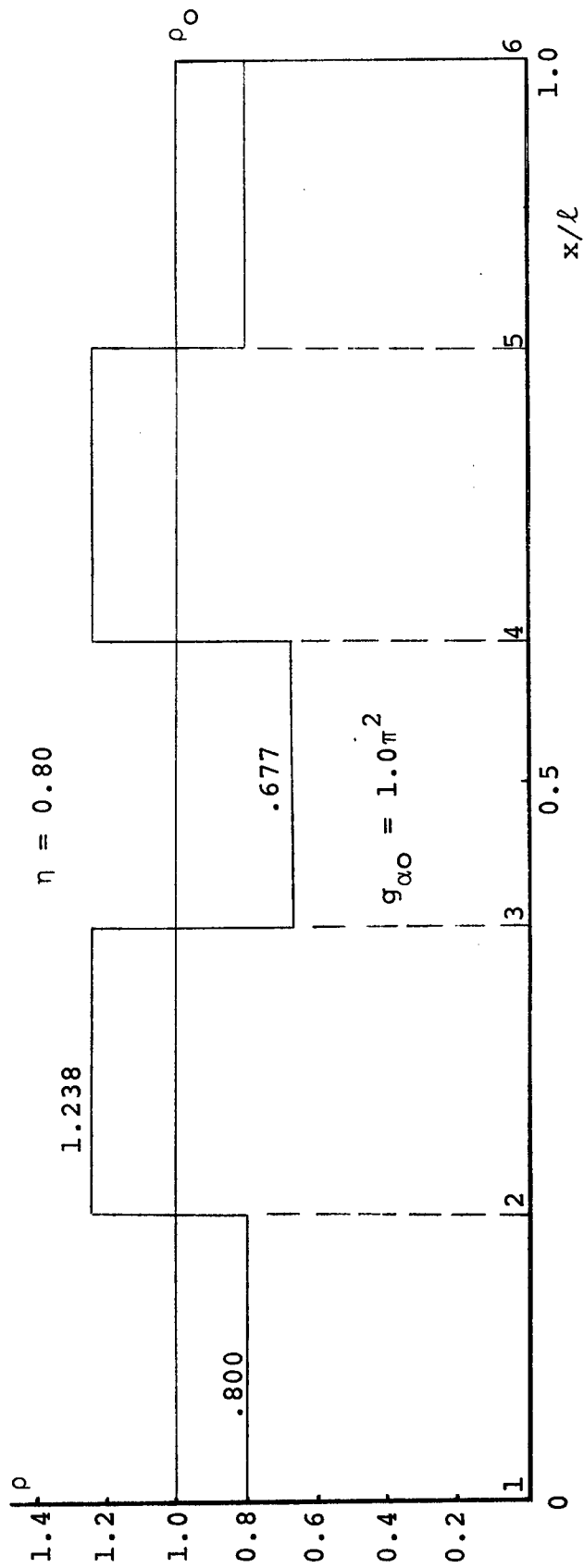
Fig. 8.3 Panel Optimization – 5 Constant Thickness Elements (No Thickness Constraint), $\alpha_o = 375.00$

dynamic and damping matrices for tapered sandwich beam element are in appendix B. This time a mass ratio ρ_i was associated with each nodal point which increased the number of design variables from 5 to 6. The merit function for this model is (using equation B.2);

$$F(\underset{\sim}{\rho}) = \frac{1}{2}\rho_1 + \sum_{i=2}^{5} \rho_i + \frac{1}{2}\rho_6 \qquad (8.4)$$

and the merit function gradient is;

$$\nabla F(\underset{\sim}{\rho})^T = \{\frac{1}{2}, 1, 1, 1, 1, \frac{1}{2}\} \qquad (8.5)$$

The results are given in table 8.4 and figure 8.4. This time the increase in flutter frequency is 0.69%. The structural weight reduction is 9.08% and the total weight reduction is 7.27%, which show a considerable improvement over constant thickness element representation. However when the optimum shape in figure 8.4 is compared with the optimum shapes obtained by control theory methods (Ref. 7, pp. 129, 132, 133) the inability of 5 tapered element model to reproduce the dip at the center became obvious. This suggested the use of 6 tapered elements.

The same problem (i.e. $g_{\alpha 0} = 1.0\pi^2$, $\alpha_0 = 375.00$, $\eta = 0.80$) was also solved by using six tapered elements with merit function;

$$F(\underset{\sim}{\rho}) = \frac{1}{2}\rho_1 + \sum_{i=2}^{6} \rho_i + \frac{1}{2}\rho_7 \qquad (8.6)$$

and merit function gradient

$$\nabla F(\underset{\sim}{\rho}) = \{1/2, 1, 1, 1, 1, 1, 1/2\} \qquad (8.7)$$
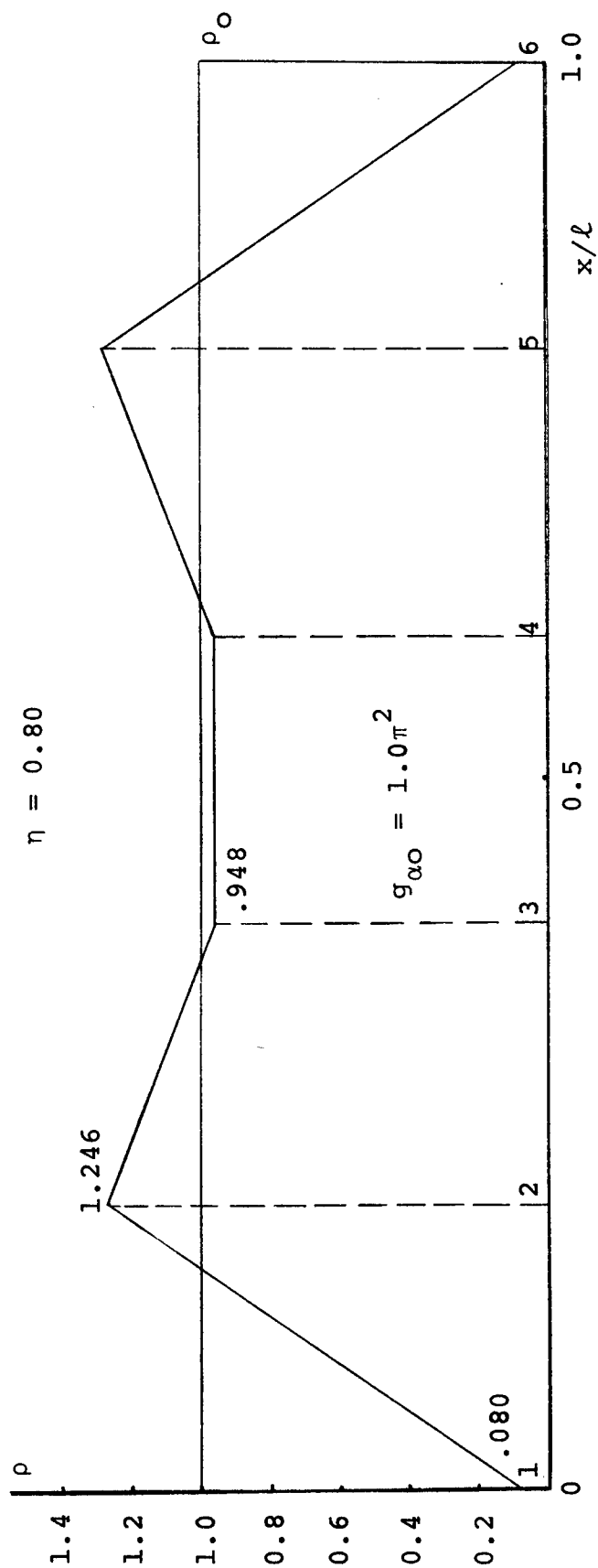
Fig. 8.4 Panel Optimization - 5 Tapered Elements (No Thickness Constraint),

$$\eta = 0.80$$

$$\alpha_o = 375.00$$

The results are in table 8.5 and figure 8.5. It can be seen that this model gave the required results as far as the optimum shape is concerned. However, it also indicated the necessity of using some sort of thickness constraints. Without increasing the number of constraints two different approaches were tried with some success:

1) Once the condition $\rho_i < \rho_{min}$ is encountered ρ_i was replaced by ρ_{min} and this design variable was excluded from the rest of the optimization process.

2) Every time the condition $\rho_i < \rho_{min}$ is encountered ρ_i was replaced by ρ_{min} but kept as a design variable.

Both of these methods were effective in applying the thickness constraints. However both had undesirable aspects: Method 1) reduced the size of the optimization problem, which meant solving not the original problem but a projection of it on a subspace. The optimum design obtained this way was not the true optimum. Method 2) interfered with the calculations of the gradient projection method which either meant more iter-actions or no convergence.

After the gradient projection routine, which could handle multiple constraints, was developed for the delta wing problem, it was applied to the panel problem. The same struc-tural model was used (i.e. six tapered elements), $\rho_{min} = 0.10$ and $\eta = 0.70$ were chosen to form a better comparison with the optimum shape given by Weisshaar (Ref. 7, p. 129). Each thick-ness constraint was handled as a separate constraint according
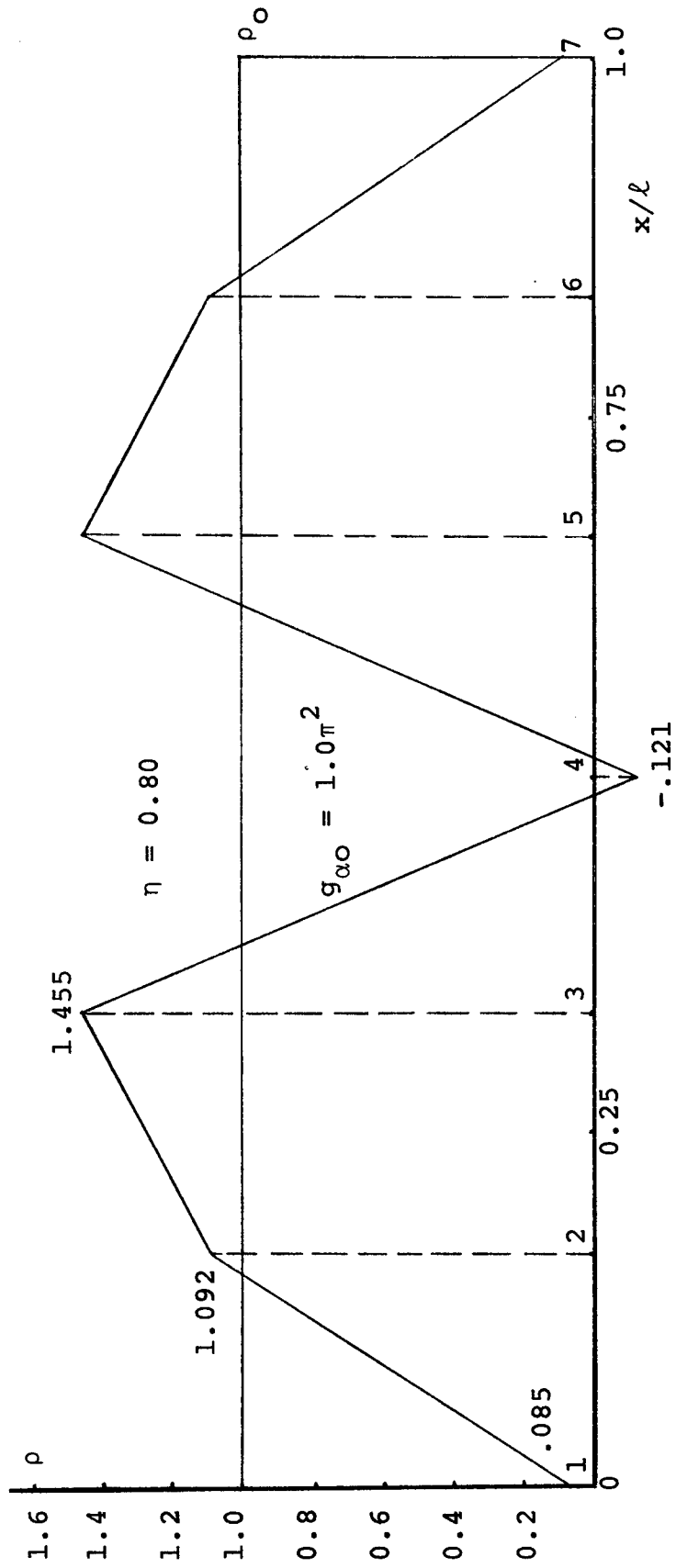
Fig. 8.5 Panel Optimization - 6 Tapered Elements (No Thickness Constraint),

$\alpha_o = 375.00$

to the equations (5.32) and (7.24). Different damping values were used to investigate the effect of damping on the optimized shape and weight reduction. $g_{\alpha O} = 0.01\pi^2$ was used instead of of zero damping. This was done to avoid trouble in calculating the eigenvectors, since at flutter there are repeated eigenvalues for zero damping and repeated eigenvalues cause problems with inverse iteration.

The results of importance are given in tables 8.6-9. In figure 8.6 the optimum shape for $g_{\alpha O} = 0.01\pi^2$ is plotted against the control theory result given by Weisshaar who uses zero damping and the same ρ_{min} and η. This plot shows that the six tapered element model is very efficient in approximating the optimum shape. In figure 8.7 all the optimum shapes for different dampings are plotted.

The results show that the damping practically has no effect on the optimum shape up to $g_{\alpha O} = 1.0\pi^2$. For $g_{\alpha O} = 1.5\pi^2$ the optimum shape is somewhat changed but still similar. However for $g_{\alpha O} = 2.0\pi^2$ the optimum shape is drastically effected. The results also show that the effect of damping on weight reduction is favorable, however slight, up to $g_{\alpha O} = 1.5\pi^2$. The structural and total weight reductions for different models and for different damping values are given in table 8.10. Percentages taken from Weisshaar's work (Ref. 7) belong to the optimum shape reproduced in figure 8.6.

The increases in the flutter frequency from initial to final design are 4.45%, 6.32%, 8.72% and 63.8% for $g_{\alpha O}$; $0.01\pi^2$, $1.0\pi^2$, $1.5\pi^2$, and $2.0\pi^2$ respectively.

TABLES 8.6 - 9 PANEL OPTIMIZATION WITH DIFFERENT
DAMPING VALUES - 6 TAPERED ELEMENTS
(THICKNESS CONSTRAINTS)

$g_{\alpha o} = 0.01\pi^2$		$\eta = 0.70$		$\rho_{min} = 0.1$		$\alpha_o = 343.1375$
	$F(\underset{\sim}{\rho})$	ρ_1	ρ_2	ρ_3	ρ_4	λ_f
INITIAL	6.000	1.000	1.000	1.000	1.000	$0.0461 \mp i\ 32.404$
FINAL	5.146	0.1000	1.0853	1.3878	0.1000	$0.0477 \mp i\ 33.845$

$g_{\alpha o} = 1.0\pi^2$		$\eta = 0.70$		$\rho_{min} = 0.1$		$\alpha_o = 375.000$
	$F(\underset{\sim}{\rho})$	ρ_1	ρ_2	ρ_3	ρ_4	λ_f
INITIAL	6.000	1.000	1.000	1.000	1.000	$0.0021 \mp i\ 33.068$
FINAL	5.053	0.1000	1.0933	1.3332	0.1000	$0.0024 \mp i\ 35.161$

$g_{\alpha o} = 1.5\pi^2$		$\eta = 0.70$		$\rho_{min} = 0.1$		$\alpha_o = 414.375$
	$F(\underset{\sim}{\rho})$	ρ_1	ρ_2	ρ_3	ρ_4	λ_f
INITIAL	6.000	1.000	1.000	1.000	1.000	$0.0016 \mp i\ 33.954$
FINAL	4.852	0.1000	1.1287	1.1971	0.1000	$0.0017 \mp i\ 36.917$

$g_{\alpha o} = 2.0\pi^2$		$\eta = 0.70$		$\rho_{min} = 0.1$		$\alpha_o = 469.625$
	$F(\underset{\sim}{\rho})$	ρ_1	ρ_2	ρ_3	ρ_4	λ_f
INITIAL	6.000	1.000	1.000	1.000	1.000	$0.0016 \mp i\ 35.310$
FINAL	2.551	0.1000	0.8490	0.3263	0.1000	0.0026 ∓ 57.830
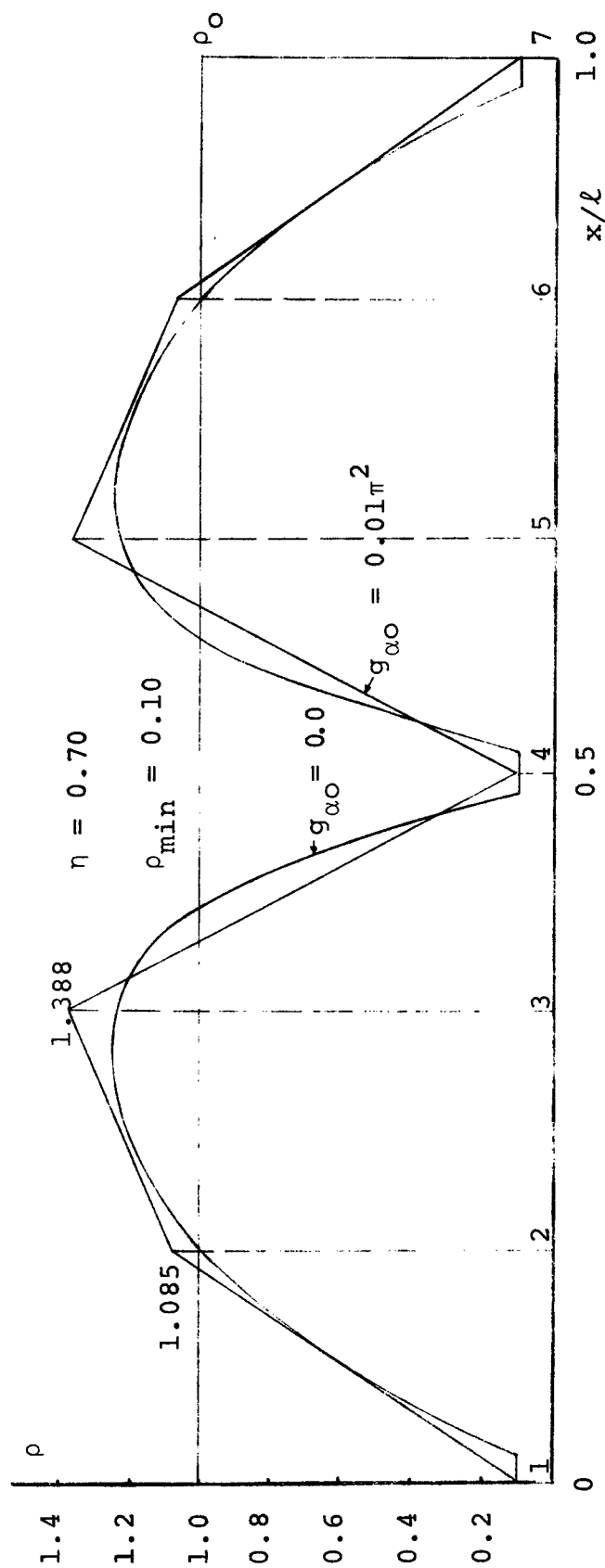
Fig. 8.6 Panel Optimization With Thickness Constraints – 6 Tapered Elements vs.
Control Theory Solution by Weisshaar (Ref. 7)
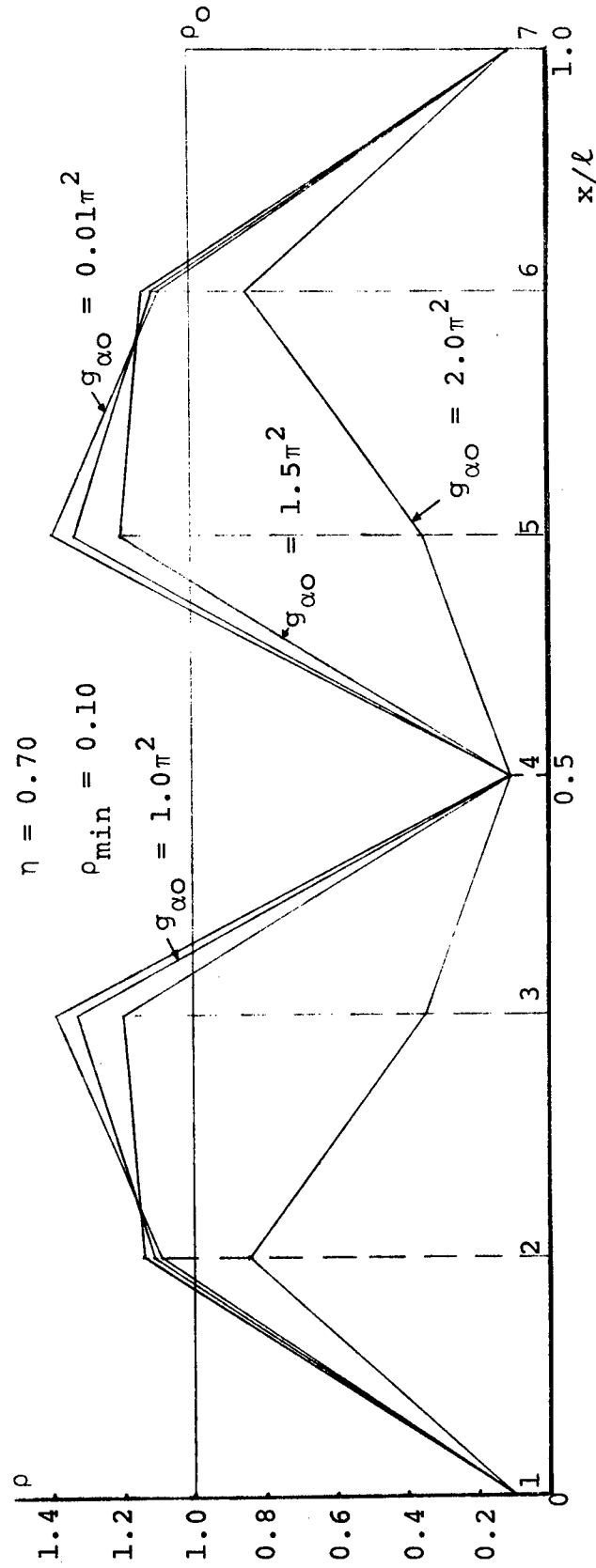
Fig. 8.7 Panel Optimization With Different Damping Values - 6 Tapered Elements
(Thickness Constraints)

TABLE 8.10   WEIGHT REDUCTIONS FOR DIFFERENT MODELS

Model	$g_{\alpha o}/\pi^2$	TWR	SWR
5 C.T. Elements $\eta = 0.80$	1.0	3.97%	4.96%
5 Tapered Elements $\eta = 0.80$	1.0	7.27%	9.08%
6 Tapered Elements $\eta = 0.70, \rho_{min} = 0.10$	0.01	9.97%	14.25%
	1.0	11.06%	15.80%
	1.5	13.39%	19.13%
	2.0	40.23%	57.45%
Control Theory Solution By Weisshaar (Ref. 7), $\eta = 0.70$, $\rho_{min} = 0.10$	0.0	11.51%	16.44%

TWR: % Total Weight Reduction

SWR: % Structural Weight Reduction

TWR = η SWR

Damping values over $g_{\alpha o} = 1.0\pi^2$ are rare for most lifting surfaces; however, they are possible, especially for members where a special viscous core material is used for noise suppression.

To give an idea of the optimization process, step by step results are given in table 8.11 for the $g_{\alpha o} = 1.0\pi^2$ case. The step size, R_q, pattern for this run was predetermined, using earlier experience with single constraint gradient projection algorithm. In figure 8.8 merit function and flutter constraint values are plotted against step sizes (positive constraint values indicate constraint violation). The option of reducing step size when a new thickness constraint is encountered (Equation 6.38) has not been used for these runs.

q	R_q	ρ_1	ρ_2	ρ_3	ρ_4	$F(\underset{\sim}{\rho})$	λ_f	C_f (10^{-2})
0		1.000	1.000	1.000	1.000	6.000	$0.0021 \mp i\ 33.068$	0.00
1	0.4	0.7794	0.9547	1.1028	0.8065	5.701	$0.0883 \mp i\ 33.431$	8.63
2	0.4	0.5546	0.9674	1.1845	0.5937	5.452	$0.0601 \mp i\ 33.878$	5.80
3	0.2	0.4460	0.9895	1.2196	0.4798	5.344	$0.0190 \mp i\ 34.144$	1.69
4	0.2	0.3409	1.0136	1.2535	0.3597	5.235	$0.0219 \mp i\ 34.451$	1.99
5	0.1	0.2922	1.0284	1.2717	0.2952	5.188	$0.0081 \mp i\ 34.621$	0.61
6	0.1	0.2462	1.0436	1.2899	0.2271	5.140	$0.0085 \mp i\ 34.812$	0.64
7	0.1	0.2041	1.0598	1.3089	0.1549	5.096	$0.0091 \mp i\ 35.025$	0.71
8	0.1	0.1672	1.0767	1.3288	0.0780	5.056	$0.0103 \mp i\ 35.267$	0.82
9	0.05	0.1357	1.0778	1.3329	0.1000	5.057	$0.0075 \mp i\ 35.167$	0.54
10	0.05	0.1020	1.0868	1.3381	0.1000	5.052	$0.0086 \mp i\ 35.150$	0.66
11	0.01	0.0958	1.0904	1.3381	0.1000	5.053	$0.0023 \mp i\ 35.148$	0.02
12	0.01	0.1000	1.0933	1.3332	0.1000	5.053	$0.0024 \mp i\ 35.161$	0.03

TABLE 8.11 STEP BY STEP OPTIMIZATION - 6 TAPERED ELEMENTS

$(g_{\alpha o} = 1.0 \pi^2,\ \eta = 0.70,\ \rho_{min} = 0.10,\ \alpha_o = 375.00)$
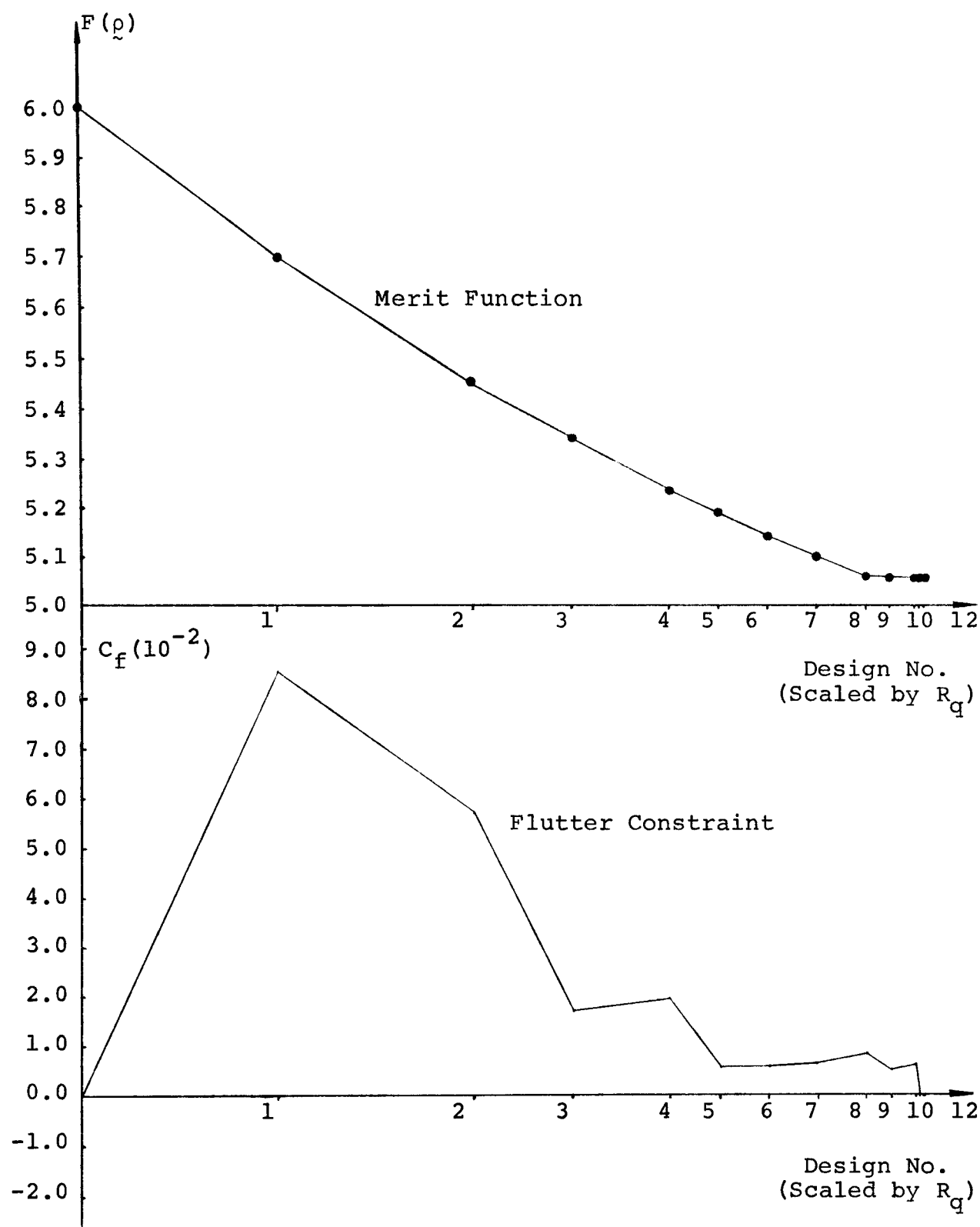
Fig. 8.8 Progress of Panel Optimization - 6 Tapered Elements

$(g_{\alpha o} = 1.0\pi^2, \quad \eta = 0.70, \quad \rho_{min} = 0.10, \quad \alpha_o = 375.00)$

CHAPTER 9

CANTILEVERED DELTA-WING OPTIMIZATION

The results of semi-infinite panel optimization showed that the aeroelastic optimization approach presented in chapters 2, 3, 4, 5, 6 and 7 is basically feasible. The second problem attempted here is the minimum-weight design of a cantilevered delta wing with flutter, stress and thickness constraints. This problem is two dimensional and considerably larger in size compared to the panel problem. The same structural model is used in the optimization problem with three different combinations of constraints: 1) Flutter and thickness constraints 2) Stress and thickness constraints 3) Flutter, stress and thickness constraints. The multiple-constraint gradient projection routine which was discussed in Chapter 6 was first applied to the optimization problems including the flutter constraint.

9.1 Structural Model

The structural model is a cantilevered delta wing with aspect ratio 1. It is assumed to be of sandwich construction with constant core thickness d and with variable skin thickness t. The air flow is assumed to be parallel to the cantilevered edge and at both sides of the wing. Figure 9.1 shows the plan view of the delta wing. The finite element lay-out, numbering of the nodal points and the elements are also shown in figure 9.1. The length of the clamped edge is L, which is used to
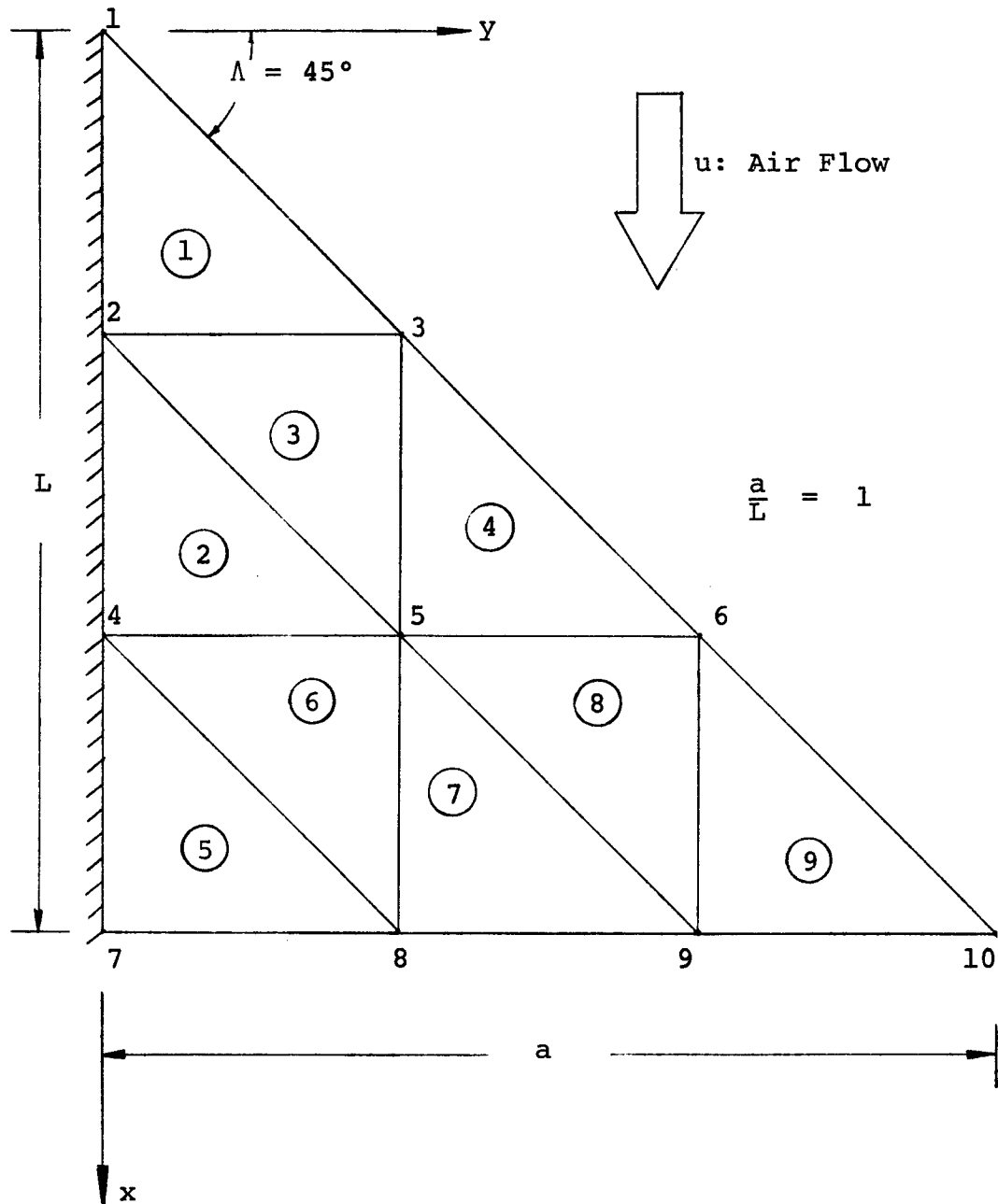
Fig. 9.1 Cantilevered Delta Wing in Supersonic
Flow - Finite Element Grid

scale all finite element dimensions.

A high-precision triangular plate bending element developed by Cowper (Ref. 22) and others is used for the finite elements. A design variable ρ_i is associated with each nodal point. The cover skin thickness variation within an element is assumed to be linear. The equations for the generation of element stiffness and mass matrices for a constant thickness plate element are given in reference 22. These equations are modified to obtain the equations for a sandwich plate with linear cover skin thickness distribution. The equations for the generation of element aerodynamic and damping matrices are derived. The element characteristics, and the equations for the generation of element mass, stiffness, aerodynamic and damping matrices are given in appendix C. The actual element matrices are generated numerically inside the computer.

There are six nodal point degrees of freedom, namely the transverse deflection and its first and second derivatives (W, W_x, W_y, W_{xx}, W_{xy}, W_y). The system, therefore, has 60 degrees of freedom before the boundary conditions are applied. Prescribed boundary conditions are applied for the nodal points on the clamped edge, which are 1, 2, 4 and 7 (Figure 9.1). The fixed-edge condition implies that $W = W_y = 0$ along the x-axis, from which we also get $W_x = W_{xy} = W_{xx} = 0$. Therefore nodal points 1, 2, 4, and 7 will only have W_{yy} freedom. Enforcement of the prescribed boundary conditions reduces the system degrees of freedom to 40. These boundary conditions are essential for any type of structural analysis, and they can be assumed suffi-

cient for a load-deflection or a dynamic (natural frequencies, flutter boundaries etc.) type analysis. However the second derivatives of the transverse deflection (W_{xx}, W_{xy}, W_{yy}) obtained this way for nodal points on free edges (nodal points 3, 6, 10, 9 and 8 at figure 9.1) will not satisfy the free edge natural boundary conditions for plate-bending moments (bending moments and second derivatives are related through equations 3.2). For the structural model used in optimization, in order to obtain more realistic stress constraints for free edge nodal points, these degrees of freedoms are constrained to satisfy the free edge conditions. These natural boundary conditions reduce the number of system degrees of freedom to 29 (the algebraic details for the application of boundary conditions are presented in appendix C).

The 40 degree of freedom system is used to obtain the natural frequencies and flutter boundaries of the delta wing which are compared to the results given in literature (Refs. 22, 6). The 29 degree of freedom system is also used in the same calculations to see the effect of additional constraining on natural frequencies and flutter boundaries. Only the 29 degree of freedom system is used for the optimization procedures.

Poisson's ratio $\nu = 0.3$ and skin mass ratio $\eta = 0.80$ is used in all the calculations presented below.

9.2 Natural Frequencies

Natural frequencies are calculated to check the accuracy of the derivation of system mass and stiffness matrices.

TABLE 9.1 NATURAL FREQUENCIES OF THE DELTA WING

Mode No.	Natural Frequencies Given by Cowper et al (Ref. 22)	Natural Frequencies of 40 D.O.F. System	Natural Frequencies of 29 D.O.F. System	% Difference
1	36.6419	36.6419	37.0083	1.0%
2	139.3265	139.3265	142.7298	2.4%
3	194.1408	194.1408	198.3996	2.2%
4	333.829	333.829	338.277	1.3%
5	455.374	455.374	459.011	0.8%
6	593.238	593.238	617.275	4.0%
7	671.342	671.342	727.063	8.4%
8	811.612	811.612	848.693	4.5%
9	969.650	969.650	1030.104	6.2%
10	1126.614	1126.614	1171.494	4.0%

The equation;

$$M_{\approx O}^{-1} \, K_{\approx O} \, W_{\sim} = \omega_n^2 \, W_{\sim} \qquad (9.1)$$

is used for this purpose. In reference 22 the first 10 natural frequencies are given for a cantilevered triangular plate with aspect ratio 1 and Poisson's ratio $\nu = 0.3$. The finite element lay out is exactly the same. There, actual material and dimensional properties are used. Since the matrices derived here are non-dimensional, a comparison is obtained by scaling the natural frequencies obtained here with a factor such that the first natural frequencies are identical. Both 40 and 29 degree of freedom systems are used in these calculations. The scaling factor is obtained with respect to the first natural frequency of the 40 degree of freedom system. The results are presented in Table 9.1. The natural frequencies obtained by the 40 degree of freedom system are exactly the same as the ones given by the authors of reference 22. The natural frequencies obtained by 29 degree of freedom system are slightly higher because of the extra constraining. On the average, the first five frequencies are 1.5% higher, and the last five frequencies are 5.4% higher.

9.3 Flutter Boundaries

In reference 6 Olson gives the flutter boundaries for cantilevered delta wings, for different sweepback angles Λ (Figure 9.1) and for different finite element grids. He uses the same aerodynamics with zero damping and the same finite elements. For $\Lambda = 45°$ and for 3 x 3 grid the flutter boundary is

TABLE 9.2 CRITICAL EIGENVALUES FOR 40 D.O.F. SYSTEM

$$(g_{\alpha o} = 0.2468)$$

α_o	$\lambda_1 = (\beta_1 \mp i\, \omega_1)/\omega o$	$\lambda_2 = (\beta_2 \mp i\, \omega_2)/\omega o$
0.0	$- 0.1234 \mp i\ \ 6.172$	$- 0.1234 \mp i\ 23.473$
70.0	$- 0.1234 \mp i\ 14.196$	$- 0.1234 \mp i\ 21.418$
86.245	$- 0.1213 \mp i\ 18.567$	$- 0.1255 \mp i\ 18.573$
86.3	$+ 0.0688 \mp i\ 18.572$	$- 0.3156 \mp i\ 18.572$
86.4	$+ 0.2583 \mp i\ 18.577$	$- 0.5051 \mp i\ 18.577$
88.0	$+ 1.1949 \mp i\ 18.653$	$- 1.4416 \mp i\ 18.653$

TABLE 9.3 CRITICAL EIGENVALUES FOR 29 D.O.F. SYSTEM

$$(g_{\alpha o} = 0.2468)$$

α_o	$\lambda_1 = (\beta_1 \mp i\, \omega_1)/\omega o$	$\lambda_2 = (\beta_2 \mp i\, \omega_2)/\omega o$
86.35	$- 0.1234 \mp i\ 16.275$	$- 0.1234 \mp i\ 21.535$
91.00	$- 0.1234 \mp i\ 17.281$	$- 0.1234 \mp i\ 20.976$
95.00	$- 0.1234 \mp i\ 18.682$	$- 0.1234 \mp i\ 19.963$
95.50	$- 0.1234 \mp i\ 19.159$	$- 0.1234 \mp i\ 19.536$
*95.60	$+ 0.0754 \mp i\ 19.352$	$- 0.3221 \mp i\ 19.352$
107.00	$+ 2.8007 \mp i\ 19.914$	$- 3.0475 \mp i\ 19.914$

*Indicates The Value Used For Optimization

given as α_{cr} = 86.254. Here the eigenvalues of the $\underset{\sim}{C}_o$ matrix
are calculated for increasing α_o values. A damping value of
$g_{\alpha o}$ = $0.025\pi^2$ (= 0.2468) is used. In table 9.2 the first two
eigenvalue pairs for the 40 degree of freedom system are pre-
sented. α_{cr} is determined roughly to be α_{cr} = 86.3. The slight
difference can be explained with the existence of small damping
which does tend to increase the α_{cr}. Table 9.3 is for the 29
degree of freedom system where α_{cr} is determined roughly to be
α_{cr} = 95.6. This is a 10.8% increase from the α_{cr} for the 40
degree of freedom system. The calculation of the flutter boun-
dary is a stability problem and the elimination of any existing
free edge moments could explain the rather considerable improve-
ment on the flutter boundary (for the 40 degree of freedom sys-
tem the free edge moments are not zero). The increase in the
flutter frequency is 4.2%.

Using a proper scaling factor the flutter frequency for
the 40 degree of freedom system is found to be in very good
agreement with the results given by Olson (Ref. 6).

9.4 Optimization Results

Using equation (C.64) given in appendix C for the weight
of a triangular element, the merit function can be derived to
be;

$$F(\underset{\sim}{\rho}) = \rho_1 + 3\rho_2 + 3\rho_3 + 3\rho_4 + 6\rho_5 + 3\rho_6 + \rho_7 + 3\rho_8$$
$$+ 3\rho_9 + \rho_{10} \qquad (9.2)$$

From which the merit function gradients are obtained as;

$$\nabla F(\underset{\sim}{\rho})^T = \{1, \ 3, \ 3, \ 3, \ 6, \ 3, \ 1, \ 3, \ 3, \ 1\} \qquad (9.3)$$

These expressions are used in obtaining all of the following optimization results.

9.4.1 Optimization with Flutter and Thickness Constraints

The first results presented here are for the optimization of the delta wing with flutter and thickness constraints. The gradients of the flutter constraint are checked numerically (as described for the panel problem) and found to be extremely accurate. The 29 degree of freedom system is used in obtaining the system matrices. Other parameters for the optimization are: $g_{\alpha o} = 0.025\pi^2$, $\alpha_{cr} = 95.6$ (From table 9.3) and $\eta = 0.80$. The small damping value is used to separate critical eigenvalues at flutter which increases the efficiency in calculating the corresponding eigenvectors.

In table 9.4 the step sizes, the design variables, the merit function, the flutter eigenvalue, the flutter constraint and the active thickness constraints are presented for 21 design steps. The flutter constraint is kept active for all design steps and it is defined as $C_f = (\beta_{fq} - \beta_{fo})/\omega_o$ since β_{fo} corresponding to $\alpha_{cr} = 95.6$ was slightly greater than zero. These results were obtained in four different computer runs; the first three runs for six design steps each and the last run for three design steps. On the University of Texas at Austin CDC 6600 each design step took approximately 21 seconds. The

TABLE 9.4 DELTA WING OPTIMIZATION WITH FLUTTER
AND THICKNESS CONSTRAINTS

Given R_q	0.4	0.4	0.4	0.3	0.3	
R_q	0.4	0.4	0.4	0.290	0.3	
Design No.(q)	0	1	2	3	4	5
ρ_1	1.000	0.9684	0.9414	0.9222	0.9169	0.8977
ρ_2	1.000	0.8933	0.7977	0.7214	0.6881	0.6218
ρ_3	1.000	0.9476	0.9202	0.9225	0.9376	0.8769
ρ_4	1.000	0.8604	0.7233	0.5924	0.5086	0.4180
ρ_5	1.000	0.8473	0.6863	0.5072	0.3390	0.1118
ρ_6	1.000	1.0985	1.1789	1.2272	1.2037	1.0982
ρ_7	1.000	0.9748	0.9506	0.9292	0.9162	0.8901
ρ_8	1.000	0.8340	0.6664	0.5015	0.3979	0.3067
ρ_9	1.000	0.7697	0.5287	0.2773	0.1000	0.1
ρ_{10}	1.000	0.8947	0.7876	0.6809	0.6129	0.5730
$F(\rho)$	27.000	24.132	21.243	18.302	15.988	13.296
$\beta_{f/\omega o}$	0.0754	-0.0764	-0.0778	-0.0793	-0.0818	-0.0903
$\omega_{f/\omega o}$	19.352	18.618	17.827	17.035	16.624	16.393
C_f	0.00	-0.1518	-0.1532	-0.1547	-0.1572	-0.1657
Thc. Con.	–	–	–	–	9	9
$\Delta F/R_q$		-7.17	-7.22	-7.35	-7.98	-8.97	-7.28

$$g_{\alpha o} = 0.025\pi^2, \quad \alpha_{cr} = 95.6, \quad \eta = 0.80, \quad C_f = (\beta_{fq} - \beta_{fo})/\omega_o$$

TABLE 9.4 (Continued)   DELTA WING OPTIMIZATION WITH FLUTTER
AND THICKNESS CONSTRAINTS

Given R_q	0.3	0.2	0.2	0.2	0.2	0.2
R_q	.091	0.2	0.164	0.2	0.139	0.182
Design No.(q)	6	7	8	9	10	11
ρ_1	0.8796	0.8470	0.8189	0.7749	0.7401	0.7125
ρ_2	0.5721	0.4775	0.3977	0.2800	0.1973	0.1000
ρ_3	0.8367	0.7487	0.6756	0.5741	0.5015	0.4020
ρ_4	0.3804	0.2941	0.2257	0.1422	0.1000	0.1
ρ_5	0.1000	0.1	0.1	0.1	0.1	0.1
ρ_6	1.0860	1.0159	0.9601	0.8956	0.8456	0.7408
ρ_7	0.8769	0.8477	0.8240	0.7925	0.7715	0.7369
ρ_8	0.2641	0.1739	0.1000	0.1	0.1	0.1
ρ_9	0.1	0.1	0.1	0.1	0.1	0.1
ρ_{10}	0.5594	0.5295	0.5032	0.4611	0.4247	0.3990
$F(\underset{\sim}{\rho})$	12.634	11.254	10.123	8.904	8.069	7.077
β_{f}/ω_o	-0.0904	-0.0905	-0.0906	-0.0908	-0.0914	-0.0916
ω_{f}/ω_o	16.330	16.741	17.120	17.678	18.171	19.515
C_f	-0.1658	-0.1659	-0.1660	-0.1622	-0.1668	-0.1670
Thc. Con.	5,9	5,9	5,8,9	5,8,9	4,5,8,9	2,4,5 8,9
$\Delta F/R_q$	-6.90	-6.88	-6.10	-6.00	-5.47	-4.52

$$g_{\alpha o} = 0.025\pi^2, \quad \alpha_{cr} = 95.6, \quad \eta = 0.80, \quad C_f = (\beta_{fq} - \beta_{fo})/\omega_o$$

TABLE 9.4 (Continued)   DELTA WING OPTIMIZATION WITH FLUTTER
AND THICKNESS CONSTRAINTS

Given R_q	0.2	0.1	0.1	0.1	0.1	0.1	
R_q	0.2	0.1	0.1	0.1	0.1	0.1	
Design No. (q)	12	13	14	15	16	17
ρ_1	0.6837	0.6524	0.6373	0.6221	0.6164	0.5955
ρ_2	0.1	0.1	0.1	0.1	0.1	0.1
ρ_3	0.2611	0.3077	0.2262	0.3052	0.2133	0.2854
ρ_4	0.1	0.1	0.1	0.1	0.1	0.1
ρ_5	0.1	0.1	0.1	0.1	0.1	0.1
ρ_6	0.6115	0.5786	0.5284	0.5428	0.5444	0.5369
ρ_7	0.6886	0.6638	0.6390	0.6280	0.5985	0.5826
ρ_8	0.1	0.1	0.1	0.1	0.1	0.1
ρ_9	0.1	0.1	0.1	0.1	0.1	0.1
ρ_{10}	0.3824	0.3106	0.3101	0.2534	0.2790	0.2153
$F(\rho)$	6.173	6.086	5.650	5.847	5.567	5.660
$\beta_{f/\omega o}$	2.527	-0.0421	4.191	1.429	3.994	2.419
$\omega_{f/\omega o}$	32.107	24.034	31.752	26.760	31.818	27.107
C_f	2.452	-0.1175	4.116	1.353	3.918	2.343
Thc. Con.	2,4,5 8,9	2,4,5 8,9	2,4,5 8,9	2,4,5 8,9	2,4,5 8,9	2,4,5 8,9
$\Delta F/R_q$	-0.87		-4.35		+1.97		-2.81		+0.93	

$$g_{\alpha o} = 0.025\pi^2, \quad \alpha_{cr} = 95.6, \quad \eta = 0.80, \quad C_f = (\beta_{fq} - \beta_{fo})/\omega_o$$

TABLE 9.4 (Continued) DELTA WING OPTIMIZATION WITH FLUTTER
AND THICKNESS CONSTRAINTS

Given R_q	0.1	0.05	0.05	0.05
R_q	0.1	0.05	0.05	0.05
Design No.(q)	18	19	20	21
ρ_1	0.6006	0.5988	0.5907	0.5766
ρ_2	0.1	0.1	0.1	0.1
ρ_3	0.2154	0.2614	0.2205	0.2437
ρ_4	0.1	0.1	0.1	0.1
ρ_5	0.1	0.1	0.1	0.1
ρ_6	0.5900	0.6004	0.5757	0.5521
ρ_7	0.5568	0.5577	0.5456	0.5358
ρ_8	0.1	0.1	0.1	0.1
ρ_9	0.1	0.1	0.1	0.1
ρ_{10}	0.2551	0.2388	0.2354	0.2021
$F(\underset{\sim}{\rho})$	5.629	5.781	5.560	5.502
$\beta_{f/\omega o}$	2.897	−0.0084	2.311	1.838
$\omega_{f/\omega o}$	32.060	24.514	31.794	27.754
C_f	2.822	−0.0838	2.236	1.762
Thc. Con.	2,4,5 8,9	2,4,5 8,9	2,4,5 8,9	2,4,5 8,9
$\Delta F/R_q$	−0.32	+3.04	−4.40	−1.17

$$g_{\alpha o} = 0.025\pi^2, \quad \alpha_{cr} = 95.6, \quad \eta = 0.80, \quad C_f = (\beta_{fq} - \beta_{fo})/\omega_o$$

calculation of the eigenvalues and the left and right hand eigenvectors corresponding to the flutter eigenvalue of the $\underset{\approx}{C}$ matrix takes approximately 14 seconds.

Table 9.4 reveals that the first thickness constraint violation occurs at the 4th design step at nodal point 9 which is the reason for reduction of R_3 (i.e. norm of the design change vector from ρ_3 to ρ_4) from 0.30 to 0.290. The second thickness constraint is encountered at the 6th design step for nodal point 5 which causes R_5 to be reduced from 0.3 to 0.091. Thickness constraints for nodal points 8, 4 and 2 are encountered at design steps 8, 10 and 11 respectively. Each time a new thickness constraint is encountered there is a reduction in the given step size due to the provision discussed in Chapter 6 (Equation 6.38).

Until the 11th design step the flutter constraint is closely followed within the feasible region. At design steps 12, 14, 16, 18 and 20 the flutter occurs involving the second and third modes. To clarify this phenomenon the first three eigenvalue pairs are given in table 9.5 for several optimization steps. It can be seen that the imaginary parts of the eigenvalues of the second and third modes come closer as the optimization progresses until the 12th design step where they become close enough for the energy transfer necessary for the flutter phenomenon.

In figure 9.2 the merit function $F(\rho)$ and flutter constraint C_f are plotted against step sizes. It is interesting to note that there is very little weight reduction after 11th de-

**TABLE 9.5   FIRST THREE EIGENVALUE PAIRS
DURING OPTIMIZATION**

| Design No. (q)	$\lambda_1 = (\beta_1 \mp i\, \omega_1)/\omega_0$	$\lambda_2 = (\beta_2 \mp i\, \omega_2)/\omega_0$	$\lambda_3 = (\beta_3 \mp i\, \omega_3)/\omega_0$
0	$0.075 \mp i\ 19.35$	$-\ 0.322 \mp i\ 19.35$	$-\ 0.123 \mp i\ 38.03$
5	$-\ 0.090 \mp i\ 16.39$	$-\ 0.192 \mp i\ 25.87$	$-\ 0.276 \mp i\ 42.30$
10	$-\ 0.091 \mp i\ 18.17$	$-\ 0.209 \mp i\ 26.94$	$-\ 0.345 \mp i\ 39.29$
11	$-\ 0.092 \mp i\ 19.51$	$-\ 0.208 \mp i\ 27.75$	$-\ 0.387 \mp i\ 37.33$
12	$-\ 0.099 \mp i\ 22.49$	$+\ 2.527 \mp i\ 32.11$	$-\ 3.192 \mp i\ 32.49$
13	$-\ 0.042 \mp i\ 24.03$	$-\ 0.214 \mp i\ 29.27$	$-\ 0.510 \mp i\ 34.74$
14	$-\ 0.093 \mp i\ 25.71$	$+\ 4.191 \mp i\ 31.75$	$-\ 4.914 \mp i\ 32.06$
15	$+\ 1.429 \mp i\ 26.76$	$-\ 1.746 \mp i\ 27.23$	$-\ 0.473 \mp i\ 35.36$
16	$-\ 0.079 \mp i\ 25.71$	$+\ 3.994 \mp i\ 31.82$	$-\ 4.741 \mp i\ 32.14$
17	$+\ 2.419 \mp i\ 27.11$	$-\ 2.754 \mp i\ 27.46$	$-\ 0.474 \mp i\ 35.46$
18	$-\ 0.063 \mp i\ 24.54$	$+\ 2.897 \mp i\ 32.06$	$-\ 3.655 \mp i\ 32.42$
19	$-\ 0.008 \mp i\ 24.51$	$-\ 0.235 \mp i\ 29.58$	$-\ 0.556 \mp i\ 34.57$
20	$-\ 0.030 \mp i\ 25.44$	$+\ 2.311 \mp i\ 31.79$	$-\ 3.107 \mp i\ 32.22$
21	$+\ 1.838 \mp i\ 27.75$	$-\ 2.116 \mp i\ 28.27$	$-\ 0.550 \mp i\ 34.09$
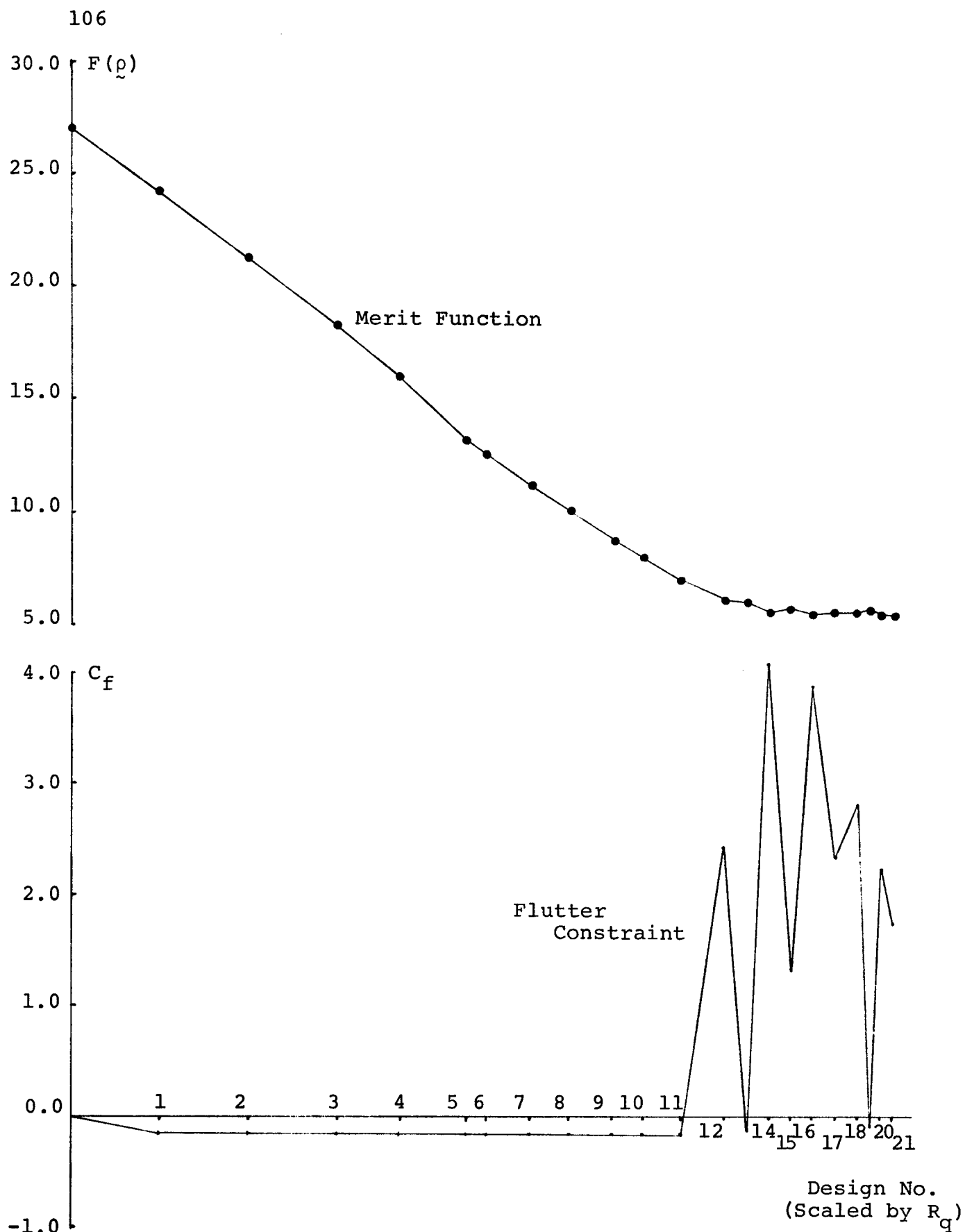
Fig. 9.2 Progress of Delta Wing Optimization with Flutter and
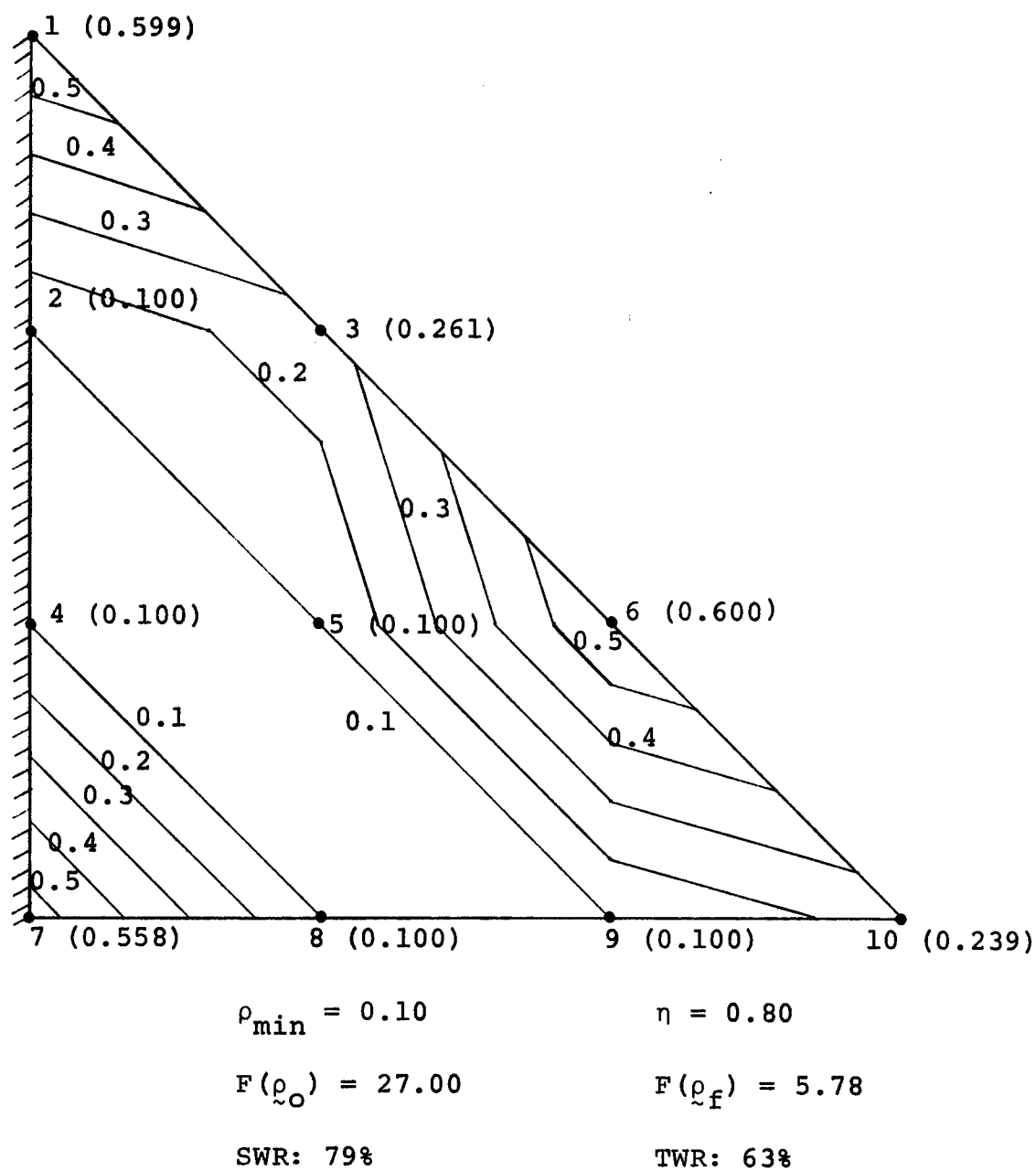Thickness Constraints

Fig. 9.3 Skin Thickness Contours for Minimum-Weight
Design with Flutter and Thickness Constraints

sign which is in the feasible region. The main reason to carry the optimization beyond this point was to see the behaviour of the flutter constraint. At design step 19 the merit function is $F(\rho_{19}) = 5.781$ which is minimum among feasible designs. This correspond to 78.6% structural and 62.9% total weight reduction. It can be shown that the weight reduction at the 11th design step corresponds to 94% of the weight reduction achieved at the 19th design step. It is interesting to note that using smaller step sizes and greater number of design cycles best possible was to obtain $F(\rho) = 5.700$. The corresponding thickness distribution was very similar to the design vector ρ_{19} of table 9.4.

In figure 9.3 the plan view of the delta wing with skin thickness contours corresponding to the minimum-weight design (ρ_{19}) is presented.

9.4.2 Optimization with Stress and Thickness Constraints

The second set of results presented here are for the optimization of the delta wing to satisfy stress and thickness constraints. The stress constraints are placed at the nodal points where the constraints can be evaluated directly from the second derivatives contained in the nodal point degrees of freedom (Equation 5.26). It was assumed that the delta wing is uniformly loaded. The load level is so adjusted that the nodal point with the highest combined stress (Equation 5.23) is at yield for the initial uniform design. The stress constraints are scaled so that $C_s = -100$ means zero stress and $C_s = 0$ means yield.

The significant facts about 22 design steps are presented in table 9.6. These results were obtained in a single run which took approximately 90 seconds on the CDC 6600. Each design cycle takes little less than 4 seconds. Successively smaller values of ε (same as defined in Chapter 6) were used to determine critical stress constraints ($C_s \geq -\varepsilon$). The values employed were: $\varepsilon = 25$ for the first 6 design steps, $\varepsilon = 15$ for the following 6 design steps and $\varepsilon = 5$ after the 12th design step. In table 9.6 the values of the critical stress constraints are given. The only active constraint for designs 0, 1, 2, and 3 is the stress constraint at nodal point 7. The reduction of R_3 from 0.30 to 0.115 is due to the violation of stress constraint at nodal point 8. The reductions in R_6, R_8, R_9 and R_{10} are due to the violation of thickness constraints at nodal points 9, 6, 2 and 3 respectively. The reduction in the number of active stress constraints at design step 12 is due to the decrease in the value of ε from 15 to 5. The reductions in R_{12}, R_{15} and R_{17} are due to the stress constraint violations at nodal points 8, 9 and 4. The reduction in R_{21} is due to the thickness constraint violation at nodal point 1. At the 22nd design step there are all together 10 active constraints (5 thickness, 5 stress constraints) and that is equal to the number of design variables. This indicates that any further improvement is not possible. Although the merit function is slightly lower for ρ_{19}, ρ_{22} is a better design with respect to the value of the stress constraint at nodal point 9.

TABLE 9.6   DELTA WING OPTIMIZATION WITH STRESS
AND THICKNESS CONSTRAINTS

Given R_q	0.4	0.4	0.4	0.3	0.3	
R_q	0.4	0.4	0.4	0.115	0.3	
Design No.(q)	0	1	2	3	4	5
ρ_1	1.000	0.9552	0.9101	0.8645	0.8511	0.7923
ρ_2	1.000	0.8786	0.7572	0.6354	0.6002	0.4677
ρ_3	1.000	0.8767	0.7545	0.6337	0.5996	0.5074
ρ_4	1.000	0.9587	0.9220	0.8913	0.8854	0.8752
ρ_5	1.000	0.7551	0.5132	0.2759	0.2104	0.2032
ρ_6	1.000	0.8684	0.7367	0.6050	0.5671	0.4349
ρ_7	1.000	1.0729	1.1476	1.2241	1.2474	1.3095
ρ_8	1.000	0.8477	0.6909	0.5286	0.4793	0.5662
ρ_9	1.000	0.8638	0.7262	0.5861	0.5445	0.3783
ρ_{10}	1.000	0.9554	0.9107	0.8656	0.8525	0.7906
$F(\underset{\sim}{\rho})$	27.000	23.396	19.810	16.250	15.242	13.800
Thc. Con.	–	–	–	–	–	–
S.Con.	7	7	7	7	7,8	7,8
C_{s2}	–	–	–	–	–	–
C_{s4}	–	–	–	–	–	–
C_{s7}	0.0	0.22	0.36	0.63	0.47	0.05
C_{s8}	–	–	–	–	-10.16	-10.05
C_{s9}	–	–	–	–	–	–
$\Delta F/R_q$	-9.01	-8.96	-8.90	-8.77	-4.80	-4.81

$\varepsilon = 25$ for $q = 0 - 5$

TABLE 9.6 (Continued) DELTA WING OPTIMIZATION WITH STRESS AND THICKNESS CONSTRAINTS

Given R_q	0.3	0.2	0.2	0.2	0.2	0.2
R_q	0.3	0.187	0.2	0.079	0.038	0.2
Design No. (q)	6	7	8	9	10	11
ρ_1	0.7330	0.6952	0.6441	0.6254	0.6149	0.5347
ρ_2	0.3354	0.2519	0.1405	0.1141	0.1000	0.1
ρ_3	0.4156	0.3576	0.2787	0.2463	0.2277	0.1020
ρ_4	0.8633	0.8553	0.8479	0.8549	0.8581	0.8301
ρ_5	0.1960	0.1946	0.1929	0.1786	0.1685	0.1490
ρ_6	0.3074	0.2325	0.1385	0.1000	0.1	0.1
ρ_7	1.3693	1.4066	1.4611	1.4803	1.4907	1.5616
ρ_8	0.6540	0.7088	0.7716	0.8099	0.8288	0.8953
ρ_9	0.2082	0.1000	0.1	0.1	0.1	0.1
ρ_{10}	0.7281	0.6882	0.6340	0.6100	0.5963	0.5108
$F(\underset{\sim}{\rho})$	12.358	11.476	10.728	10.463	10.357	9.884
Thc. Con.	–	9	9	6,9	2,6,9	2,6,9
S.Con	7,8	7,8	4,7,8	4,7,8	4,7,8	4,7,8
C_{s2}	–	–	–	–	–	–
C_{s4}	–	–	-12.84	-12.81	-12.79	-12.71
C_{s7}	0.05	0.02	-0.04	-0.03	-0.03	0.10
C_{s8}	-9.64	-9.29	-8.84	-8.70	-8.66	-8.10
C_{s9}	–	–	–	–	–	–
$\Delta F/R_q$	-4.71	-3.74	-3.36	-2.81	-2.36	-2.17

$\varepsilon = 15$ for $q = 6 - 11$

TABLE 9.6   (Continued)   DELTA WING OPTIMIZATION
WITH STRESS AND THICKNESS CONSTRAINTS

Given R_q	0.2	0.1	0.1	0.1	0.1	0.1
R_q	.003	0.031	0.1	0.1	0.099	0.1
Design No. (q)	12	13	14	15	16	17
ρ_1	0.5343	0.5290	0.4726	0.4160	0.3600	0.2976
ρ_2	0.1	0.1	0.1	0.1	0.1	0.1
ρ_3	0.1000	0.1	0.1	0.1	0.1	0.1
ρ_4	0.8297	0.8289	0.7944	0.7592	0.7244	0.6742
ρ_5	0.1487	0.1269	0.1179	0.1096	0.1022	0.1175
ρ_6	0.1	0.1	0.1	0.1	0.1	0.1
ρ_7	1.5628	1.5722	1.6149	1.6569	1.6981	1.7365
ρ_8	0.8964	0.8788	0.8978	0.9159	0.9330	0.9226
ρ_9	0.1	0.1	0.1	0.1	0.1	0.1
ρ_{10}	0.5092	0.5043	0.4463	0.3880	0.3300	0.2880
$F(\rho)$	9.877	9.690	9.517	9.344	9.174	9.017
Thc. Con.	2,3,6,9	2,3,6,9	2,3,6,9	2,3,6,9	2,3,6,9	2,3,6,9
S.Con	7	7,8	7,8	7,8	7,8,9	7,8,9
C_{s2}	-	-	-	-	-	-
C_{s4}	-12.71	-13.57	-12.53	-11.30	-9.92	-5.21
C_7	0.09	0.10	0.01	0.01	0.01	0.05
C_{s8}	-8.10	-0.62	-0.61	-0.60	-0.59	-0.49
C_{s9}	-	-	-	-	-0.01	0.38
$\Delta F/R_q$	-6.14	-1.72	-1.73	-1.72	-1.56	-1.46

$\epsilon = 5$ for $q = 12 - 22$

TABLE 9.6 (Continued) DELTA WING OPTIMIZATION WITH STRESS AND THICKNESS CONSTRAINTS

Given R_q	0.1	0.1	0.1	0.1	0.1
R_q	.098	0.1	0.1	0.1	0.098
Design No. (q)	18	19	20	21	22
ρ_1	0.2330	0.1594	0.1022	0.1543	0.1000
ρ_2	0.1	0.1	0.1	0.1	0.1
ρ_3	0.1	0.1	0.1	0.1	0.1
ρ_4	0.6248	0.6120	0.6603	0.6123	0.6589
ρ_5	0.1334	0.1132	0.1207	0.1115	0.1195
ρ_6	0.1	0.1	0.1	0.1	0.1
ρ_7	1.7754	1.8032	1.7417	1.8039	1.7440
ρ_8	0.9126	0.9424	0.9253	0.9449	0.9274
ρ_9	0.1	0.1	0.1	0.1	0.1
ρ_{10}	0.2534	0.3019	0.2856	0.3110	0.2887
$F(\underset{\sim}{\rho})$	8.874	8.807	8.811	8.810	8.808
Thc. Con.	2,3,6,9	2,3,6,9	2,3,6,9	2,3,6,9	1,2,3,6,9
S.Con	4,7,8,9	2,4,7,8,9	2,4,7,8,9	2,4,7,8,9	2,4,7,8,9
C_{s2}	-	-3.94	-3.63	-3.37	-3.09
C_{s4}	-0.01	-0.06	0.01	0.00	0.01
C_{s7}	0.05	-0.01	0.00	0.01	0.01
C_{s8}	-0.39	-0.30	-0.30	-0.31	-0.31
C_{s9}	0.35	0.72	0.08	0.15	0.12
$\Delta F/R_q$		-0.67	+0.04	-0.01	-0.01

$\varepsilon = 5$ for q = 12 - 22

Fig. 9.4 Progress of Delta Wing Optimization with Stress and
Thickness Constraints

Fig. 9.5 Skin Thickness Contours for Minimum-Weight
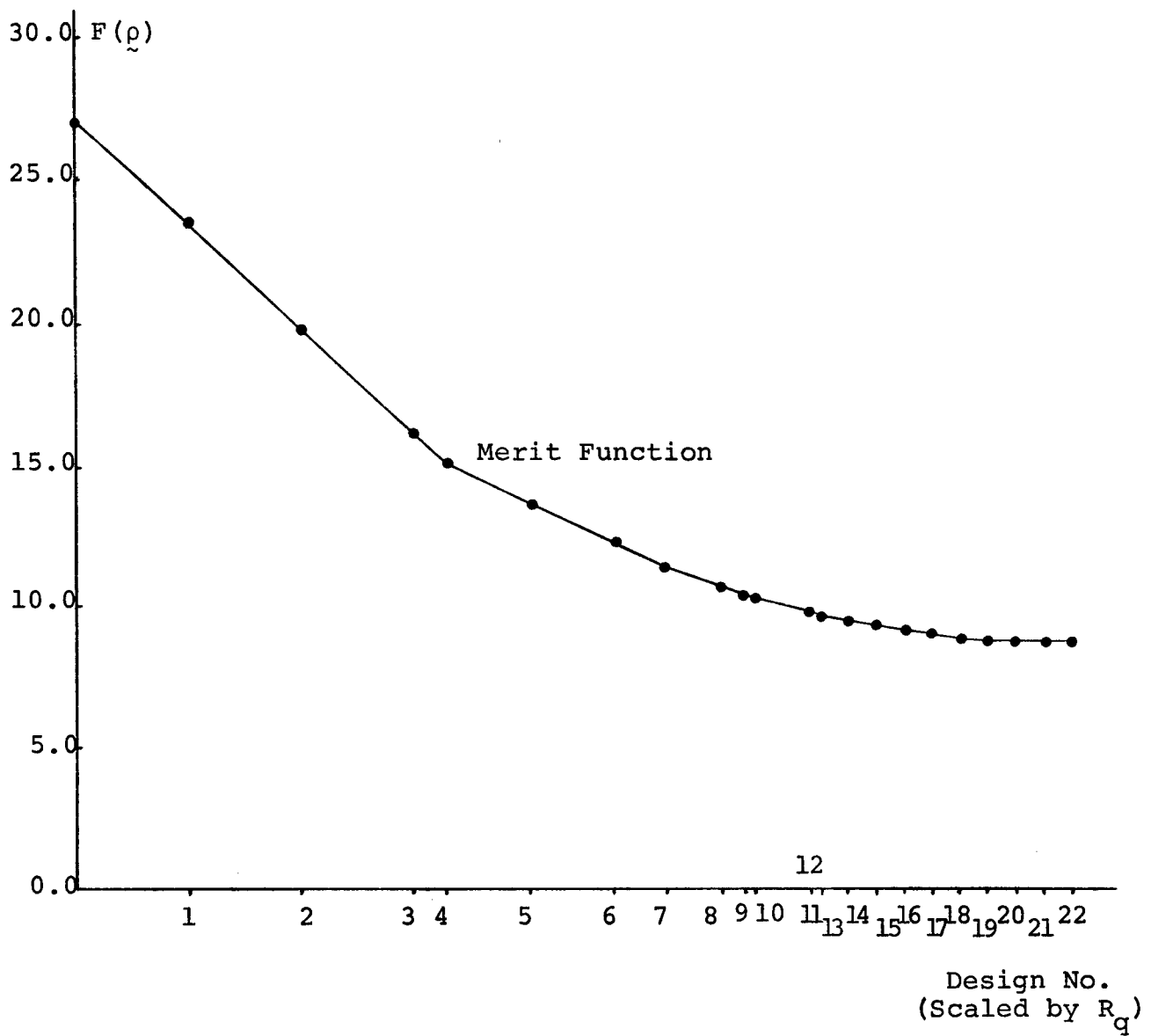Design with Stress and Thickness Constraints

$F(\rho_{22}) = 8.808$ correspond to 67.5% structural and 54% total weight reduction.

In figure 9.4 the merit function $F(\rho)$ is plotted against step sizes. Again it can be seen that the improvement in the merit function after 11th design step is poor compared to the number of design cycles. $F(\rho_{11}) = 9.884$ approximately correspond to 94% of the weight reduction achieved at 22nd design step. Using smaller step sizes and greater number of design cycles best possible was to obtain $F(\rho) = 8.765$ with similar thickness distribution.

Skin thickness contours corresponding to the minimum-weight design (ρ_{22}) satisfying stress and thickness constraints are presented in figure 9.5.

9.4.3 Optimization with Flutter, Stress and Thickness Constraints

Finally the delta wing was optimized to satisfy the flutter, stress and thickness constraints. The flutter constraint was considered active at all design steps, stress and thickness constraints became active as they were violated.

Table 9.7 presents the results for 18 design steps. These results were obtained in three different computer runs, six design steps for each run. On the CDC 6600 each design cycle took approximately 24.5 seconds which included the calculation of the flutter constraint, the flutter constraint gradients, the critical stress constraints, the gradients of the critical stress constraints, critical thickness constraints and

TABLE 9.7 DELTA WING OPTIMIZATION WITH FLUTTER STRESS AND THICKNESS CONSTRAINTS

Given R_q	0.4	0.4	0.4	0.3	0.3	
R_q	0.4	0.4	0.4	0.263	0.3	
Design No. (q)	0	1	2	3	4	5
ρ_1	1.000	0.9649	0.9341	0.9107	0.9051	0.8695
ρ_2	1.000	0.8935	0.7970	0.7181	0.7031	0.5729
ρ_3	1.000	0.9444	0.9125	0.9089	0.9164	0.9245
ρ_4	1.000	0.9252	0.8504	0.7769	0.7513	0.7261
ρ_5	1.000	0.8439	0.6806	0.5011	0.3275	0.2710
ρ_6	1.000	1.0836	1.1509	1.1886	1.1597	0.9637
ρ_7	1.000	1.0643	1.1219	1.1702	1.1890	1.2886
ρ_8	1.000	0.8117	0.6211	0.4344	0.3477	0.4381
ρ_9	1.000	0.7623	0.5159	0.2603	0.1000	0.1
ρ_{10}	1.000	0.8938	0.7860	0.6783	0.6161	0.5096
$F(\underset{\sim}{\rho})$	27.000	24.248	21.469	18.627	16.610	15.469
$\beta_f/\omega o$	0.075	-0.078	-0.079	-0.081	-0.084	-0.080
$\omega_f/\omega o$	19.35	18.67	17.93	17.16	16.84	18.13
C_f	0.00	-0.153	-0.154	-0.156	-0.159	-0.155
Thc. Con.	–	–	–	–	9	9
S.Con.	7	7	7	4,7	4,7,8	4,7,8
C_{s2}	–	–	–	–	–	–
C_{s4}	–	–	–	-23.0	-23.11	-22.83
C_{s7}	0.00	-0.21	-.56	-1.35	-2.08	-2.16
C_{s8}	–	–	–	–	-21.85	-21.32
$\Delta F/R_q$	-6.88	-6.95	-7.11	-7.66	-3.80	-3.26

$\varepsilon = 25$ for $q = 0 - 5$

TABLE 9.7 (Continued) DELTA WING OPTIMIZATION
WITH FLUTTER STRESS AND THICKNESS CONSTRAINTS

Given R_q	0.3	0.2	0.2	0.2	0.2	0.2
R_q	0.3	0.088	0.137	0.108	0.2	0.2
Design No. (q)	6	7	8	9	10	11
ρ_1	0.8086	0.7953	0.7665	0.7417	0.7402	0.7112
ρ_2	0.3855	0.3533	0.2941	0.2145	0.2324	0.2400
ρ_3	0.9599	0.9190	0.8763	0.9135	1.0004	1.0803
ρ_4	0.7084	0.7026	0.7160	0.6974	0.6893	0.7072
ρ_5	0.1770	0.1416	0.1000	0.1	0.1	0.1
ρ_6	0.9066	0.8672	0.8004	0.7660	0.6035	0.4475
ρ_7	1.3985	1.4144	1.4543	1.4855	1.4833	1.4581
ρ_8	0.5489	0.5082	0.5680	0.5822	0.5873	0.5942
ρ_9	0.1	0.1	0.1	0.1	0.1	0.1
ρ_{10}	0.3950	0.3837	0.3500	0.3266	0.2515	0.1656
$F(\underset{\sim}{\rho})$	14.492	13.794	13.235	12.975	12.714	12.442
$\beta_f/\omega o$	-0.083	-0.084	-0.086	-0.086	-0.086	-0.090
$\omega_f/\omega o$	17.78	17.92	18.24	17.98	19.29	20.36
C_f	-0.158	-0.159	-0.161	-0.161	-0.161	-0.165
Thc. Con.	9	9	5,9	5,9	5,9	5,9
S.Con.	7	7,8	7,8	2,7,8	2,7,8	2,7,8
C_{s2}	-	-22.31	-23.26	-3.74	-4.03	-4.30
C_{s4}	-22.37	-21.01	-22.42	-17.92	-18.26	-18.43
C_{s7}	-2.14	-2.11	-2.10	-2.06	-2.00	-1.91
C_{s8}	-20.71	-3.32	-2.93	-2.77	-2.34	-1.82
$\Delta F/R_q$	-7.92	-4.07	-2.42	-1.31	-1.36	-2.60

$\varepsilon = 15$ for q = 6 - 11

TABLE 9.7 (Continued) DELTA WING OPTIMIZATION
WITH FLUTTER STRESS AND THICKNESS CONSTRAINTS

Given R_q	0.2	0.1	0.1	0.1	0.1	0.1	0.1
R_q	0.2	0.024	0.1	0.1	0.1	0.047	0.1
Design No. (q)	12	13	14	15	16	17	18
ρ_1	0.6776	0.6740	0.6565	0.6403	0.6297	0.6186	0.6018
ρ_2	0.2238	0.2204	0.2074	0.1910	0.1856	0.1627	0.1450
ρ_3	1.0757	1.0574	0.9636	0.8859	0.8115	0.7828	0.7120
ρ_4	0.7342	0.7348	0.7358	0.7392	0.7351	0.7340	0.7383
ρ_5	0.1	0.1	0.1	0.1	0.1	0.1	0.1
ρ_6	0.2649	0.2549	0.2555	0.2093	0.2741	0.2561	0.2014
ρ_7	1.4519	1.4567	1.4762	1.4978	1.5081	1.5220	1.5426
ρ_8	0.6292	0.6355	0.6540	0.6827	0.6803	0.6947	0.7256
ρ_9	0.1	0.1	0.1	0.1	0.1	0.1	0.1
ρ_{10}	0.1086	0.1000	0.1	0.1	0.1	0.1	0.1
$F(\rho)$	11.922	11.839	11.582	11.262	11.198	11.032	10.711
$\beta_f/\omega o$	-0.100	0.356	-0.092	4.928	-0.025	-0.028	5.549
$\omega_f/\omega o$	21.77	39.41	22.78	39.07	24.77	25.06	37.15
c_f	-0.175	0.280	-0.167	4.852	-0.100	-0.103	5.474
Thc. Con.	5,9	5,9,10	5,9,10	5,9,10	5,9,10	5,9,10	5,9,10
S.Con.	2,7,8	2,7,8	2,7,8	2,7,8	7,8	2,7,8	2,7,8
c_{s2}	-4.54	-4.55	-4.70	-4.81	-5.06	-.31	-.45
c_{s4}	-18.27	-18.19	-17.82	-17.42	-16.89	-15.65	-15.08
c_{s7}	-1.79	-1.79	-1.79	-1.78	-1.71	-1.71	-1.70
c_{s8}	-.82	-.82	-.73	-.58	-.27	-.24	-.07
$\Delta F/R_q$		-3.37	-2.58	-3.19	-0.65	-3.54	-3.20

$\varepsilon = 5$ for $q = 12 - 18$

their gradients and the calculation of $\Delta\rho_{\sim q}$ using the gradient projection algorithm. In the determination of active stress constraints, $\varepsilon = 25$ was used for the first run, $\varepsilon = 15$ was used for the second run and $\varepsilon = 5$ was used for the last run. The reductions in R_3, R_7, R_{12} are for thickness constraint violations at nodal points 9, 5 and 10 respectively. The reductions in R_6, R_8, R_{16} are for stress constraint violations at nodal points 8, 2 and 2 respectively.

From table 9.7 it can be seen that until the 12th design step the flutter constraint is closely followed within the feasible region. At design step 13, 15 and 18 the flutter occurs between second and third modes. It is easier to observe this phenomenon from table 9.8 where first three eigenvalue pairs during the optimization are given. As has previously been discussed for the optimization with only flutter and thickness constraints; the imaginary parts of the second and third eigenvalue pairs come closer during the optimization until the 13th design step where they are close enough for the flutter to occur.

At the 17th design step the merit function is $F(\rho_{\sim 17}) = 11.032$, which is minimum among feasible designs. This correspond to 59.2% structural and 47.4% total weight reduction. This time the merit function at the 11th design step, $F(\rho_{\sim 11}) = 12.442$, corresponds to 91% of the weight reduction achieved at 17th design step. Using smaller step sizes and greater number of design steps, best design obtained had a merit function $F(\rho_{\sim}) = 10.990$. The corresponding thickness dis-

TABLE 9.8   FIRST THREE EIGENVALUE PAIRS
DURING OPTIMIZATION

Design No. (q)	$\lambda_1 = (\beta_1 \mp i\, \omega_1)/\omega_0$	$\lambda_2 = (\beta_2 \mp i\, \omega_2)/\omega_0$	$\lambda_3 = (\beta_3 \mp i\, \omega_3)/\omega_0$
0	$0.075 \mp i\ 19.35$	$-0.322 \mp i\ 19.35$	$-0.123 \mp i\ 38.03$
5	$-0.080 \mp i\ 18.13$	$-0.236 \mp i\ 24.59$	$-0.243 \mp i\ 42.38$
10	$-0.086 \mp i\ 19.29$	$-0.295 \mp i\ 26.53$	$-0.289 \mp i\ 41.44$
11	$-0.090 \mp i\ 20.36$	$-0.332 \mp i\ 29.32$	$-0.311 \mp i\ 42.15$
12	$-0.100 \mp i\ 21.77$	$-0.437 \mp i\ 37.22$	$-0.333 \mp i\ 40.72$
13	$-0.100 \mp i\ 21.97$	$-1.143 \mp i\ 39.14$	$+0.356 \mp i\ 39.41$
14	$-0.092 \mp i\ 22.78$	$-0.636 \mp i\ 38.05$	$-0.169 \mp i\ 39.17$
15	$-0.094 \mp i\ 23.80$	$-5.762 \mp i\ 38.96$	$+4.928 \mp i\ 39.07$
16	$-0.025 \mp i\ 24.77$	$-0.517 \mp i\ 32.98$	$-0.352 \mp i\ 40.34$
17	$-0.028 \mp i\ 25.06$	$-0.576 \mp i\ 34.52$	$-0.314 \mp i\ 38.96$
18	$-0.050 \mp i\ 26.32$	$-6.453 \mp i\ 37.05$	$+5.549 \mp i\ 37.15$
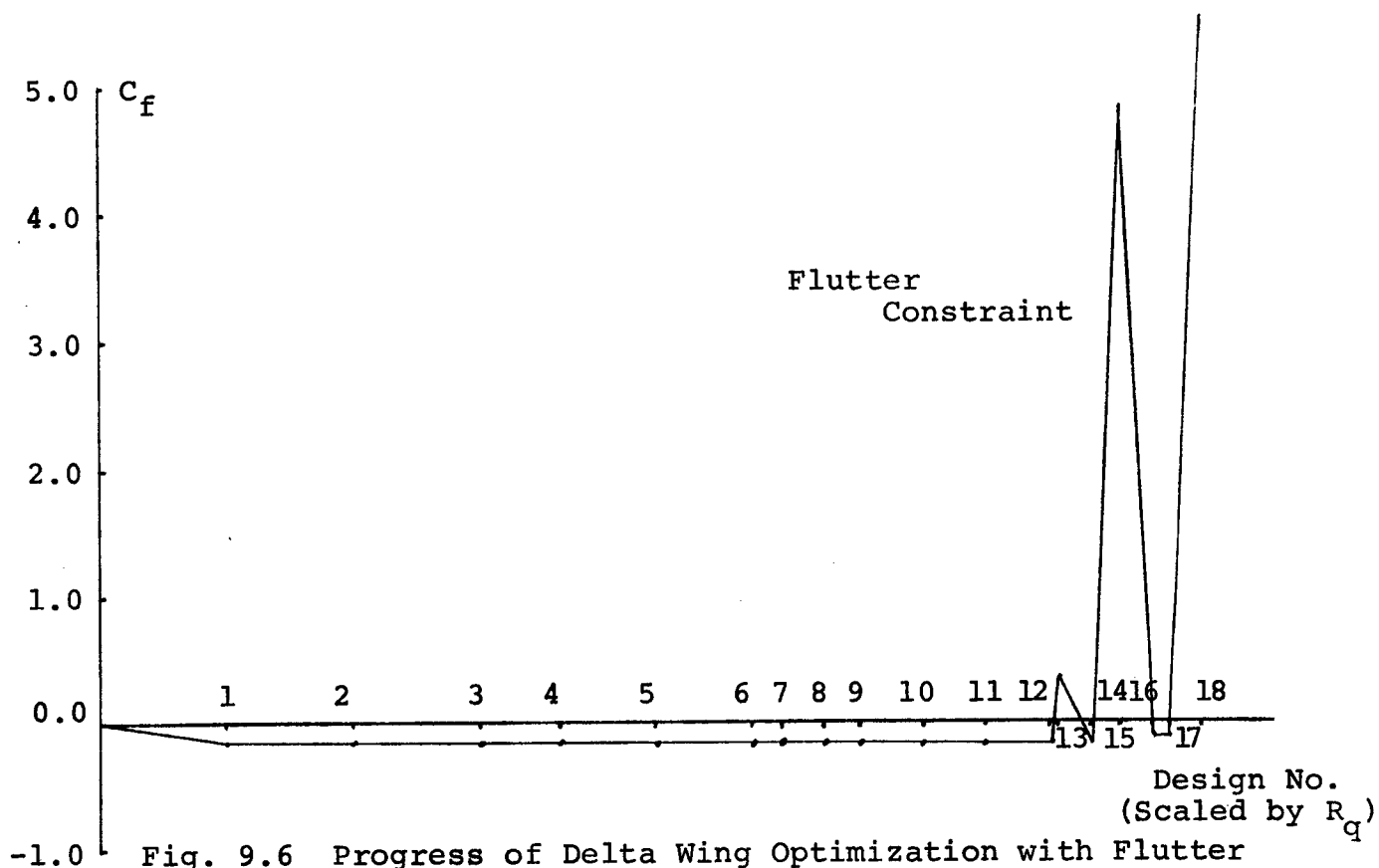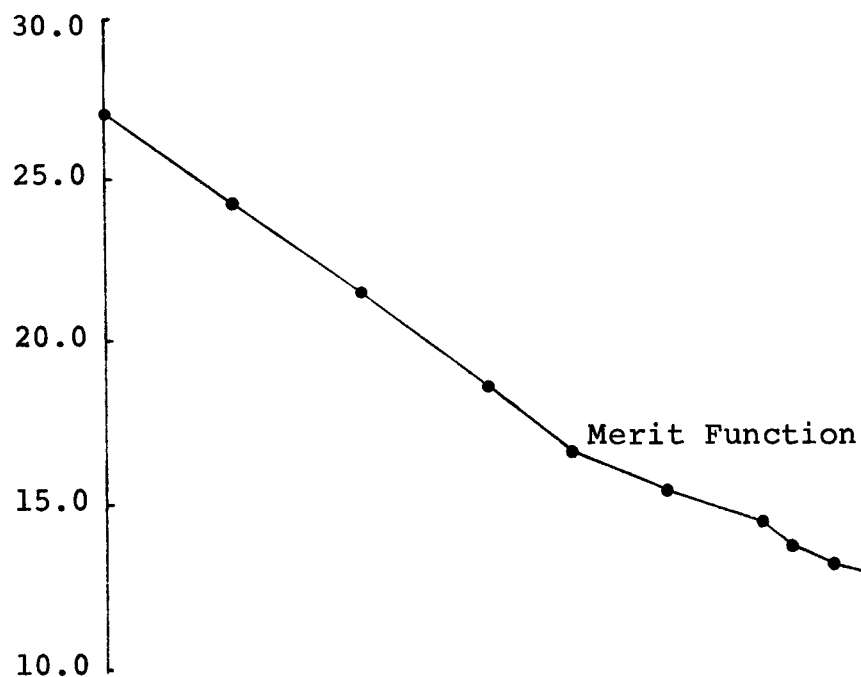
Fig. 9.6 Progress of Delta Wing Optimization with Flutter
Stress and Thickness Constraints
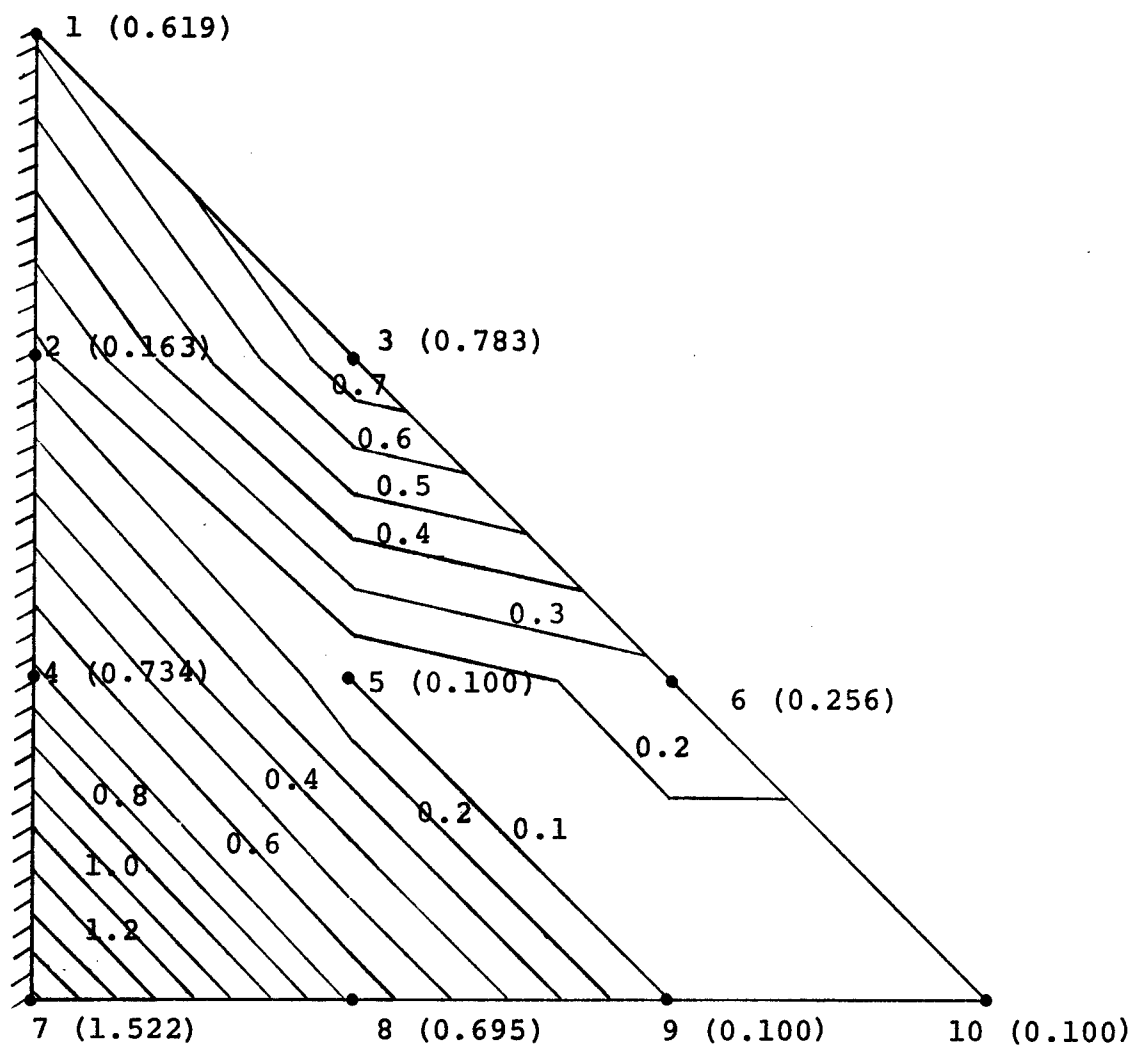
Fig. 9.7 Skin Thickness Contours for Minimum - Weight
Design with Flutter, Stress and Thickness Constraints

tribution was very close to the ρ_{17} of table 9.7.

In figure 9.6 the merit function $F(\rho)$ and flutter constraint C_f are plotted against step sizes. The kink at the merit function plot for design number 6 is due to the reduction of ε from 25 to 15 which releases some of the active stress constraints.

Skin thickness contours corresponding to the minimum-weight design (ρ_{17}) satisfying flutter, stress and thickness constraints are presented in figure 9.7.

9.5 Discussion of Results

The same step size, R_q, pattern was used to obtain the minimum-weight designs of a cantilevered delta wing with three different set of constraints. Each time more than 90% of the total weight reduction was obtained within 11 design cycles. It was found out that with a little experience with a particular optimization problem; the determination of a suitable step size pattern is not very difficult. Experiences with different step size patterns also showed that the number of design cycles and the final minimum-weight design are not very sensitive to small changes in step size patterns. These results are very encouraging as to the capabilities of the multi-constraint gradient projection algorithm.

It was also found out that the minimum-weight design for stress and thickness requirements is radically different from the minimum-weight design for flutter and thickness re-quirements. This substantiates the results reported by the

Langley Research Center (Ref. 29).

Experimenting with stress optimization showed that using a large value for ε initially and then gradually reducing it is effective in reducing the number of design steps required to obtain the minimum-weight design.

The observation of the flutter constraint revealed that towards the end of the optimization procedure, flutter involving modes other than the initial two modes does occur. However it also became evident that any improvement in merit function, after such phenomenon is encountered, would be insignificant unless, possibly multiple flutter constraints were employed. This possibility has not been investigated within the scope of this study.

It is interesting to note that a design was formed by taking the larger of the two nodal point thicknesses between the minimum-weight design which only satisfy stress and thickness constraints and the minimum-weight design which only satisfy flutter and thickness constraints. This design had a merit function $F(\rho) = 11.292$ and satisfied all stress constraints but failed to satisfy the flutter constraint.

CHAPTER 10

CONCLUSIONS AND SUGGESTIONS

10.1 Conclusions

The conclusions obtained from this study can be summarized as follows:

1. The proposed procedures for handling the flutter constraint has been proved to be very satisfactory.

2. The analytical expressions for the calculation of flutter and stress constraint gradients proved to be both accurate and time saving.

3. The proposed optimization algorithm which is based on gradient projection concept, was proved to be very effective in obtaining approximate feasible minimum-weight designs within few (10-11) design cycles. It was also found out that the efficiency decreases as the optimum design is approached.

4. Experience with panel and delta wing optimization problems suggested that establishing a step size pattern for a particular structural optimization problem is not a very difficult task and that once this pattern is set, it can be used to optimize the same structural model with different combinations of constraints. However, more research is required in order to establish more concrete conclusions.

5. Results of panel optimization indicated that the effect of damping on minumum-weight designs was negligible for

practical damping values. However results also suggested that large savings are possible for members where a high structural damping is introduced for special reasons.

6. Results of delta wing optimization showed that optimum designs for stress and for flutter requirements are radically different. This fact provides the motivation for combined (aeroelastic-stress) optimization approach.

10.2 Suggestions for Further Research

Several suggestions for the extension of this work are listed in the following:

1. Introduction of the capability to handle multiple flutter constraints: The results of cantilevered delta wing optimization showed that; a) flutter could occur between modes other than the initial two modes. b) multiple mode pairs could be involved at a particular design step. Such a capability therefore could be very effective in handling such situations and possibly will produce better designs.

2. Introduction of a procedure to determine the step sizes automatically: It is conceivable that a procedure can be developed which automatically determines step sizes, possibly using constraint gradient information of earlier design steps. However for the present it seems that the best method to determine the step size pattern for an unfamiliar structural optimization problem is to run the optimization interactively.

3. Introduction of modal representation to reduce the

size of the eigenvalue problem which represents the flutter constraint. Such a development would involve the calculation of required number of natural modes and the reduction of system matrices using these modes. Relative effectiveness of, keeping the initial mode shapes throughout the entire optimization or updating the mode shapes as the design changes, should be investigated.

4. A study should be conducted to determine the relative efficiency of the different optimization algorithms on aeroelastic-stress optimization problems.

APPENDIX A

CONSTANT THICKNESS SANDWICH BEAM ELEMENT
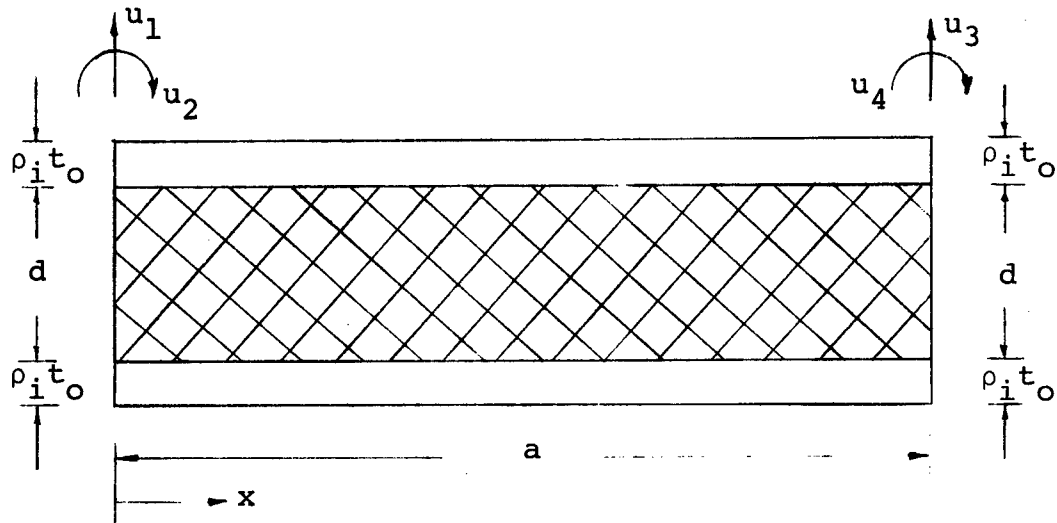
Fig. A.1 Constant Thickness Sandwich Beam Element

Figure A.1 shows the cross section and the degrees of freedom of typical element. A design variable ρ_i is associated with each element. We have

$$\rho(x) \;=\; \rho_i \qquad\qquad (A.1)$$

and

$$F_e(\rho) \;=\; \rho_i \qquad\qquad (A.2)$$

where $F_e(\rho)$ is the merit function associated with an element.

In the following, non-dimensional element stiffness, mass, aerodynamic and damping matrices are given in the form that they were employed in equations (5.3) and (5.4).

A.1 Stiffness Matrix

$$\bar{\underset{\approx}{K}}_e(\rho) = \rho_i \begin{bmatrix} 12 & 6 & -12 & 6 \\ 6 & 4 & -6 & 2 \\ -12 & -6 & 12 & -6 \\ 6 & 2 & -6 & 4 \end{bmatrix} \tag{A.3}$$

A.2 Mass Matrix

$$\bar{\underset{\approx}{M}}_e(\rho) = (\rho\,\eta + 1 - \eta)/420n_e^4 \begin{bmatrix} 156 & 22 & 54 & -13 \\ 22 & 4 & 13 & -3 \\ 54 & 13 & 156 & -22 \\ -13 & -3 & -22 & 4 \end{bmatrix} \tag{A.4}$$

·where η is same as defined in equation (3.8)

A.3 Aerodynamic Matrix

$$\bar{\underset{\approx}{A}}_e = \frac{1}{60n_e^3} \begin{bmatrix} -30 & 6 & 30 & -6 \\ -6 & 0 & 6 & -1 \\ -30 & -6 & 30 & 6 \\ 6 & 1 & -6 & 0 \end{bmatrix} \tag{A.5}$$

A.4 Damping Matrix

$$\underset{\approx}{\bar{D}}_e = \frac{1}{420n_e{}^4} \begin{bmatrix} 156 & 22 & 54 & -13 \\ 22 & 4 & 13 & -3 \\ 54 & 13 & 156 & -22 \\ -13 & -3 & -22 & 4 \end{bmatrix} \qquad (A.6)$$

In all the above expressions n_e is

$$n_e = \frac{\ell}{a} \qquad (A.7)$$

where ℓ has the same meaning as was defined in Chapter 5, section 5.1. For the panel problem, ℓ was taken to be the span length.
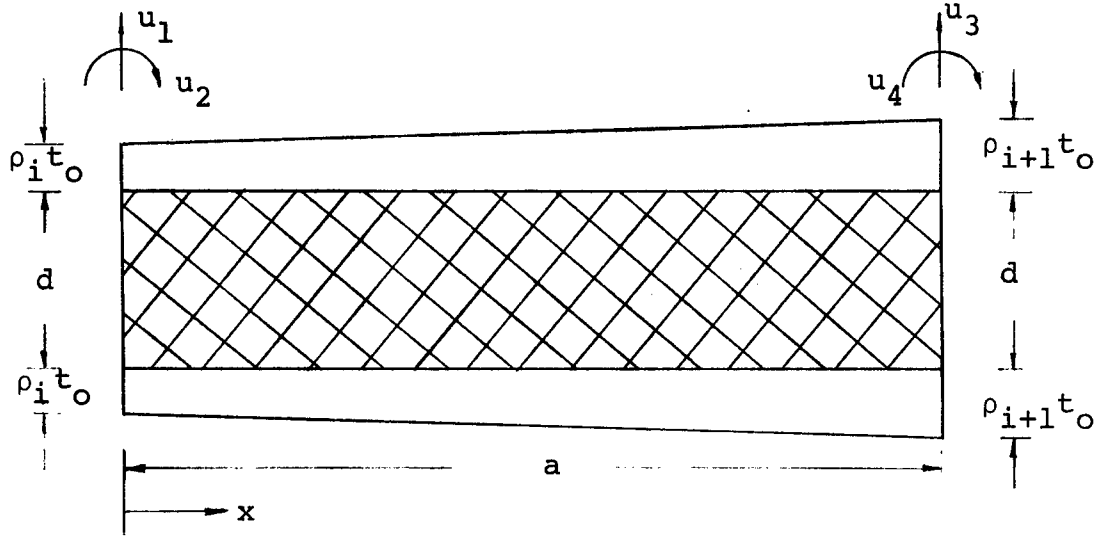
TAPERED SANDWICH BEAM ELEMENT

Fig. B.1   Tapered Sandwich Beam Element

Figure B.1 shows the main properties of a typical element.   A design variable ρ_i is associated with each nodal point and we have

$$\rho(x) \;=\; \rho_i \;+\; (\rho_{i+1} - \rho_i)x/a \qquad\qquad \text{(B.1)}$$

and

$$F_e(\rho) \;=\; \tfrac{1}{2}(\rho_i + \rho_{i+1}) \qquad\qquad \text{(B.2)}$$

Non-dimensional element stiffness, mass, aerodynamic and damping matrices as they were used in equations (5.3) and (5.4) are given in the following.

B.1 Stiffness Matrix

$$\bar{\underset{\sim}{K}}_e(\rho) = \rho_i \begin{bmatrix} 12 & 6 & -12 & 6 \\ 6 & 4 & -6 & 2 \\ -12 & -6 & 12 & -6 \\ 6 & 2 & -6 & 4 \end{bmatrix} + (\rho_{i+1}-\rho_i) \begin{bmatrix} 6 & 2 & -6 & 4 \\ 2 & 1 & -2 & 1 \\ -6 & -2 & 6 & -4 \\ 4 & 1 & -4 & 3 \end{bmatrix} \quad (B.3)$$

B.2 Mass Matrix

$$\bar{\underset{\sim}{M}}_e(\rho) = \frac{(\rho_i\eta + 1-\eta)}{420 n_e^4} \begin{bmatrix} 156 & 22 & 54 & -13 \\ 22 & 4 & 13 & -3 \\ 54 & 13 & 156 & -22 \\ -13 & -3 & -22 & 4 \end{bmatrix}$$

$$+ \frac{(\rho_{i+1} - \rho_i)\eta}{840 n_e^4} \begin{bmatrix} 72 & 14 & 54 & -12 \\ 14 & 3 & 14 & -3 \\ 54 & 14 & 240 & -30 \\ -12 & -3 & -30 & 5 \end{bmatrix} \quad (B.4)$$

where η is same as defined in equation (3.8)

B.3 Aerodynamic Matrix

$$\underset{\sim}{\bar{A}}e = \frac{1}{60n_e^3}\begin{bmatrix} -30 & 6 & 30 & -6 \\ -6 & 0 & 6 & -1 \\ -30 & -6 & 30 & 6 \\ 6 & 1 & -6 & 0 \end{bmatrix} \tag{B.5}$$

B.4 Damping Matrix

$$\underset{\sim}{\bar{D}}e = \frac{1}{420n_e^4}\begin{bmatrix} 156 & 22 & 54 & -13 \\ 22 & 4 & 13 & -3 \\ 54 & 13 & 156 & -22 \\ -13 & -3 & -22 & 4 \end{bmatrix} \tag{B.6}$$

In all the above expressions n_e is

$$n_e = \frac{\ell}{a} \tag{B.7}$$

where ℓ is a convenient scaling dimension as was defined in section 5.1. For the panel problem the span length ℓ was used for this purpose.

APPENDIX C

HIGH PRECISION TRIANGULAR SANDWICH PLATE BENDING
ELEMENT WITH LINEAR THICKNESS VARIATION

Figure C.1 shows the plan view of a typical element. It has a core of constant thickness d and cover skins with linear thickness variation. Each nodal point has 6 degrees of freedom $(W, W_x, W_y, W_{xx}, W_{xy}, W_{yy})$. The deflection $W(\xi, \eta)$ within a triangular element is taken as a quintic polynomial (Ref. 22).

$$W(\xi, \eta) = a_1 + a_2\xi + a_3\eta + a_4\xi^2 + a_5\xi\eta + a_6\eta^2 + a_7\xi^3$$
$$+ a_8\xi^2\eta + a_9\xi\eta^2 + a_{10}\eta^3 + a_{11}\xi^4 + a_{12}\xi^3\eta$$
$$+ a_{13}\xi^2\eta^2 + a_{14}\xi\eta^3 + a_{15}\eta^4 + a_{16}\xi^5 + a_{17}\xi^3\eta^2$$
$$+ a_{18}\xi^2\eta^3 + a_{19}\xi\eta^4 + a_{20}\eta^5 \qquad (C.1)$$

or

$$W(\xi, \eta) = \sum_{i=1}^{20} a_i \, \xi^{m_i} \eta^{n_i} \qquad (C.2)$$

For vectors

$$\underset{\sim}{a}^T = \{a_1, a_2, \ldots, a_{20}\} \qquad (C.3)$$

and

$$\underset{\sim}{W}_e^T = \{W_1, W_{x1}, W_{y1}, W_{xx1}, W_{xy1}, W_{yy1}, W_2, \ldots, W_3, \ldots\} \qquad (C.4)$$

we have the relationship

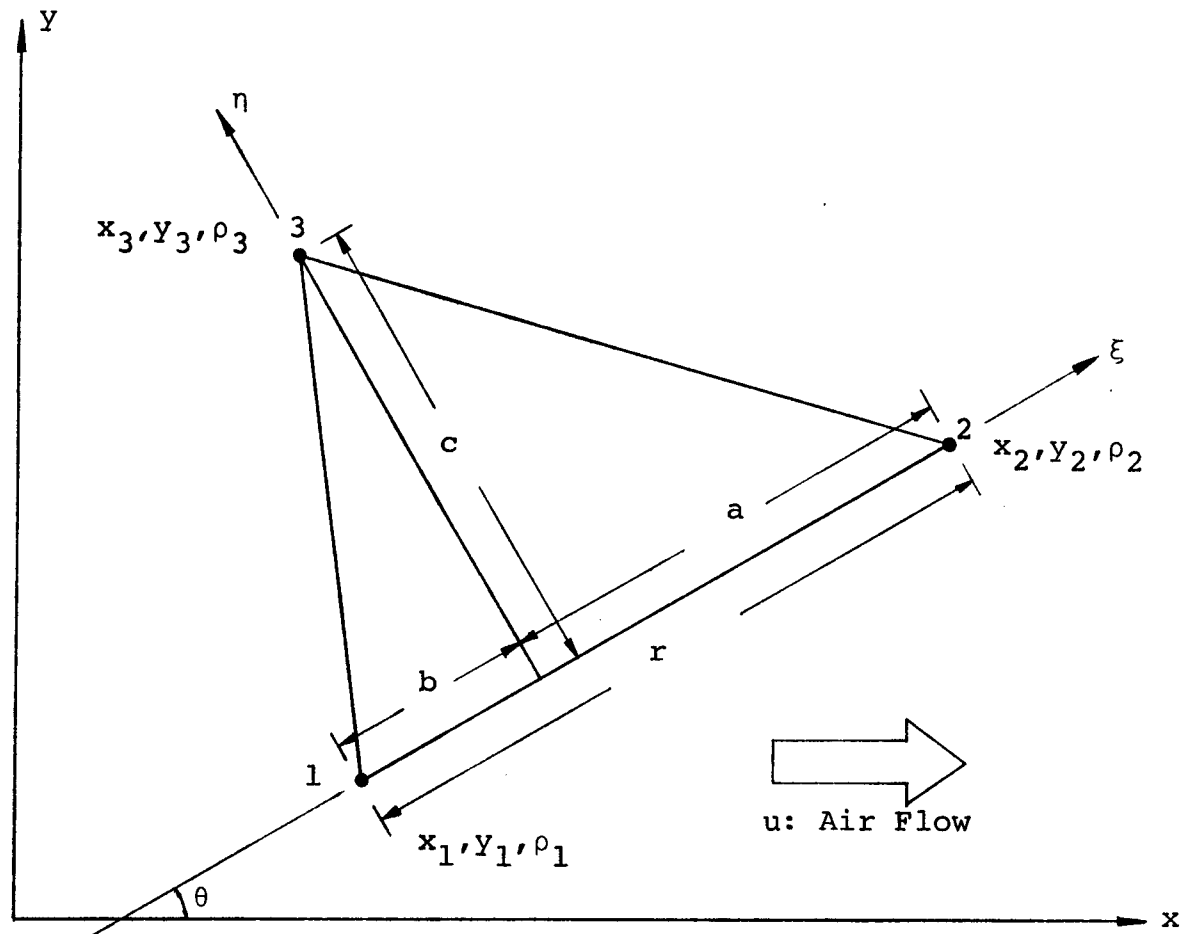$$\underset{\sim}{a} = \underset{\approx}{T} \, \underset{\approx}{R} \, \underset{\sim}{W}_e \qquad (C.5)$$

135

Fig. C.1   Triangular Sandwich Plate Bending Element

where $\underset{\sim}{R}$ transforms nodal point degree of fredoms from local

coordinates (ξ,η) to global coordinates (x,y), and $\underset{\sim}{T}$ transforms

polynomial coefficients to nodal point degree of freedoms in

local coordinates. Details of the derivation of $\underset{\sim}{T}(a,b,c)$ and

$\underset{\sim}{R}(\theta)$ can be found in reference 22 where $\underset{\sim}{T}^{-1}$ is given in table

1 and $\underset{\sim}{R}$ is given in table 2.

Using equation (C.5) for $\underset{\sim}{a}$ we can write,

$$W(\xi,\eta) \;=\; \underset{\sim}{\Phi}^T \; \underset{\approx}{T} \; \underset{\approx}{R} \; \underset{\sim}{W}_e \tag{C.6}$$

where

$$\underset{\sim}{\Phi}^T \;=\; \{\xi^{m_1}\eta^{n_1}, \; \xi^{m_2}\eta^{n_2}, \ldots, \; \xi^{m_{20}}\eta^{n_{20}}\} \tag{C.7}$$

with

$$\underset{\sim}{m}^T \;=\; \{0,1,0,2,1,0,3,2,1,0,4,3,2,1,0,5,3,2,1,0\} \tag{C.7a}$$

and

$$\underset{\sim}{n}^T \;=\; \{0,0,1,0,1,2,0,1,2,3,0,1,2,3,4,0,2,3,4,5\} \tag{C.7b}$$

which gives us $W(\xi,\eta)$ in terms of nodal point degree of freedoms.

For linear cover skin thickness variation we can
write $\rho(\xi,\eta)$ as

$$\rho(\xi,\eta) \;=\; \{1 \; \xi \; \eta\} \begin{Bmatrix} \alpha_1 \\ \alpha_2 \\ \alpha_3 \end{Bmatrix} \tag{C.8}$$

From equation (C.8) we obtain;

$$\begin{Bmatrix} \rho_1 \\ \rho_2 \\ \rho_3 \end{Bmatrix} \;=\; \begin{bmatrix} 1 & -b & 0 \\ 1 & a & 0 \\ 1 & 0 & c \end{bmatrix} \begin{Bmatrix} \alpha_1 \\ \alpha_2 \\ \alpha_3 \end{Bmatrix} \tag{C.9}$$

138

or

$$\begin{Bmatrix} \alpha_1 \\ \alpha_2 \\ \alpha_3 \end{Bmatrix} = \begin{bmatrix} a/r & b/r & 0 \\ -1/r & 1/r & 0 \\ -a/cr & -b/cr & 1/c \end{bmatrix} \begin{Bmatrix} \rho_1 \\ \rho_2 \\ \rho_3 \end{Bmatrix} \qquad (C.10)$$

where $r = a + b$ (Fig. C.1). Thus we have

$$\rho(\xi,\eta) = \{1 \;\; \xi \;\; \eta\} \begin{bmatrix} a/r & b/r & 0 \\ -1/r & 1/r & 0 \\ -a/cr & -b/cr & 1/c \end{bmatrix} \begin{Bmatrix} \rho_1 \\ \rho_2 \\ \rho_3 \end{Bmatrix} \qquad (C.11)$$

which gives us $\rho(\xi,\eta)$ in terms of nodal point design parameters.

In the following the element stiffness, mass, aerodynamic and damping matrices are developed based on the above relations and the formulas given in reference 22 for a constant thickness plate.

C.1 Stiffness Matrix

Using classical bending theory of plates, we can write the strain energy for an element as

$$U_e = \frac{1}{2}D_o \iint\limits_{A_e} \rho(\xi,\eta)\{W_{\xi\xi}^2 + W_{\eta\eta}^2 + 2\nu W_{\xi\xi}W_{\eta\eta} + 2(1-\nu)W_{\xi\eta}^2\}d\xi d\eta \qquad (C.12)$$

where D_o is the initial flexural rigidity as discussed in Chapter 3, ν is the Poisson's ratio and the integration is over the area of the element.

Using expressions (C.6) for $W(\xi,\eta)$ and (C.11) for $\rho(\xi,\eta)$ and carrying the integrations over the area we obtain

$$U_e = \frac{1}{2} D_0 \underset{\sim}{W}_e^T \underset{\approx}{R}^T \underset{\approx}{T}^T \underset{\approx}{k} \underset{\approx}{T} \underset{\approx}{R} \underset{\sim}{W}_e \qquad (C.13)$$

where

$$\underset{\approx}{k} = \rho_1 \underset{\approx}{k}^1 + \rho_2 \underset{\approx}{k}^2 + \rho_3 \underset{\approx}{k}^3 \qquad (C.14)$$

The elements of $\underset{\approx}{k}^1$, $\underset{\approx}{k}^2$ and $\underset{\approx}{k}^3$ are generated in the computer according to the following expressions:

Define

$$a_{ij}^m = m_i m_j (m_i - 1)(m_j - 1) \qquad (C.15)$$

$$a_{ij}^n = n_i n_j (n_i - 1)(n_j - 1) \qquad (C.16)$$

$$a_{ij}^{mn} = 2(1 - \nu) m_i m_j n_i n_j + \nu\, m_i n_j (m_i - 1)(n_j - 1)$$
$$+ \nu\, m_j n_i (m_j - 1)(n_i - 1) \qquad (C.17)$$

$$m_{ij} = m_i + m_j \qquad (C.18)$$

$$n_{ij} = n_i + n_j \qquad (C.19)$$

Here m_i, m_j, n_i, n_j are the same as the exponents of equations (C.2) and (C.7).

Also define

$$F^1_{ij} = a^m_{ij} F(m_{ij} - 4, n_{ij}) + a^n_{ij} F(m_{ij}, n_{ij} - 4)$$
$$+ a^{mn}_{ij} F(m_{ij} - 2, n_{ij} - 2) \tag{C.20}$$

$$F^2_{ij} = a^m_{ij} F(m_{ij} - 3, n_{ij}) + a^n_{ij} F(m_{ij} + 1, n_{ij} - 4)$$
$$+ a^{mn}_{ij} F(m_{ij} - 1, n_{ij} - 2) \tag{C.21}$$

$$F^3_{ij} = a^m_{ij} F(m_{ij} - 4, n_{ij} + 1) + a^n_{ij} F(m_{ij}, n_{ij} - 3)$$
$$+ a^{mn}_{ij} F(m_{ij} - 2, n_{ij} - 1) \tag{C.22}$$

where $F(m,n)$ means (Ref. 22)

$$F(m,n) = \iint_{A_e} \xi^m \eta^n d\xi d\eta = c^{n+1} \{a^{m+1} - (-b)^{m+1}\} \frac{m!n!}{(m+n+2)!} \tag{C.23}$$

Finally we have

$$k^1_{ij} = \frac{a}{r} F^1_{ij} - \frac{1}{r} F^2_{ij} - \frac{a}{cr} F^3_{ij} \tag{C.24}$$

$$k^2_{ij} = \frac{b}{r} F^1_{ij} + \frac{1}{r} F^2_{ij} - \frac{b}{cr} F^3_{ij} \tag{C.25}$$

$$k^3_{ij} = \frac{1}{c} F^3_{ij} \tag{C.26}$$

where a, b, c and r are the element dimensions (Fig. C.1).

Thus the element stiffness matrix is

$$\underset{\sim}{K}_e = D_o \underset{\sim}{R}^T \underset{\sim}{T}^T \{\rho_1 \underset{\sim}{k}^1 + \rho_2 \underset{\sim}{k}^2 + \rho_3 \underset{\sim}{k}^3\} \underset{\sim}{T} \underset{\sim}{R} \tag{C.27}$$

or

$$\bar{\underset{\sim}{K}}_e(\rho) = \underset{\sim}{R}^T \underset{\sim}{T}^T \{\rho_1 \underset{\sim}{k}^1 + \rho_2 \underset{\sim}{k}^2 + \rho_3 \underset{\sim}{k}^3\} \underset{\sim}{T} \underset{\sim}{R} \tag{C.28}$$

C.2 Mass Matrix

For sinusoidal time dependence, the kinetic energy of an element can be written as

$$T_e = \frac{1}{2}\omega^2 \iint\limits_{A_e} m(\xi,\eta) \ W^2 \ d\xi \ d\eta \tag{C.29}$$

where ω is the frequency and $m(\xi,\eta)$ is

$$m(\xi,\eta) = m_o \{\rho(\xi,\eta)\eta_m + 1 - \eta_m\} \tag{C.30}$$

as described in Chapter 3. Here η_m is the same as η (Eq. 3.8) of the text. Substituting the expression (C.30) for $m(\xi,\eta)$ and the expression (C.6) for $W(\xi,\eta)$ in equation (C.29) and carrying out the integration we obtain;

$$T_e = \frac{1}{2}\omega^2 m_o \ \underset{\sim}{W}_e^T \ \underset{\sim}{R}^T \ \underset{\sim}{T}^T \underset{\sim}{m} \ \underset{\sim}{T} \ \underset{\sim}{R} \ \underset{\sim}{W}_e \tag{C.31}$$

where

$$\underset{\sim}{m} = \eta_m \{\rho_1 \underset{\sim}{m}^1 + \rho_2 \underset{\sim}{m}^2 + \rho_3 \underset{\sim}{m}^3\} + (1 - \eta_m)\underset{\sim}{m}^c \tag{C.32}$$

The elements of $\underset{\sim}{m}^1$, $\underset{\sim}{m}^2$, $\underset{\sim}{m}^3$ and $\underset{\sim}{m}^c$ are generated in the computer according to the following expressions:

Define

$$F_{ij}^1 = F(m_{ij}, \ n_{ij}) \tag{C.33}$$

$$F_{ij}^2 = F(m_{ij} + 1, \ n_{ij}) \tag{C.34}$$

$$F_{ij}^3 = F(m_{ij}, n_{ij} + 1) \qquad\qquad (C.35)$$

where m_{ij}, n_{ij} and $F(m,n)$ have the same meaning as in equations (C.18), (C.19) and (C.23) for the stiffness matrix. In terms of the above definitions we have

$$m_{ij}^1 = \frac{a}{r} F_{ij}^1 - \frac{1}{r} F_{ij}^2 - \frac{a}{cr} F_{ij}^3 \qquad\qquad (C.36)$$

$$m_{ij}^2 = \frac{b}{r} F_{ij}^1 + \frac{1}{r} F_{ij}^2 - \frac{b}{cr} F_{ij}^3 \qquad\qquad (C.37)$$

$$m_{ij}^3 = \frac{1}{c} F_{ij}^3 \qquad\qquad (C.38)$$

$$m_{ij}^c = F_{ij}^1 \qquad\qquad (C.39)$$

where a, b, c and r are the element dimensions (Fig. C.1).

Thus the element mass matrix is

$$\underset{\sim}{M}_e = m_0 \ \underset{\sim}{R}^T \ \underset{\sim}{T}^T \ \{\eta_m [\rho_1 \underset{\sim}{m}^1 + \rho_2 \underset{\sim}{m}^2 + \rho_3 \underset{\sim}{m}^3] + (1 - \eta_m) \ \underset{\sim}{m}^c\} \ \underset{\sim}{T} \ \underset{\sim}{R}$$
$$(C.40)$$

or

$$\underset{\sim}{\bar{M}}_e(\rho) = \underset{\sim}{R}^T \ \underset{\sim}{T}^T \ \{\eta_m [\rho_1 \underset{\sim}{m}^1 + \rho_2 \underset{\sim}{m}^2 + \rho_3 \underset{\sim}{m}^3] + (1 - \eta_m) \ \underset{\sim}{m}^c\} \ \underset{\sim}{T} \ \underset{\sim}{R}$$
$$(C.41)$$

C.3 Aerodynamic Matrix

We can use equations (4.10) and (4.11) to derive the aerodynamic matrix. Since the air flow is on both sides of the delta wing, there will be an additional factor of 2. Noting the similarity between equations (4.8) and (C.6) we can write;

$$\underset{\approx}{a}_e = 2\left[\frac{2q}{(M_\infty^2 - 1)^{1/2}}\right]\iint\limits_{A_e} \underset{\sim}{\Phi}\,\frac{\partial}{\partial x}\,\underset{\sim}{\Phi}^T\,d\xi d\eta \tag{C.42}$$

from which we can define

$$\underset{\approx}{a} = \iint\limits_{A_e} \underset{\sim}{\Phi}\,\frac{\partial}{\partial x}\,\underset{\sim}{\Phi}^T\,d\xi d\eta \tag{C.43}$$

For the angle θ (Figure C.1) between the two coordinate systems we have

$$\frac{\partial}{\partial x}\,\underset{\sim}{\Phi}^T = \frac{\partial}{\partial \xi}\,\underset{\sim}{\Phi}^T \cos\theta - \frac{\partial}{\partial \eta}\,\underset{\sim}{\Phi}^T \sin\theta \tag{C.44}$$

Using equation (C.7) for $\underset{\sim}{\Phi}^T$, we obtain

$$a_{ij} = \iint\limits_{A_e} \{m_i\,\xi^{m_i+m_j-1}\,\eta^{n_i+n_j}\cos\theta - n_i\,\xi^{m_i+m_j}\,\eta^{n_i+n_j-1}\sin\theta\}d\xi d\eta \tag{C.45}$$

or

$$a_{ij} = m_i\,F(m_{ij}-1,\,n_{ij})\cos\theta - n_i\,F(m_{ij},\,n_{ij}-1)\sin\theta \tag{C.46}$$

where m_{ij}, n_{ij} and $F(m,n)$ have the same meaning as in equations (C.18), (C.19) and (C.23) for the stiffness matrix. From the above definitions we can write

$$\underset{\approx}{\bar{A}}_e = 2\,\underset{\approx}{R}^T\,\underset{\approx}{T}^T\,\underset{\approx}{a}\,\underset{\approx}{T}\,\underset{\approx}{R} \tag{C.47}$$

C.4 Damping Matrix

Using equation (4.13) and replacing $\underset{\sim}{f}$ by $\underset{\sim}{\Phi}$ we can write

$$\underset{\approx}{d}_e = 2\left(\frac{2q}{u}\frac{M_\infty^2 - 2}{(M_\infty^2-1)^{3/2}}\right)\mu \iint_{A_e} \underset{\sim}{\Phi}\ \underset{\sim}{\Phi}^T\ d\xi d\eta \qquad (C.48)$$

where the factor 2 accounts for the air flow on both sides of the element. We can define

$$\underset{\approx}{d} = \iint_{A_e} \underset{\sim}{\Phi}\ \underset{\sim}{\Phi}^T\ d\xi d\eta \qquad (C.49)$$

and using equation (C.7) for $\underset{\sim}{\Phi}^T$ we obtain

$$d_{ij} = \iint_{A_e} \xi^{m_i+m_j}\ \eta^{n_i+n_j}\ d\xi d\eta \qquad (C.50)$$

or

$$d_{ij} = F(m_{ij}, n_{ij}) = m_{ij}^C \qquad (C.51)$$

where m_{ij}^C was defined by equations (C.33) and (C.39). From the above expressions and from equation (4.12) we obtain

$$\underset{\approx}{\bar{D}}_e = 2\underset{\sim}{R}^T\ \underset{\approx}{T}^T\ \underset{\approx}{m}^C\ \underset{\approx}{T}\ \underset{\sim}{R} \qquad (C.52)$$

It should be noted that when deriving matrices $\underset{\approx}{\bar{K}}_e(\rho)$, $\underset{\approx}{\bar{M}}_e(\rho)$, $\underset{\approx}{\bar{A}}_e$ and $\underset{\approx}{\bar{D}}_e$ the element dimensions are scaled by ℓ as discussed in Chapter 5. For the delta wing problem the length of the cantilevered edge, L, (Fig. 9.1) is used for this purpose.

C.5 Boundary Conditions

In this section equations for applying the free edge natural (force) boundary conditions on deflection curvatures are derived.
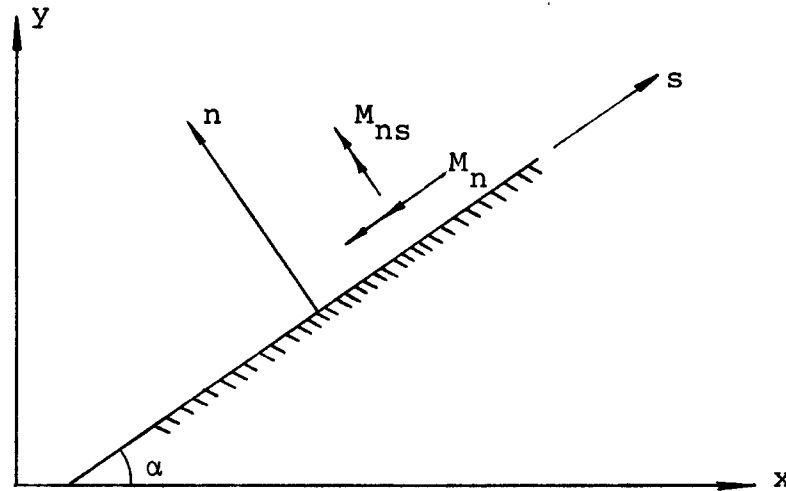

Fig. C.2 Plate Free Edge and Free Edge Moments

In figure C.2 a free edge that makes an angle α with the x-axis is shown. For the (n,s) coordinate system the free edge plate-bending moments are M_n and M_{ns}. Free edge natural boundary conditions given by Kirchhoff (Ref. 31) are

$$M_n = 0 \qquad (C.53)$$

$$Q_n - \frac{\partial M_{ns}}{\partial s} = 0 \qquad (C.54)$$

where Q_n is the free edge shear force. Equation (C.54) requires the calculation of transverse displacement third derivatives.

For simplicity it was replaced in the present optimization
study by the equation

$$M_{ns} = 0 \qquad (C.55)$$

which assumes $Q_n = 0$. Using equation (3.2) which relates plate-
bending moments to deflection curvatures we can reduce equations
(C.53) and (C.55) to

$$W_{nn} + \nu\, W_{ss} = 0 \qquad (C.56)$$

$$(1 - \nu)\, W_{ns} = 0 \qquad (C.57)$$

where ν is the Poisson's ratio. Employing second degree tensor
transformation (Ref. 22) we can write

$$W_{ss} = W_{xx} \cos^2\alpha + 2W_{xy} \sin\alpha \cos\alpha + W_{yy} \sin^2\alpha \qquad (C.58)$$

$$W_{nn} = W_{xx} \sin^2\alpha - 2W_{xy} \sin\alpha \cos\alpha + W_{yy} \cos^2\alpha \qquad (C.59)$$

$$W_{ns} = -W_{xx} \sin\alpha \cos\alpha + W_{xy} (\cos^2\alpha - \sin^2\alpha)$$

$$+ W_{yy} \sin\alpha \cos\alpha \qquad (C.60)$$

Substituting these expressions for W_{ss}, W_{nn} and W_{ns}
in equations (C.56) and (C.57) we obtain

$$W_{xx}(\sin^2\alpha + \nu \cos^2\alpha) + W_{yy}(\cos^2\alpha + \nu \sin^2\alpha)$$

$$- 2W_{xy} (1 - \nu) \sin\alpha \cos\alpha = 0 \qquad (C.61)$$

$$W_{xx} \sin\alpha \cos\alpha - W_{yy} \sin\alpha \cos\alpha - W_{xy} (\cos^2\alpha - \sin^2\alpha) = 0$$

$$(C.62)$$

which are the constraint equations used on the curvatures of free edge nodal points (i.e. nodal points 3, 6, 10, 9 and 8, Fig. 9.1) for the delta wing problem.

It should be noted that the authors of reference 22 do not approve such attempts to satisfy natural boundary conditions only at the nodal points (see Ref. 22, section 2.6 for a detailed discussion).

C.6   Merit Function

We can define

$$F_e(\rho) \;=\; \iint\limits_{A_e} \rho(\xi,\eta)\,d\xi\,d\eta \qquad\qquad (C.63)$$

where $F_e(\rho)$ is the merit function associated with an element. Using equation (C.11) for $\rho(\xi,\eta)$ we obtain

$$F_e(\rho) \;=\; \frac{A_e}{3}\,(\rho_1 + \rho_2 + \rho_3) \qquad\qquad (C.64)$$

which can be used to derive the merit function for the system.

REFERENCES

1.   Ashley, H., and McIntosh, S.C., "Application of Aeroelas-
     tic Constraints in Structural Optimization", Twelfth
     International Congress of Applied Mechanics. Stanford
     University, August 1968.

2.   Dugundji, J., "Theoretical Considerations of Panel Flutter
     at High Supersonic Mach Numbers", AIAA Journal, 4,
     July 1966.

3.   Bisplinghoff, R.L., and Ashley, H., "Principles of Aero-
     elasticity", John Wiley and Sons, New York, 1962.

4.   Turner, M.J., "Optimization of Structures to Satisfy
     Flutter Requirements", AIAA Structural Dynamics Con-
     ference, New Orleans, 1969.

5.   Olson, M.D., "Finite Elements Applied to Panel Flutter",
     AIAA Journal, 5, December 1967.

6.   Olson, M.D., "Some Flutter Solutions Using Finite Elements",
     AIAA Structural Dynamics Conference, New Orleans, 1969.

7.   Weisshaar, T. A., "An Application of Control Theory Methods
     to the Optimization of Structures Having Dynamic or
     Aeroelastic Constraints", AFOSR Scientific Report,
     Sudaar 412.

8.   Craig, Jr., R.R., "Optimization of a Supersonic Panel Sub-
     ject to a Flutter Constraint - a Finite-Element Solu-
     tion", AIAA Structural Dynamics Conference, Ananeim,
     California, 1971.

9. Rudisill, C.S. and Bhatia, K.G., "Optimization of Complex
    Structures to Satisfy Flutter Requirements", AIAA
    Journal, Vol. 9, No. 8, August 1971.

10. Fox, R.L., Miura, H., and Rao, S.S., "Automated Design
    Optimization of Supersonic Airplane Wing Structures
    Under Dynamic Constraints", AIAA Structural Dynamics
    Conference, San Antonio, 1972.

11. Rogers, L.C., "Derivatives of Eigenvalues and Eigenvectors"
    AIAA Journal, 8, May 1970.

12. Van de Vooren, A.I., "Theory and Practice of Flutter Calcu-
    lations for Systems with Many Degrees of Freedom",
    Doctoral thesis, Leyden, Holland, 1952.

13. Pope, G.G. and Schmit, L.A., Eds., "Structural Design
    Applications of Mathematical Programming Techniques",
    AGARDograph No. 149, Feb., 1971.

14. Leitmann, G., "Optimization Techniques", Academic Press,
    1962.

15. Fox, R.L., "Optimization Methods for Engineering Design",
    Addison-Wesley, 1971.

16. Przemieniecki, J.S., "Theory of Matrix Structural Methods",
    McGraw-Hill, New York, 1968.

17. Zienkiewicz, "The Finite Element Method in Engineering
    Science", McGraw-Hill, New York, 1971.

18. Wilkinson, J.H., "The Algebraic Eigenvalue Problem",
    Clarendon Press, London, 1965.

19. Rao, S.S., "Automated Optimum Design of Aircraft Wings to
    Satisfy Strength, Stability, Frequency and Flutter

Requirements", Doctoral thesis, Case Western Reserve
University, January, 1972.

20. Miura, H., "An Optimal Configuration Design of Lifting Sur-
face Type Structures Under Dynamic Constraints",
Doctoral thesis, Case Western Reserve University,
January, 1972.

21. Gwin, L.B. and McIntosh, Jr. S.C., "A Method of Minimum-
Weight Synthesis for Flutter Requirements", Technical
Report AFFDL-TR-72-22, Part I, June 1972.

22. Cowper, G.R., Kosko, E., Lindberg, G.M., Olson, M.D.,
"A High Precision Triangular Plate-Bending Element",
NRCC Aeronautical Report LR-514, Ottowa, December 1968.

23. Houbolt, J.C., "A Study of Several Aerothermoelastic Pro-
blems of Aircraft Structures", Mitteilung aus dem
Institüt für Flugzengstatik und Leichtbau, Nr.5, E.T.H.,
Zürich, 1958.

24. Cannon, R.H., "Dynamics of Physical Systems", McGraw-Hill,
New York, 1967.

25. Turner, M.J., "Proportioning Members of a Structure for
Maximum Stiffness with Given Weight", report by Vought-
Sikorsky Aircraft, January 1942.

26. Turner, M.J., "Design of Minimum Mass Structures with
Specified Natural Frequencies", AIAA Journal, Vol. 5,
No. 3, March 1967.

27. Bryson, A.E., and Ho, Y.C., "Applied Optimal Control",
Blaisdell, Waltham, Mass., 1969.

28. Rubin, C.P., "Dynamic Optimization of Complex Structures", AIAA Structural Dynamics Conference, New Orleans, 1969.

29. Stroud, W.J., Dexter, C.B., Stein, M., "Automated Preliminary Design of Simplified Wing Structures to Satisfy Strength and Flutter Requirements", Langley Research Center, NASA TN D-6534.

30. Pierson, B.L., "Application of a Gradient Projection Optimal Control Method to a Class of Panel Flutter Optimization Problems", Technical Report, Iowa State University, ERI-AMES-73186, August, 1973.

31. Timoshenko, S.P., and Woinowsky-Kreiger, S., "Theory of Plates and Shells", McGraw-Hill, New York, 1959.

VITA

Ibrahim Onur Erbuğ was born in Gaziantep, Turkey, on November 2, 1946, the son of Ayşe Melek Erbuğ and Mustafa Safi Erbuğ. After graduating from Ankara Atatürk High School in Ankara, Turkey, he entered the Middle East Technical University at Ankara in October 1963. In June 1967, he received the degree of Bachelor of Science in Civil Engineering from the Middle East Technical University. In September 1967, he entered the Graduate School of The University of Texas at Austin. He was awarded the degree of Master of Science in Civil Engineering from The University of Texas at Austin in May, 1969. During his graduate studies toward a Ph.D. degree at The University of Texas at Austin, he received a NATO Scholarship from the Scientific and Technical Research Council of Turkey. He was also employed several semesters as a Research Assistant by the Civil Engineering Department, by the Bureau of Engineering Research and by the Aerospace Engineering Department of The University of Texas at Austin. In the Spring semester of 1974 he was employed as a Teaching Assistant by the Civil Engineering Department.

Permanent address: 111 Nene Hatun Cad.
                          Çankaya - Ankara, Turkey

This dissertation was typed by Bettye Lofton and Miriam Riskind.